

MODELING COUPLED WATER-HEAT FLOW AND IMPACTS
UPON CHEMICAL TRANSPORT IN MULCHED SOIL BEDS

By

DILIP SHINDE

A DISSERTATION PRESENTED TO THE GRADUATE SCHOOL
OF THE UNIVERSITY OF FLORIDA IN PARTIAL FULFILLMENT
OF THE REQUIREMENTS FOR THE DEGREE OF
DOCTOR OF PHILOSOPHY

UNIVERSITY OF FLORIDA

1997

I dedicate this work to my parents, father (late) Krishna Rao Shinde and mother Vatsala Shinde, who instilled in me the importance of education and knowledge.

ACKNOWLEDGMENTS

I express my sincere gratitude to Professors R.S. Mansell (chair) and A.G. Hornsby (cochair) for their guidance and support during this research work. Appreciation is also extended to the members of my advisory committee: Professors P.S.C. Rao, B.L. McNeal, and F. S. Zazueta; for useful comments, help and support.

I would like to extend my appreciation and thanks to Dr. B.P. Mohanty (Univ. of California, Riverside) for providing numerous technical literature citations. Thanks are also due to Professor P.N. Kizza for encouragement and support. I would like to also thank Dr. A. Akpoji and Ron Jessup for useful discussions on finite element methods and numerical programming, respectively. I acknowledge Dr. John L. Neiber (Agric. Eng. Dep., Univ. of Minnesota) for providing the FORTRAN code used extensively in creating finite element-mesh in this work.

I take this opportunity to thank also 'The Rotary Foundation of The Rotary International' for the prestigious 'FREEDOM FROM HUNGER' scholarship to enhance my knowledge and join the fight to free the world from hunger.

I would like to acknowledge the substantial financial support provided by Professor A.G. Hornsby during the latter part of this research. I would also like to acknowledge the facilities and partial financial support provided by Professors R.S. Mansell and B.L. McNeal, respectively, during this research.

Lastly, appreciation is extended to my family for their help and support.

TABLE OF CONTENTS

ACKNOWLEDGMENTS	iii
LIST OF TABLES	vii
LIST OF FIGURES	ix
ABSTRACT	xi
INTRODUCTION	1
Coupled Versus Uncoupled Flow Processes in Soil	1
Soil Thermal Regime	2
Non-isothermal Soil Conditions	3
Mechanistic Mathematical Modeling	4
Hypothesis	6
Objectives	7
REVIEW OF LITERATURE	8
Isothermal Water Flow in Porous Media	9
Soil Temperature and Heat Flow	11
Soil Thermal and Water Regimes under Mulching	15
Coupled Heat and Water Flows	19
Philip-de Vries Theory (PDT)	20
Application of Philip-de Vries Theory	22
Solute Transport during Coupled Heat and Water Flow	24
Temperature Effects on Solute Transport	27
Summary	29
MATHEMATICAL MODEL	31
Liquid and Vapor Water Flow in Soil	32
Heat Flow in Soil	32
Transport of Multiple Species of Solutes in Soil	33
Energy Balance at the Soil/Atmosphere Interface	34

Initial and Boundary Conditions	38
Input Parameter Requirements	39
MODEL VERIFICATION AND VALIDATION	44
Isothermal Water Flow	45
Uncoupled Heat Flow	46
Coupled Water and Heat Flow	47
Isothermal 1-D Solute Transport during Steady Water Flow	48
Isothermal 2-D Solute Transport during Steady Water Flow	49
Isothermal 1-D Solute Transport with Nitrification Chain during Steady Water Flow	51
Isothermal 1-D Solute Transport involving Gas Flow	52
Summary	54
MODEL APPLICATION	55
Fate and Transport of Methyl Bromide Fumigation in Soils	55
Transport Mechanisms for MBr Fumigant in Soil	59
Fate of MBr Fumigant in Soil	60
Permeation/Transmission of MBr through Polyethylene Mulch	63
Modeling of MBr Transport during Fumigation	68
Analysis of Fate and Transport of MBr Fumigant	72
Approach	73
Methodology	75
Results and Discussion	79
Plastic-Mulching of Soil Beds to Control MBr Loss to the Atmosphere	79
Non-Isothermal versus Isothermal Soil-Conditions	85
Variable Water Saturation of Soil	87
Depth of Fumigation Injection	97
Effect of Irrigation (Water Dousing of the Bed Surface)	96
Fumigation Efficiency Analysis	101
Hydrolysis of MBr (Sensitivity Analysis)	107
Diurnal Water and Heat Dynamics in a Plastic Covered Soil Bed ..	108
Summary and Conclusions	119
APPENDIX A SOIL MOISTURE FLOW	122
APPENDIX B SOIL HEAT FLOW	125
APPENDIX C CHEMICAL TRANSPORT	127
APPENDIX D NUMERICAL APPROACH	132

LIST OF REFERENCES	142
BIOGRAPHICAL SKETCH	153

LIST OF TABLES

<u>Table</u>	<u>page</u>
2-1. Average thermal properties of major soil constituents at 20 °C and 1 atm (Ghildyal and Tripathi, 1987)	12
2-2. Short-wave optical properties of five plastic mulches used in commercial crop production. Data adapted from Ham et al. (1993)	17
5-1. Earlier estimates for source-contributions of MBr to the atmosphere (Grojesan, 1991; Khalil et al., 1993; Lobert et al., 1990; Manó and Andreae, 1994; Yagi et al., 1993; and Zurer, 1993)	56
5-2. A recently revised budget for atmospheric MBr (Yvon-Lewis and Butler, 1997)	57
5-3. Selected chemical and physical properties of MBr (CH ₃ Br) (Adapted from Hacherl, 1994)	58
5-4. Measured degradation rate coefficient and half life of MBr as a function of soil water content (Adapted from Jin and Jury, 1996)	63
5-5. Rate of escape of MBr through several films at various temperatures (Adapted from Kolbezen and Abu-El-Haj, 1977)	65
5-6. Physical Properties for 5 distinct horizons of a profile of Arredondo fine sand soil	77
5-7. Parameter values for 5 distinct horizons of a profile of Arredondo fine sand soil	78
5-8. Material balance (unit: %) of MBr under measured and enhanced levels of diffusion coefficient for plastic mulch	84
5-9. Material balance (unit: %) of MBr for fumigation under isothermal and non-isothermal conditions	86

5-10. Material balance of MBr (unit: %) under different water saturations for one and 3 days after fumigant injection	90
5-11. Material balance of MBr (unit: %) during fumigation under different water saturations for 65-cm injection zone	98
5-12. Material balance (unit: %) of MBr under water dousing and no-dousing ..	100

LIST OF FIGURES

<u>Figure</u>	<u>page</u>
2-1. Measurements of soil temperature at 10-cm depth beneath five different plastic mulches and a bare plot near Manhattan, KS on day 196 of the year 1991. Adapted from Ham et al. (1993)	18
4-1. Observed and computed distributions of water content in a sand column during constant flux infiltration	45
4-2. Observed and computed temperatures for two depths in a field soil	46
4-3. Observed and computed water content after 31 days under the influence of both matric head and thermal gradients	48
4-4. Observed and computed breakthrough curves for boron	49
4-5. Location of solute concentration fronts for three times as estimated numerically and with the analytical solution	50
4-6. Analytically determined and numerically computed concentration profiles at 200 hours	52
4-7. Analytically determined and numerically computed concentration profiles at 1, 3, and 5 hours	53
5-1. Temperature dependence of MBr diffusion in water (Data from Maharajh and Walkley, 1973)	60
5-2. Laboratory-measured and estimated Henry's Law constants at different temperatures for partitioning of MBr into water (Adapted from Mutziger et al., 1996)	61
5-3. MBr emission fluxes in plastic mulched beds during fumigation at the University of Florida Green Acres Experimental Station located near Gainesville, FL.	66
5-4. MBr diffusion through black LDPE of different thicknesses (Data from Hacherl, 1994; and Kolbezan and Abu-El-Haj, 1977)	68

5-5. Simulated and measured flux density through plastic-mulched surface. Adapted from Wang et al. (1997)	71
5-6. Schematic of the discretized simulation domain of the soil bed	76
5-7. Measured and elevated levels of diffusion coefficients through 1.25-mil black LDPE plastic-mulch used in model simulations	80
5-8. Losses of MBr to the atmosphere through soil bed and furrow surfaces using measured and elevated diffusion coefficients for MBr through plastic mulch	81
5-9. MBr total concentration ($\mu\text{mol cm}^{-3}$) contours and gaseous MBr flux vectors ($\mu\text{mol cm}^{-2} \text{hr}^{-1}$) in the bed 6 hrs after injection of MBr fumigant. .	82
5-10. Emission fluxes of MBr through bed and furrow under isothermal and non- isothermal transport of fumigant	85
5-11. Emission fluxes of MBr through bed and furrow during fumigation performed under different profile water-saturation scenanos	88
5-12. Contours of water content ($\text{cm}^3 \text{cm}^{-3}$), temperature ($^{\circ}\text{C}$), and MBr concentration (μmol) with gaseous fluxes ($\mu\text{mol cm}^{-2} \text{hr}^{-1}$) of MBr under 2 different soil-water saturation scenarios after fumigation	91
5-13. Emission fluxes of MBr under different water saturations for a 66-cm injection zone during the first 3 days after fumigant injection	97
5-14. Effect of water dousing on the MBr emission fluxes from the soil bed during fumigation	99
5-15. Contours of water content, temperature, and MBr concentration with gaseous fluxes of MBr at 9 hours after fumigation under water dousing and no-dousing on the bed-surface	100
5-16. Soil sterilization zones for different scenarios 3 days after MBr fumigation using different criteria	104
5-17. Loss of MBr (unit: %) under different rates of hydrolysis of MBr	107
5-18. Diurnal water and heat dynamics in a mulched bed for a wet soil.	113
5-19. Diurnal water and heat dynamics in a mulched bed for a dry soil.	116
D4-1 Linear triangular element	136

Abstract of Dissertation Presented to the Graduate School
of the University of Florida in Partial Fulfillment of the
Requirements for the Degree of Doctor of Philosophy

MODELING COUPLED WATER-HEAT FLOW AND IMPACTS
UPON CHEMICAL TRANSPORT IN MULCHED SOIL BEDS

By

Dilip Shinde

December 1997

Chair: Robert S. Mansell

Cochair: Arthur G. Hornsby

Major Department: Soil and Water Science

Plastic-covered soil bed systems are widely used in the southeastern United States for vegetable and fruit production. Plastic-mulching results in highly variable and transient soil thermal regimes both in space and time under atmospheric influences (e.g., solar radiation, wind, etc.). Much evidence exists that water flow is affected by non-isothermal conditions and vice-versa. In this work, a two-dimensional model for simultaneously describing chemical transport and coupled water-heat flows in plastic-covered soil beds was developed with many improvements over earlier efforts. Realistic plastic-mulch boundary conditions are thoroughly described by including optical properties of the plastic mulch into the energy balance at the soil/atmospheric interface along with other atmospheric influences of weather components. This model provides opportunity to consider the

effect of coupled water-heat flows upon estimates of chemical transport (both in the liquid and gaseous phases) in plastic-mulch culture production systems.

Chemical transport in soil beds in the model utilize consideration of chemical existence in solid, liquid, and gas phases. Temperature dependence of the rates of chemical reactions and volatilization is described efficiently by incorporating temperature dependence in fate and transport coefficients. The model uniquely provides opportunity to simulate coupled water-heat flow and multiple-solute transport with a complex plastic-mulch atmospheric boundary for realistic field situations.

The model was used to analyze the fate and transport of methyl bromide (MBr) during fumigation of mulched soil beds. MBr, a highly volatile pesticide, is widely used in California, Florida, and Hawaii for its broad-spectrum efficiency in controlling insects, fungi, and weeds. Unfortunately, MBr is a major environmental hazard due to its depletion effect on the atmosphere ozone layer. Model analyses revealed that non-isothermal conditions should be considered in the accurate description of MBr fate and transport. Modeling results indicate that utilizing a relatively wet soil profile, deeper injection, and water dousing on the bed-surface before installation of plastic mulch will decrease atmospheric emissions of MBr. However, deeper injection of MBr fumigant, although environmentally less hazardous, may decrease effective sterilization of crop root zones in the soil.

CHAPTER 1 INTRODUCTION

Coupled Versus Uncoupled Flow Processes in Soil

Flow of water, air, and heat in soil is generally assumed to be uncoupled, that is, the driving forces causing individual flow are generally considered to be mutually independent. Darcy's equation for liquid water flow, based upon spatial gradients of soil-water potential, and Fourier's equation for heat flow based upon spatial gradients of soil temperature, provide two examples of uncoupled flow processes. In nature, however, water is also known to move in response to molecular forces, such as thermal and osmotic gradients. Similarly, considerable heat flow may occur as latent heat by water vapor diffusion in the air-filled soil pores, and as sensible heat transfer due to liquid and vapor movement. In a partially saturated soil, flow of water due to thermal gradients occurs through zones occupied by liquid as well as air, and is assisted by multiple condensation and evaporation cycles (Philip and de Vries, 1957). Thus, transport processes occurring in the soil under field conditions are intricate and complex.

Diffusion theory indicates that water molecules are in constant thermal motion, accompanied by jump-like transitions from one temporary equilibrium state to another (Ghildyal and Tripathi, 1987). The frequency of transition and the number

of molecules traversing a certain section of the liquid is highly dependent upon the temperature gradient and causes self thermo-diffusion of water. As temperature gradients are accompanied by gradients of surface tension at the air-water interface, there is a possibility of thermo-capillary flow and thermo-capillary film flow of water in the liquid phase (Ghildyal and Tripathi, 1987). Thermo-capillary flow occurs in those capillaries where liquid-water menisci exist. Here, temperature variation induces the variation of capillary pressure and a corresponding shift of the liquid column. Thermo-capillary film flow is caused due to gradients of surface tension (change in water affinity with change in temperature) at the water-film surface. Both of these mechanisms contribute significantly to the total thermal water transfer under moderate to high water content conditions. Movement of water in the liquid state due to changes in the volume of entrapped air with temperature has also been observed (Ghildyal and Tripathi, 1987). In water-saturated or nearly saturated soil, the entrapped air may cause direct transport of water through the pressure it exerts and, in unsaturated soil, through an apparent increase in the temperature coefficient of the matric potential. Convective flow of water vapor may also occur due to differences in the densities of cold and warm air.

Soil Thermal Regime

The thermal regime of a soil depends upon radiative solar heat flux into the soil and upon heat-transfer processes occurring in the soil and between the soil and air which, in turn, depend on the thermal characteristics of soil solids, gases, and water. The soil thermal regime, which greatly modifies the overlying microclimate,

is generally characterized in terms of soil temperature. Soil temperature fluctuations are especially important since they impact physical, chemical, and biological processes in the soil.

The source of heat for soil is incoming net solar radiation. On a clear day, Geiger (1957) described the typical distribution of incoming solar radiation as: 1) global radiation, which is the sum of the direct-beam penetration to the earth (19 %) and the diffuse-sky radiation (26 %); 2) scattered radiation returned to outer space (11 %); 3) radiation reflected by clouds (28 %); and 4) radiation absorbed by the atmosphere (15 %).

Non-isothermal Soil Conditions

Much published literature confirms that soil-water movement is affected by spatial gradients of both temperature and water potential. Thus, under non-isothermal conditions, movement of water (both liquid water and vapor tend to move from regions of high to low temperature) through soil should be considered for both liquid and vapor phases. Non-isothermal conditions have broader implications in that solute-transport mechanisms are associated with water movement, and the fate and transport of volatile organic chemicals are also influenced by the soil thermal environment.

The influence of thermal gradients upon water movement in soils has largely been observed in two areas (Jury, 1973): 1) in the hot, dry surface layer of a bare soil where the interface between the soil and atmosphere causes water movement to be largely in the vapor phase; and 2) deeper in the soil where thermal gradients persist

over seasons and can slowly transport liquid upward or downward. In the special case of plastic-mulched soil, imposed thermal gradients tend to be greater at the soil surface and the mulch also provides a partial barrier to vapor flow between the soil and atmosphere and causes a return flow of water after condensation under the mulch.

Both water movement and contaminant transport are influenced by temperature gradients in soils. Natural temperature gradients are usually highest during daytime (midday) near the land surface, but the relatively small geothermal gradient below the level of seasonal temperature variation can be a significant factor in determining the percolation of water in deep unsaturated zones (Evans and Nicholson, 1987).

Mechanistic Mathematical Modeling

Mechanistic mathematical models provide powerful tools to describe and interpret flow and transport processes in soil-water systems. Bear and Verruijt (1987) defined a model as a 'simplified version of the real system that approximately simulates the excitation-response relations of the latter'. The first step in modeling involves the construction of a conceptual model of the problem, consisting of a set of assumptions that reduce the real problem and the real domain to simplified versions (ultimately permitting mathematical description of the processes) that are acceptable in view of the modeling objectives. In the second step, the conceptual model is expressed in the form of a mathematical model (Bear and Verruijt, 1987). Properly posed mathematical models for initial-value problems involving mass and

energy transport in porous media require (i) appropriate differential transport equations, (ii) initial conditions in the flow domain, and (iii) boundary conditions imposed along the surfaces of the flow domain. Models are essential in performing complex analyses and in making informed predictions. Friedman et al. (1984) stated that, in some cases, models have increased the accuracy of estimates of future events to a level far beyond 'best judgement' decisions. Anderson and Woessner (1992) emphasized that models provide the best way to make an informed analysis or prediction concerning consequences for a proposed action. The authors further stated that models can also be used in an interpretive sense to gain insight into the controlling parameters in a site-specific setting or as a framework for assembling and organizing field data and formulating ideas about system dynamics.

Schwarzenbach et al. (1993) defined a model in the following way: 'A model is an imitation of reality which stresses those aspects that are assumed to be important and omits all properties considered to be nonessential'. These authors summarized the role of modeling explicitly in the following ways:

- 1) Mathematical models allow knowledge acquired for different systems and/ or different situations to be combined in order to provide the ultimate aim of constructing general theories. Models permit making predictions, which then must be verified by measurement.
- 2) Classic scientific theories begin as models, and it is only long-time positive experience with some of these models which leads scientists to believe that they are more true and fundamental than others and should thus bear the name 'law'.

- 3) In environmental sciences, models serve to sort out alternative explanations for observations made in nature which cannot be controlled in the same way as conditions for a laboratory experiment can be controlled.
- 4) Models should always be constructed to transfer the knowledge acquired in one system to another situation, thus enabling a deeper understanding of the processes responsible for the measured data. A model should be applied in order to design new experiments or observation programs that are critical for the testing of hypotheses.
- 5) Real observations are always superior to outputs produced by a given model. But model results can help us examine various scenarios and likely future outcomes regarding the behavior of environmental systems for which real data would never be collected as frequently and as ubiquitously as needed.

Hypothesis

The soil thermal regime within plastic-mulched soil beds is well-known to be influenced by interactions between the overlying atmosphere and the plastic-covered soil surface. The resulting non-isothermal conditions affect water flow and redistribution. Hence, coupling of water and heat flows is necessary to model effectively both components within the vadose zone, especially the crop root zone. The hypothesis here is that model description of chemical transport within plastic-mulched soil beds under non-isothermal field conditions requires the utilization of coupled water and heat flows in order to provide realistic results for management

practices such as fumigation with methyl bromide to control pathogens. Impacts of this coupled process upon chemical fate (transformations, microbial degradation, etc.) and transport are expected to be particularly significant for volatile chemicals such as methyl bromide that may appear in aqueous, gaseous, and solid phases of soil water systems. Information obtained here regarding the dynamics of the fate and transport of methyl bromide during fumigation of agricultural soils should also be useful in evaluating future fumigation with fumigants other than methyl bromide, which will no longer be used in this country after the year 2001.

Objectives

This research was performed to model and investigate the interactive flows of water, heat, and solutes in non-isothermal soil environments (the vadose zone) in order to minimize empiricism from existing knowledge of such systems. The following objectives were formulated:

1) Develop a mathematical model describing the coupled processes of water, heat and chemical transport (2-D) for mulched soil-bed systems, where solar energy imposes non-isothermal conditions.

2) Verify, validate, evaluate, and refine the model as needed for cases of both coupled and uncoupled flows of water, heat and chemicals with existing appropriate models (analytical) and published data.

3) Use model simulations to determine impacts of coupled water and heat transport due to non-isothermal conditions upon the transport of a volatile pesticide such as methyl bromide during fumigation of plastic-covered soil beds.

CHAPTER 2 REVIEW OF LITERATURE

The rate of liquid water movement in soil is important to the study of solute transport, nutrient availability, efficacy of pesticides, and also water availability to crop root systems during agricultural production. Physical properties of the soil influence water movement in two important ways: the size distribution and structural arrangement of soil particles determine the pore space configuration through which water moves; and the interaction between the soil and water gives rise to water-moving forces. In water-saturated soils such as occur below groundwater tables where pores are completely filled with water, the fluid is a single phase and forces originating from gravity, including the pressure gradient, determine the direction and magnitude of flow. The energy potential for the pore water under saturated conditions is generally positive, or greater than the atmospheric pressure. The saturated flow process for the simple isothermal case is described mathematically by Darcy's equation and Laplace's equation.

Generally, under field conditions, soil pores are incompletely or partially saturated and the energy potential of water is negative (i.e. a suction), being less than atmospheric pressure. It depends not only upon position in the gravitational field, but also upon sorptive forces associated with interfacial boundaries. If the unfilled pore space is filled with gases such as air, movement in the resulting

composite system of solid, liquid and gaseous phases is referred to as unsaturated flow. This flow condition in soil is particularly important when the groundwater table occurs at considerable depth below the soil surface (below the vadose zone).

Isothermal Water Flow in Porous Media

Under saturated conditions where the pores of the soil system are completely filled with water, the transmission coefficient (i.e., hydraulic conductivity) depends principally upon the viscosity ($\mu_w(T)$) and density ($\rho_w(T)$) (both being functions of temperature, T) of the water and the nature of the porous media. The volumetric flux of water flow through soil or other porous material is usually given by Darcy's equation as

$$q_L = -K \nabla P \quad [2.1]$$

where q_L is liquid flux, K is hydraulic conductivity, and P is hydraulic pressure of the water.

Except for the isothermal saturated condition, Darcy's equation, as originally postulated, does not apply precisely to water flow through soil. However, this equation has been used since 1856 for describing liquid flow through porous material with little reservation.

Under unsaturated conditions when the soil contains both liquid and gaseous phases, the most frequently used modification of Darcy's equation involves substituting the matric-potential gradient for the hydraulic pressure gradient as the driving force. Under these conditions, hydraulic conductivity is no longer a constant

but is a function of capillary potential as well as temperature, which yields

$$q_L = -K(h, T) \nabla H ; \quad H = h(\theta_L, T) + z_g, \quad K = \frac{k_p \rho_w(T) g_f}{\mu_w(T)} \quad [2.2]$$

Here H is total potential, h is matric potential, z_g is gravitational potential (i.e., elevation), θ_L is liquid volumetric water content, T is temperature, k_p is intrinsic permeability and g_f is the acceleration of gravity. Under isothermal conditions the temperature dependence is eliminated and total potential gradient is the driving force. Richards (1931) derived the equation of isothermal flow through a porous medium by using the continuity equation (describing mass conservation) and Darcy's equation. Assuming that the medium is incompressible, the continuity equation for water flow through a homogenous medium was given as

$$\frac{\partial(\rho_L \theta_L)}{\partial t} = -\nabla \rho_L q_L \quad [2.3]$$

where t is time and ρ_L is the liquid density. In very dry soils, the capillary or matric potential attains great negative values and, in the unsaturated region above a water table, the capillary driving force dominates the gravitational force.

Isothermal theory has limited application for soils under actual field conditions, where heat flow is transient in time and varies in space. It has been observed that heat is evolved at the wetting front when water infiltrates a very dry soil of fine texture (Anderson and Linville, 1960). Cooling of soil occurs when water is evaporated from soil (Wiegand and Taylor, 1962) and warming occurs due to release of thermal energy during condensation of water vapor. Absorption of solar radiation at the soil surface and chemical or biological activity within the soil may

also result in temperature gradients. Thus, temperature gradients must be included in the flow equation in order to effectively describe water flow in surface soil characterized by transient thermal regimes.

Soil Temperature and Heat Flow

Under field conditions, the profiles of soil temperature change rapidly during a normal day. When incoming solar radiation falls on the soil surface the soil surface becomes heated, causing a difference of temperature between the surface and the subsoil. This difference causes heat to flow downwards as a temperature wave. As the heat wave penetrates slowly downward in response to soil thermal properties, moisture content, and structure of the soil, a phase shift occurs in the temperature curve with depth which leads to a time lag in the occurrence of temperature maxima at different depths in the soil. Also, the amplitude of the temperature wave decreases with soil depth due to storage of thermal energy. During night time, when the soil surface cools down, the lower portion of the soil profile remains warmer than the air temperature. Annual temperature fluctuations extend much deeper into the soil compared to diurnal changes, and are also in general periodic in nature.

Soil texture has a distinct influence on soil heat flux and, hence, on soil temperature. The amplitude of the daily temperature wave decreases in the order sand > loam > peat > clay. This order can be attributed to the greater heat capacity of the finer-textured materials and their normally greater thermal conductivities.

Table 2-1. Average thermal properties of major soil constituents at 20 °C and 1 atm (Ghildyal and Tripathi, 1987).

Material	Specific Heat (cal g ⁻¹ °C ⁻¹)	Volumetric Heat Capacity (cal cm ⁻³ °C ⁻¹)	Thermal Conductivity (10 ⁻³ cal cm ⁻¹ s ⁻¹ °C ⁻¹)	Thermal Diffusivity (10 ⁻³ cm ² s ⁻¹)
Quartz	0.175	0.46	20.00	43.00
Other Minerals	0.175	0.46	7.00	15.00
Organic Matter	0.46	0.60	0.60	1.00
Water	1.00	1.00	1.42	1.42
Air	0.24	0.00029	0.062	0.21

Sandy soils generally hold less water and usually drain faster than finer-textured soils. At low water contents, air occupies much of the pore space and hydraulic conductivity of the soil becomes limited. As such, thermal capacity and conductivity of soil with a low degree of water saturation is governed by the volumetric content of water, which has the highest heat capacity (Table 2-1) among the substances commonly found in soils. Because of very small thermal diffusivity, air provides thermal insulation against rapid changes in temperature.

Three mechanisms by which heat flow occurs in soils include conduction, convection and radiation (Hillel, 1980). Radiative heat transfer is of importance only in dry soils at high temperatures and within large pores. It is the least-important mechanism, and is often neglected. Convection can be separated into two components, forced and free. Forced convection is mostly negligible, with the exception of infiltration during irrigation or heavy rain. Free convection occurs as a result of fluid density gradients. Convective heat transport in the vapor phase can be partitioned into sensible and latent heat components. The sensible heat capacity of

soil air is very low (Table 2-1) and, as soil air flow is most often small, latent heat transport is of primary importance. Latent heat transport occurs when a fluid such as water changes phase and is transported as a new phase (such as vapor). Vaporization of liquid water requires heat (540 cal g^{-1}) that is transported in the vapor phase through a vapor-phase gradient and may be released during condensation at a location different from where the liquid originated.

A very simple theory of heat transfer in soils is based upon uncoupled mass and heat flows and considers only heat conduction, without regard for any other transport mechanisms which may actually occur. The thermal flux in the soil (assuming that thermal gradients do not result in water flow) is defined from Fourier's first law of heat conduction as

$$q_h = -\lambda \nabla T \quad [2.4]$$

where q_h is thermal flux and λ is thermal conductivity. Invoking the principle of energy conservation in the form of the thermal continuity equation (Hillel, 1980) provides

$$\frac{\partial T}{\partial t} = \nabla D_H \nabla T; \quad \text{with } D_H = \frac{\lambda}{C_s} \quad [2.5]$$

where D_H is thermal diffusivity and C_s is volumetric heat capacity of the soil.

Conduction of heat in soils occurs through the solid, liquid, and gaseous phases. Since these phases have different heat capacities and thermal conductivities, the main complication when solving the heat conduction equation in soils is caused by determining the average soil thermal properties. de Vries (1963) reported a method to calculate heat capacity of soil material by addition of the heat

capacities of the various constituents, weighted according to their volume fractions. The heat capacity as such can be found by adding the heat capacities of the various phases present as

$$C = \sum_i (X_{s,i} C_{s,i}) + X_w C_w + X_a C_a \quad [2.6]$$

where the subscripts *s*, *w* and *a* refer to solid, liquid water, and air phases respectively; *i* distinguishes the various materials in the solid phase; and *X* denotes the volumetric fraction of a given phase (de Vries, 1963). Thus, volumetric heat capacity for soil clearly depends upon water content.

The thermal conductivity of a soil also depends in a rather complicated way on the composition of the soil, in particular its water content. A physical model, assuming solid and gas particles to be suspended in the liquid phase, for estimating the thermal conductivity in soils was given by de Vries (1963) as

$$\lambda = \frac{X_w \lambda_w + \sum_i (k_i^* X_i \lambda_i) + k_a^* X_a \lambda_a}{X_w + \sum_i (k_i^* X_i) + k_a^* X_a} \quad [2.7]$$

The summation for this equation extends over the different solid soil constituents, which are characterized by their thermal conductivities and shapes. The multiplication factor k^* in Eq. [2.7] represents the ratio of the spatial average of the temperature gradient in the soil grains of kind *i* and the spatial average of the temperature gradient in water.

The influence of latent heat transfer in air-filled pores is proportional to the temperature gradient in these pores and can be taken into account by adding the thermal conductivity of vapor (λ_{vap}) to the thermal conductivity of dry air (λ_a). The

λ_{vap} term represents the increase in gaseous-phase thermal conductivity due to evaporation and condensation of water vapor. At complete dryness and at very low water contents, the model assumes air rather than liquid to be the continuous medium. However, at this stage (i.e. completely dry soil), de Vries (1963) proposed introduction of a multiplication factor of 1.25 to Eq. [2.7] (i.e. 1.25λ). de Vries reported that errors in calculating λ in this manner would not exceed 10 %, unless the soil grains have a different shape than those assumed.

Wescott and Wierenga (1972) demonstrated the need for coupling heat and water movement when predicting heat transfer by conduction and vapor movement for a dry soil. They found that vapor movement accounted for 40-60 % of the heat flow in the top 2 cm of the soil profile during certain periods of the day and for 20-25 % of the total heat flow even at the 25-cm depth.

Soil Thermal and Water Regimes under Mulching

Mulches are used in agriculture not only because they suppress weeds and reduce water loss from the soil surface, but because they also modify the thermal microclimate of the soil. Rosenberg et al. (1983) presented a good review of mulch effects on soil processes and defined mulching as the application or creation of any soil cover that constitutes a barrier to the transfer of either heat or vapor, or both.

Waggoner et al. (1960) applied black plastic, translucent plastic, aluminum foil, paper, and hay mulches to soil surfaces and measured the resulting alteration in surface energy balance and in soil and air temperature profiles. Black plastic

reduced the outgoing radiation as was evidenced by the greater net radiation, whereas hay and paper (and especially paper) increased it. All mulches decreased the quantity of energy consumed in evaporation by blocking the transport of vapor out of the soil. Sensible heat generated at the surface was increased by the black plastic and the hay, and the temperature of the hay and black plastic was elevated. Black plastic increased in soil temperature, whereas hay and paper had a cooling effect and decreased the amount of heat penetrating the soil. Ekern (1967) in Hawaii found that black plastic mulch reduced water use by pineapples grown in lysimeters. Note here that the well-known practice of surface mulching (for any purpose) decreases evaporative water loss by creating a layered condition in the soil due to differential water contents.

The diurnal supply of solar radiant energy at the soil surface during daylight hours and loss during night-time hours is the major determinant of the thermal microclimate of soil. The presence of mulch material at the soil surface creates a thermal layering effect (similar to the effect of soil layers within the soil). The use of nonporous mulch such as polyethylene plastic also creates a barrier to water vapor flow to the atmosphere.

Optical properties of the plastic mulches play an important role in interaction of the soil surface with the overlying atmosphere. Ham et al. (1993) reported short-wave optical properties of five plastic mulches used in commercial crop production (Table 2-2). These properties exhibited a wide range and thus helped explain earlier work by Waggoner et al. (1960) and Ekern (1967). Black and clear plastic mulches provide extremes in the absorbance of short-wave radiation. The five mulches

described in Table 2-2 were used under bedded conditions in a field and temperatures were recorded at the 10-cm depth below the mulched surface in the center of the bed (Ham et al., 1993).

Table 2-2. Short-wave optical properties of five plastic mulches used in commercial crop production. Data adapted from Ham et al. (1993).

Mulch	Reflectance	Transmittance	Absorbance
Black	0.03	0.01	0.96
Sunfilm	0.12	0.37	0.51
Al-mulch [†]	0.39	0.01	0.60
White-on-Black [†]	0.48	0.01	0.51
Clear	0.11	0.84	0.05

[†]Al-Mulch and White-on-Black were Black mulch in which the upper surface was painted with aluminum and white paint, respectively.

Diurnal measurements of soil temperature beneath the 5 mulches and a bare soil plot as recorded by Ham et al. (1993) for a summer day are given in Fig. 2-1. The highest temperatures were observed beneath the black mulch, which strongly absorbed shortwave radiation. Cooler temperatures were observed beneath the Al-mulch and White-on-Black mulches, which had lower absorbances but higher shortwave reflectances. Although clear mulches are normally used to maximize soil heating during cooler seasons, in this experiment the investigators placed the plastic covers in intimate contact with the soil to ensure a minimal average air gap between the mulch and the soil. The small air gap greatly minimized thermal contact resistance at this location. Thus, the thermal insulation due to air between the plastic sheet and the soil surface was minimized in that investigation.

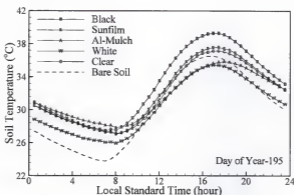


Figure 2-1. Measurements of soil temperature at the 10-cm depth beneath five different plastic mulches and a bare plot near Manhattan, KS on day 195 of the year 1991. Adapted from Ham et al. (1993).

Besides mulching, the geometry of the soil bed, the directional orientation of the beds, crop geometry (canopy structure) and the directional orientation of crop rows also influence the radiation-energy exchange with the soil surface. The amount of solar radiation reaching a horizontal unit of the surface of the earth (at a particular latitude, longitude, and elevation) depends upon a number of factors including the intensity of radiation emitted by the sun, astronomical considerations determining the position of the sun, and the transparency of the atmosphere (Rosenberg et al., 1983). The sum of direct solar radiation and diffuse sky radiation received by a unit horizontal surface is referred to as global radiation. In humid climates, clouds also play a major part in decreasing the amount of solar radiation received at a location. The vegetative canopy of growing annual crops tends to provide increasing shade for the soil surface as the growing season progresses, due

to interception of incoming solar radiation. The shadow of the growing crop results in variable radiation interception at the soil surface, thus affecting the thermal regime in the upper soil layers.

Coupled Heat and Water Flows

The energy state of water molecules in soil changes when a temperature gradient is imposed on the system, and water moves in response to this energy gradient. For the duration of the imposed temperature gradient, an irreversible and spontaneous flow of heat occurs. Thus, heat and water flow processes interact with each other and require mutual coupling. Where simultaneous movement of more than one component (like water and heat) occurs in the system, isothermal flow equations and simple equilibrium thermodynamics cannot be used to predict or describe the water flow (Enfield, 1970).

If a soil system initially at equilibrium (uniform water content with a constant water potential at constant temperature throughout) is subjected to a temperature gradient, water will flow from a warm region to a cooler region (Gurr et al., 1952; Taylor and Cavazza, 1954; Woodside and Cliffe, 1959). When the degree of water saturation in the soil is relatively high, water flow occurs primarily in the liquid phase (Taylor and Cary, 1960). When the degree of water saturation is very low, water movement occurs primarily in the vapor phase. At intermediate water contents, however, movement occurs by a combination of liquid and vapor flows (Cary and Taylor, 1962a, 1962b).

Possible magnitudes of thermally-driven flows have been summarized by Cary (1966) for various soils and commercial materials. Vapor flow in soils in response to thermal gradients of $0.01\text{ }^{\circ}\text{C}$ were observed to vary from about 0.4 to 2.0-mm day^{-1} , the same flow rates that would require pressure-head gradients of 0.05 to 2.50 m of water. Since vapor flow out of wet soils (evaporation) may range from near zero to perhaps 12 mm day^{-1} depending on climatic conditions, one can see that temperature-induced vapor flow should not be ignored.

Philip-de Vries Theory (PDT)

Approximately 40 years ago, in an attempt to describe the phenomenon of simultaneous flow where water is moved by a thermal gradient, Philip and de Vries (1957) and de Vries (1958) proposed theory and equations to describe coupled heat and water transfer in porous media, in terms of classical mechanisms of vapor diffusion and liquid movement by capillarity accounting for heat flow and its resultant effects. Philip and de Vries (1957) were apparently the first to include the interaction of vapor, liquid, and solid phases and the difference between average temperature gradients in the air-filled pores and in the soil as a whole. Taking these factors into account, an approximate analysis was developed which would predict orders of magnitude and general behavior that was in satisfactory agreement with the experimental results of Gurr et al. (1952), Jones and Kohnke (1952), Rollins et al. (1954), Smith (1943), and Staple and Lehane (1954).

Philip and de Vries (1957) separated the isothermal and thermal components of vapor transfer to show the effect of relative humidity. They separated the vapor

flux into two components: 1) one due to temperature gradients; and 2) another due to moisture gradients. In the saturation range where liquid transfer occurs, the liquid flux for water was separated into components caused by temperature gradients, water gradients and gravity. Philip and de Vries (1957) suggested that interaction between vapor and liquid phases occurs as a series of evaporation and condensation steps coupled with liquid flow through so-called 'liquid islands'. When a temperature gradient is applied across a soil, water evaporates at the warm end of the pores and diffuses as vapor, due to a vapor density gradient, towards the cooler end where condensation occurs. This process changes the curvature of the liquid menisci of a liquid island, which continues until capillary liquid flows through the island, produced by the growing difference of both curvatures, equals the rate of condensation and evaporation. The overall effect is a decrease in the tortuous path length and an increase in the cross-sectional area available for vapor diffusion.

Philip and de Vries (1957) presented the simultaneous equations of continuity describing water and heat transfer under the combined influence of water and temperature gradients as

$$\frac{\partial \theta}{\partial t} = \nabla \cdot (D_T^w \nabla T) + \nabla \cdot (D_0^w \nabla \theta) + Kk, \quad \frac{\partial T}{\partial t} = \nabla \cdot (\lambda \nabla T) - L \nabla \cdot (D_0^v \nabla \theta) \quad [2.8]$$

where D_T^w is thermal water diffusivity, D_0^w is isothermal water diffusivity, k is the vertical unit vector, D_0^v is isothermal vapor diffusivity, and L is the latent heat of vaporization. Note that the existence of soil-water hysteresis may, however, invalidate the use of Eq. [2.8] (de Vries, 1958).

Application of Philip-de Vries Theory

Various applications and verifications of PDT have been documented. Barnes and Allison (1984) applied PDT for non-isothermal conditions to develop a model for distribution of deuterium and ^{18}O in dry soils. The model was later verified by the same investigators (Barnes et al., 1989), with the experimental data showing satisfactory results. However, they emphasized that the assumption of constant tortuosity for both liquid and vapor movement is questionable. They reported that, in moderately dry soils the liquid tortuosity factor is probably reduced, and vapor diffusion may be enhanced by the presence of 'liquid islands'. Scanlon (1992) used a model developed with PDT to evaluate liquid and vapor water flow in desert soils of Texas using ^{36}Cl and ^3H tracers. Observed and predicted potentials with the model showed good agreement. Scanlon (1992) concluded from simulation results that thermal vapor fluxes were downward-directed during the day and upward at night during both winter and summer. Net vapor flux was also downward during the day and upward at night.

Bach (1992) conducted isothermal and non-isothermal laboratory experiments to investigate the significance of non-isothermal water flow and to examine theoretical and numerical descriptions of the transport processes. He concluded from sensitivity analysis that, with adjustment in C_b (temperature coefficient of the matric potential), PDT provided an adequate description of the non-isothermal transport processes.

Many other applications of PDT to non-isothermal water movement have been observed to describe and simulate transport processes (Benjamin, 1989; Chung and Horton, 1987; de Silans et al., 1989; Mahrer et al., 1984; Milly, 1984; Nassar and Horton, 1992; Noborio, 1995; Sophocleous, 1979; and Yakirevich et al., 1997). Cassel et al. (1969) concluded that PDT showed acceptable agreement with observed soil water movement.

In order to account for soil inhomogeneity and hysteresis of the moisture retention process, Milly and Eagleson (1980) modified the PDT by using soil matric pressure-head gradients instead of soil moisture gradients. These authors also included effects of the heat of wetting on transport processes. A finite-element one-dimensional formulation of the governing equations showed that the model performed well in simulating highly coupled, hysteresis-affected, or very nonlinear problems. Later, Milly (1984) used this modified form to study soil-water evaporation from silt loam and sandy soils and reported that soil water evaporation was generally more sensitive to isothermal than to thermal vapor diffusion.

Published evidence thus shows that the mechanistic PDT appears to be accurate for coupled heat and water transfer in soils. This mechanistic approach to formulate expressions for the fluxes of water and heat is based upon concepts derived from fluid mechanics, mass diffusion and heat conduction.

Solute Transport during Coupled Heat and Water Flow

Simultaneous flow of solutes and water occur in most soil-water systems under field conditions. Salt concentration gradients may also be a major contributor to water movement in soils located in arid climates. Salt concentration gradients often occur within the uppermost soil profile, where evaporation selectively removes water at the soil surface and result in an accumulation of salt. Kemper and Rollins (1966) reported that, for experiments involving Wyoming Bentonite clay, soil moisture suction heads needed to be greater than 50 m of water before the osmotic potential gradient would cause significant soil water movement. Low (1965) observed that, when the solute was completely restricted by the porous medium, osmotic potential differences were as effective as pressure potential differences in causing water to move through clay under isothermal conditions. In studying water flow through a porous ceramic filter, Jackson (1967) reported that soil water flow could deviate from Darcy-type flow due to the presence of salt. In laboratory studies on clay loam and sandy loam soils, Qayyum and Kemper (1962) reported that diffusive movement of water occurred to the salt-bearing surface at soil moisture contents less than one-half of field capacity, and that viscous flow occurred at soil moisture contents higher than one-half of field capacity in closed soil columns.

Kemper and Maasland (1964) found that salt sieving increased with decreasing pore size of the soil and decreasing valence of the saturating cation. Letey and Kemper (1969) introduced a theory to describe simultaneous movement of

water and solute in soil. The theory included an equation to describe water flow and another equation to describe solute transfer. The equation for solute transfer implied that the movement of solute is controlled by Fickian diffusion and salt sieving.

In summary, temperature and osmotic gradients can induce water flow within soils. As water moves, heat and solute are transported, thus altering the driving forces (gradients). Interactions among thermal, soil moisture, and osmotic effects exist, and they differ for the liquid and vapor phases (Nassar and Horton, 1989b).

Nassar and Horton (1989b) extended the PDT, describing water transport under the combined effects of matric and osmotic pressure head gradients in unsaturated, non-isothermal, saline soil. Their theory was based upon the concept of viscous flow of liquid water under the influence of capillary, adsorptive, and osmotic forces and on a concept of vapor movement by diffusion. They presented two equations for vapor and liquid transfer as

$$\frac{q_v}{\rho_L} = -D_{TV} \nabla T - D_{\theta V} \nabla \theta_L + D_{CV} \nabla C \quad [2.9]$$

and

$$\frac{q_L}{\rho_L} = -D_{TL} \nabla T - D_{\theta L} \nabla \theta_L + D_{CL} \nabla C - Kk \quad [2.10]$$

where q_v is water vapor flux, D_{TV} is thermal vapor diffusivity, D_{TL} is thermal liquid diffusivity, $D_{\theta V}$ is isothermal vapor diffusivity, $D_{\theta L}$ is isothermal liquid diffusivity, D_{CV} is vapor diffusivity due to solute concentration, D_{CL} is liquid diffusivity due to solute concentration, and c is solute concentration.

Equations [2.9] and [2.10] were summed in order to describe the total water flux as

$$\frac{q_w}{\rho_L} = -D_T^w \nabla T - D_\theta^w \nabla \theta + D_C \nabla C - Kk \quad [2.11]$$

where $q_w = q_L + q_v$ is total water flux, $D_T^w = D_{TV} + D_{TL}$ is thermal moisture diffusivity, $D_\theta^w = D_{\theta V} + D_{\theta L}$ is isothermal moisture diffusivity, $D_C = D_{CV} + D_{CL}$ is moisture diffusivity due to solute concentration, and $\theta = \theta_v + \theta_L$ is total volumetric water content, where θ_v is water vapor content (expressed as equivalent liquid volume).

Applying the principle of heat conservation, an equation for transient heat transfer combining the effects of matric pressure head, osmotic pressure head, and temperature was formulated. For developing the solute-transport equation (non-interacting solute transfer), Nassar and Horton (1989b) included the mechanisms of molecular diffusion, hydrodynamic dispersion, thermal diffusion, mass flow of water (convection), and salt sieving.

Nassar and Horton (1989a, 1989b) conducted experimental and numerical studies of coupled heat and mass transport in closed soil columns with three different soil textures. Experimental observations for unsaturated conditions showed water accumulation within the low-temperature region of the columns, but solute accumulation within the high-temperature region. Predicted and observed results were in good agreement when initial soil-water contents were relatively large and initial solute concentrations were low. However, for small initial soil-water contents, the model underestimated soil-water contents close to the low-temperature boundaries and overestimated than near the high-temperature boundaries. For high

initial solute concentration, the theory underestimated liquid transfer toward the hot boundary temperatures. Unfortunately, the theory proposed by Nassar and Horton (1989b, 1992) is restricted to homogenous soils and cannot be used in its presented form for heterogenous soils. The water flow equation is written in terms of water content and thus does not allow simulation for multilayered soil. Furthermore, the model is primarily restricted to soil conditions of water unsaturation.

Temperature Effects on Solute Transport

The rates of most chemical reactions increase with temperature, changing their equilibrium constants (Clark, 1996). Clark further states as a rule of thumb, that the reaction rate doubles for each increase in temperature of 10 °C. Generally, the understanding of a chemical reaction is not considered complete until the sensitivity of the reaction to temperature is understood. Many chemical studies thus include experiments at different temperatures.

Daniels and Alberty (1961) and Clark (1996) discussed the influence of temperature on reaction rate in the following way. Kinetic data over a range of temperatures can usually be represented by use of an empirical equation first proposed by Arrhenius

$$k_r = F_f e^{-\frac{E_a}{R_u T}} \quad [2.12]$$

where k_r is reaction rate, F_f is a frequency factor, E_a is activation energy, and R_u is the universal gas constant. Set in logarithmic form,

$$\log k_r = -\frac{E_a}{2.303 R_u T} + \log F_f \quad [2.13]$$

According to Eq. [2.13], a straight line should be obtained when logarithm of the rate coefficient (k_r) is plotted against the reciprocal of the absolute temperature (T). The E_a can then be estimated as $-2.303 R_u$ x the slope of the line. The activation energy may be envisioned as an energy barrier that must be surmounted for the reaction to proceed. An increase in E_a indicates a slowing down of the reaction (and vice-versa). The E_a thus can be determined by measuring the reaction rate at different temperatures.

The influence of temperature on chemical processes has also been described by Stumm and Morgan (1981) through use of the Arrhenius equation. Šimůnek and Suarez (1993) described a function with some modification to account for relative change in rate coefficients with temperature as

$$f(T) = e^{\left[\frac{E_a(T - T_r)}{R_u T T_r} \right]} \quad [2.14]$$

where T_r is the reference absolute temperature and $f(T) = 1$ at $T = T_r$.

Cohen and Ryan (1989) and Cohen et al. (1988) used the relationship given by Bird et al. (1960) to describe the temperature dependence of diffusion coefficients. The chemical molecular diffusion in air as a function of temperature was estimated as

$$D_a(T) = D_a(T_r) \left[\frac{T}{T_r} \right]^{1.823} \quad [2.15]$$

where $D_a(T_r)$ is the chemical molecular diffusion coefficient in air at the reference temperature. Temperature variation of the chemical molecular diffusivity in liquid

water was estimated as

$$D_w(T) = D_w(T_r) \left[\frac{\mu_w(T_r)}{\mu_w(T)} \right] \quad [2.16]$$

where μ_w is the viscosity of liquid water.

Summary

The PDT was proposed 40 years ago to mathematically describe coupled water and heat flows in soil. It has been well-verified and applied by a number of researchers to date. The theory was extended by Milly and Eagleson (1980) to make it applicable to heterogenous media, by replacing the water content-based formulation with a matric potential-based formulation of flow equations. This advancement was a big step, as it made the theory suitable for the solution of field problems. Nassar and Horton (1989a, 1992) extended the theory to include salt effects on water flow and provided insight into additional coupling. But, this theory cannot be used to solve field problems, because Nassar and Horton used the original PDT (water content-based) formulation for modification.

Relatively little evidence exists that the potential of PDT and its modification by Milly and Eagleson (1980) has been fully exploited to use the improved estimates of water content/flow, and temperature information. Several researchers (Barnes and Allison, 1984; Barnes et al., 1989; Nassar and Horton, 1989a, 1989b; Noborio, 1995; Scanlon, 1992; and Yakirevich et al., 1997), however, utilized PDT by making use of improved estimates of water content/flow when exploring solute transport.

These investigations, however, did not attempt to use the improved estimates of temperature by inclusion of its effect on solute transport.

A need, therefore, exists to exploit the full potential of PDT in solving field problems where temperature could be highly transitional both in space and time. Furthermore, where chemical (especially volatile-compound) transport is also of concern, a need exists to use both the improved estimates of water content/flow and of temperature provided by PDT. The work reported here utilizes PDT in totality to develop a 2-D numerical model for solving problems involving the fate and transport of volatile chemicals that may exist in all three phases (*viz.* liquid, solid, and gas) of soils. Details for the developed model are presented in Chapter-3.

CHAPTER 3 MATHEMATICAL MODEL

The model developed here considers the soil to be a heterogenous isotropic medium composed of solid, liquid, and gaseous phases. The latter is assumed to be a non-interacting binary mixture of water vapor, dry air, and volatile chemicals.

Other general assumptions in the model include

1. The solid matrix is undeformable and immobile.
2. The liquid water is incompressible.
3. The density and viscosity of liquid water are not influenced by dissolved constituents.
4. Hysteresis in the relationship between capillary-pressure and hydraulic conductivity is neglected.
5. Liquid water and water vapor are in local thermodynamic equilibrium.
6. Water vapor and other gases behave as perfect gases and advective transport of these components is neglected.
7. Local thermal equilibrium exists among all phases.
8. Radiative heat transfer is negligible.
9. Thermal and matric potential gradients interact to provide heat and water flow in the porous medium.

More specific assumptions are stated as required. Additional details concerning the equations governing flow and transport are presented in the appendices.

Liquid and Vapor Water Flow in Soil

The original water content-based formulation of PDT was modified by Milly and Eagleson (1980) to provide

$$\left[\left(1 - \frac{\rho_v}{\rho_L} \right) \frac{\partial \theta_L}{\partial h} + \frac{\theta_a}{\rho_L} \frac{\partial \rho_v}{\partial h} \right] \frac{\partial h}{\partial t} = \nabla \left[(K + D_{hv}) \nabla h + D_{Tv} \nabla T + K k \right] - \left[\left(1 - \frac{\rho_v}{\rho_L} \right) \frac{\partial \theta_L}{\partial T} + \frac{\theta_a}{\rho_L} \frac{\partial \rho_v}{\partial T} \right] \frac{\partial T}{\partial t} \quad (3.1)$$

where ρ_v is vapor water density, θ_a is the volumetric air content, and D_{hv} is isothermal vapor diffusivity. Equation [3.1] describes both liquid water and vapor water flow in response to gradients of matric potential and thermal energy.

Heat Flow in Soil

Coupled heat flow in the soil in response to gradients of temperature and pressure-head has been described by (de Vries, 1958; Milly and Eagleson, 1980)

$$\left(C + H_1 \frac{\partial \rho_v}{\partial T} + H_2 \frac{\partial \theta_L}{\partial T} \right) \frac{\partial T}{\partial t} = \nabla \left[\lambda \nabla T + \rho_L L D_{hv} \nabla h - C_L (T - T_o) q_w \right] - \left(H_1 \frac{\partial \rho_v}{\partial h} + H_2 \frac{\partial \theta_L}{\partial h} \right) \frac{\partial h}{\partial t} \quad (3.2)$$

and

$$\begin{aligned} C &= C_d + C_L \rho_L \theta_L + C_v \rho_v \theta_v, \quad H_1 = [L_o + C_v(T - T_o)] \theta_v, \\ H_2 &= (C_L \rho_L - C_v \rho_v)(T - T_o) - \rho_v L_o \end{aligned} \quad [3.3]$$

where C_d is volumetric dry heat capacity of the total medium; C_L and C_v are specific heat of liquid water and vapor water, respectively; and the subscript $_o$ implies the magnitude at a designated reference level.

Transport of Multiple Species of Solutes in Soil

Following the approach of Šimůnek et al. (1992) and Šimůnek and van Genuchten (1994), in which solutes can exist in all three phases (liquid, solid, and gaseous) with non-equilibrium transport, the governing transport equations can be stated as

$$\begin{aligned} \frac{\partial \theta_L c_i}{\partial t} + \frac{\partial \rho s_i}{\partial t} + \frac{\partial \theta_a g_i}{\partial t} &= \nabla(\theta_L D_i^L \nabla c_i) + \nabla(\theta_a D_i^a \nabla g_i) - \nabla(q_L c_i) - \\ &(\mu_{L,i} + \mu_{L,i}^*) \theta_L c_i - (\mu_{s,i} + \mu_{s,i}^*) \rho s_i - (\mu_{g,i} + \mu_{g,i}^*) \theta_a g_i + \gamma_{L,i} \theta_L + \gamma_{s,i} \rho + \gamma_{g,i} \theta_a \end{aligned} \quad [3.4]$$

$$\begin{aligned} \frac{\partial \theta_L c_i}{\partial t} + \frac{\partial \rho s_i}{\partial t} + \frac{\partial \theta_a g_i}{\partial t} &= \nabla(\theta_L D_i^L \nabla c_i) + \nabla(\theta_a D_i^a \nabla g_i) - \nabla(q_L c_i) - (\mu_{L,i} + \mu_{L,i}^*) \theta_L c_i - \\ &(\mu_{s,i} + \mu_{s,i}^*) \rho s_i - (\mu_{g,i} + \mu_{g,i}^*) \theta_a g_i + \mu_{L,i-1}^* \theta_L c_{i-1} + \mu_{s,i-1}^* \rho s_{i-1} + \\ &\mu_{g,i-1}^* \theta_a g_{i-1} + \gamma_{L,i} \theta_L + \gamma_{s,i} \rho + \gamma_{g,i} \theta_a; \quad i = 2, \dots, n_s \text{ (species)} \end{aligned} \quad [3.5]$$

where s represents adsorbed concentrations; g is the gas concentration; μ_L , μ_s , and μ_g are the first-order rate constants for solutes in the liquid, solid, and gas phases, respectively; γ_L , γ_s , and γ_g are zero-order rate constants for the liquid, solid, and gas

phases, respectively; ρ is the soil bulk density; D^L is the dispersion coefficient for the liquid phase; and D^g is the diffusion coefficient for the gas phase. The subscripts L , s , and g correspond with the liquid, solid, and gas phases, respectively; the subscript i represents the i^{th} chain number; n_i is the number of solutes involved in a chain reaction; and μ_L^* , μ_s^* , and μ_g^* are first-order rate constants for solutes in the liquid, solid, and gas phases, respectively, providing the connection between individual chain species. The nine zero- and first-order rate constants in Eqs. [3.4] and [3.5] can be used to represent a variety of reactions or transformations including biodegradation, volatilization, precipitation, etc., and the effect of temperature on these coefficients is included through use of Eq. [2.14]. Equation [3.4] alone is sufficient for a single solute that does not undergo transformation to related chemical species in a 'chain' reaction. Both Eqs. [3.4] and [3.5] are required when the primary solute undergoes transformations to other species or when multiple unrelated solutes are present in the soil system.

In order to solve the solute-transport equation, a knowledge of liquid water content, air content, and volumetric flux is required. Solution of the coupled water and heat flow equations (Eqs. [3.1] and [3.2]) provides this information.

Energy Balance at the Soil/Atmosphere Interface

Interception of solar radiation, interaction with the overlying atmosphere, and loss of water through evaporation is described via an energy-balance equation for the soil surface

$$(1 - \rho_s)R_g + R_{LA} - R_{LS} = H_s + LE + G \quad [3.6]$$

where ρ_s is soil surface albedo, R_g is measured global radiation (taken as positive downward), R_{LA} is longwave sky irradiance (positive downward), R_{LS} is longwave radiation from the soil surface (positive upward), H_s is sensible air heat flux (positive upward), LE is latent heat of the evaporative flux (positive upward), and G is soil heat flux (positive downward).

The solution of Eq. [3.6] provides information for soil surface temperature and atmospheric evaporative demand (excluding transpiration) required to specify the top boundary condition of the solution domain. This equation is strictly valid only for a soil surface without a mulch cover.

The presence of a mulch cover alters interaction of the soil surface with the overlying atmosphere (as discussed earlier). An approach based on the work of Hares and Novak (1992) and Ham and Kluitenberg (1994) was adapted for conditions where the soil surface is covered with a plastic mulch such as commonly used in soil-bed systems for vegetable production in Florida. The energy balance for a plastic mulch can be defined as

$$Rn_m + H_s - C_c = 0 \quad [3.7]$$

where Rn_m is net radiation of the mulch surface and C_c represents conduction or free convection between the mulch and free soil surface. Energy balance for the soil surface beneath the thin plastic mulch can be defined as

$$Rn_s + C_c + G = 0 \quad [3.8]$$

where Rn_s is net radiation of the soil surface. These energy-balance equations

neglect heat storage within the thin plastic mulch, and the potential impacts of cuts and planting holes in the mulch is not considered. Thickness for such plastic mulches typically ranges from 0.02544 to 0.15264 mm.

Net radiation of the plastic mulch is given by (Ham and Kluitenberg, 1994)

$$Rn_m = \alpha_m R_g \left(1 + \rho^* \tau_{m,ir} \rho_s \right) \epsilon_m \epsilon_{sky} \sigma T_{sky}^4 \left(1 + \rho_{ir}^* \tau_{m,ir} (1 - \epsilon_s) \right) + \rho_{ir}^* \epsilon_m \epsilon_s \sigma T_s^4 + \rho_{ir}^* \left(\epsilon_m^2 \sigma T_m^4 \right) (1 - \epsilon_s) - 2 \sigma \epsilon_m T_m^4 \quad [3.9]$$

where T_{sky} , T_s and T_m are the temperatures of the sky (usually taken to be atmospheric temperature at 1 m above the ground surface), soil surface, and mulch, respectively; ϵ_{sky} , ϵ_s and ϵ_m are the emissivities of the sky, soil surface, and mulch, respectively; α_m is the shortwave absorbance of the mulch; $\tau_{m,ir}$ is the transmittance of the mulch in the longwave spectrum; and σ is the Stefan-Boltzmann constant. The variables ρ^* and ρ_{ir}^* represent the internal reflection functions for shortwave and longwave radiation, respectively. These functions account for multiple reflections of radiation between the mulch and soil surface, and are defined by Van de Hulst (1980) as

$$\rho^* = \left(1 - \rho_s \rho_m \right)^{-1} = 1 + \rho_s \rho_m + \rho_s^2 \rho_m^2 + \dots \quad [3.10]$$

$$\rho_{ir}^* = \left[1 - \rho_{m,ir} \left(1 - \epsilon_s \right) \right]^{-1} = 1 - \rho_{m,ir} \left(1 - \epsilon_s \right) + \rho_{m,ir}^2 \left(1 - \epsilon_s \right)^2 + \dots \quad [3.11]$$

where ρ_m is the shortwave reflectance of the lower mulch surface and $\rho_{m,ir}$ is the reflectance of the mulch in the infrared spectrum. The infinite series expansion shows here that the reflection functions account for the initial radiation in the layer and then amplify the effects via repeated reflections between the soil surface and the underside of the mulch.

Sensible heat transfer between the plastic mulch and the atmosphere is a function of the aerodynamic properties of the surface and the temperature gradient between the plastic and the boundary layer, as defined by

$$H_s = \frac{C_a (T_a - T_m)}{r_{a,h}} \quad [3.12]$$

where T_a is air temperature and $r_{a,h}$ is the aerodynamic resistance to heat transfer.

Heat transfer between the mulch and the underlying soil surface is estimated using the equation

$$C_c = \frac{T_m - T_s}{r_c} \quad [3.13]$$

where r_c represents a thermal contact resistance at the mulch-soil interface and mainly depends on the air-gap thickness between the soil surface and the mulch.

This determines whether the heat transfer is conductive or convective. Ham and Kluitenberg (1994) described the estimation procedure and presented representative values of r_c for different air gaps between the soil surface and the mulch for various plastic mulches.

Net radiation of the soil is dependent upon the global and longwave sky irradiance transmitted through the mulch, radiation emitted from the mulch and soil, and multiple scattering of radiation between the soil and mulch as given by (Ham and Kluitenberg, 1994)

$$n_s = (1 - \rho_s) \tau_m \rho^* R_s + \rho_{i,s} e_s (\tau_{m,ir} e_{s,sky} \sigma T_{sky}^4 + e_s \sigma T_m^4 + \rho_{m,ir} e_s \sigma T_s^4) - e_s \sigma T \quad [3.14]$$

Given the subsurface temperature near the surface at depth z , ground heat flux can be approximated at the future time step $p + 1$ (p being the current time) as (Horton

and Chung, 1991)

$$G = -\lambda^* \left[\frac{T_s^{p+1} - T_1^{p+1}}{\Delta z} \right] + C_s \left[\frac{(T_s^{p+1} - T_s^p) \Delta z}{2 \Delta t} \right] \quad [3.15]$$

where T_1 is soil temperature at the first node below the soil surface and $(T_s^{p+1} - T_s^p)/\Delta t$ is the rate of change in temperature with time at the surface between time steps p and $p+1$.

Initial and Boundary Conditions

Equations [3.1]-[3.5] require supplementation with appropriate initial (IC) and boundary (BC) conditions to describe a specific simulation scenario. The IC in general (at $t = 0$) are specified as $h(x, z, 0) = h_i(x, z)$, $T(x, z, 0) = T_i(x, z)$, and $c(x, z, 0) = c_i(x, z)$ respectively for Eqs. [3.1], [3.2], and [3.4], [3.5]. Here h_i , T_i , and c_i are known values of the state variables at the beginning of the simulation; and x and z represent the horizontal and vertical locations, respectively.

Boundary conditions may be defined as a specified value of matric potential/or temperature and/or solute concentration (Dirichlet-type BC), a specified water/or temperature and/or solute flux (Neumann-type BC), or a combination of the two (Cauchy-type BC). The top boundary (i.e., the soil surface) in the system under consideration is a special case of the Neumann-type BC for water (evaporative flux), dependent upon the overlying atmosphere. In general, the boundary conditions depend on the specific system being investigated.

Input Parameter Requirements

Soil input data include sand, silt, clay, and organic matter contents; bulk density; saturated hydraulic conductivity; and soil hydraulic parameters which describe the water retention curve (Eqs. [3.7]-[3.8]). For the soil/atmospheric boundary conditions, weather data such as average air temperature, air temperature daily amplitude, average dew-point temperature, dew-point temperature daily amplitude, wind speed, surface roughness length, and day-length are required inputs as well.

Soil hydraulic properties are estimated following van Genuchten (1980) as

$$\theta_L = \theta_r + \frac{\theta_s - \theta_r}{[1 + (\alpha|h|)^{\eta}]^{\frac{1}{\eta}}}; \quad \eta = 1 - \frac{1}{\eta} \quad [3.16]$$

$$K(\theta_L) = K_{sat} \frac{(1 - (\alpha|h|)^{\eta})^{-1} [1 + (\alpha|h|)^{\eta}]^{\frac{1}{\eta}}}{[1 + (\alpha|h|)^{\eta}]^{\eta/2}}$$

and,

$$\frac{\partial \theta_L}{\partial h} = -\frac{\alpha \eta (\theta_s - \theta_r)}{1 - \eta} \theta^{1/\eta} (1 - \theta^{1/\eta})^{\eta}; \quad \theta = \frac{\theta_L - \theta_r}{\theta_s - \theta_r} \quad [3.17]$$

where θ is residual water content, θ_s is saturated volumetric water content, $|h|$ is the absolute value of the matric potential, and K_{sat} is the saturated hydraulic conductivity. The parameters α , η , and η are empirical constants used to fit the moisture retention curve. The temperature dependence of matric potential (h) was described as (Philip and de Vries, 1957)

$$\frac{dh}{dT} = \frac{h}{\sigma_s} \frac{d\sigma_s}{dT} \Rightarrow = C_h h \quad [3.18]$$

and hydraulic conductivity ($K(h)$) as (Constantz, 1982)

$$K(h) = \frac{\mu_w^{ref}}{\mu_w^T} \frac{\rho_{L,T}}{\rho_{L,ref}} K_{ref}(h) \quad [3.19]$$

where σ_s is surface tension of water; C_h ($= -0.0017 \text{ } ^\circ\text{K}^{-1}$ by Milly and Eagleson, 1980) is temperature coefficient of matric potential; μ_w^{ref} and μ_w^T are dynamic viscosities at the reference temperature and soil temperature, respectively; $\rho_{L,ref}$ and $\rho_{L,T}$ are the densities of water at reference temperature and soil temperature, respectively, and $K_{ref}(h)$ is hydraulic conductivity at the reference temperature.

The dependence of θ_L upon temperature can be determined as (Milly and Eagleson, 1980)

$$\frac{\partial \theta_L}{\partial T} = -C_h \frac{\partial \theta_L}{\partial h} h \exp[-C_h \cdot (T - T_0)] \quad [3.20]$$

Water vapor density is given by Marshall and Holmes (1979) as

$$\rho_v = g_s \rho_L \phi \left[\frac{M_w}{R_u T} \right] \quad [3.21]$$

where ϕ is water vapor pressure and M_w is the molecular weight of water. Water vapor pressure is related to soil water matric potential by the relation (Marshall and Holmes, 1979)

$$\phi = \phi_s \exp \left[\frac{g_s h M_w}{R_u T} \right] \quad [3.22]$$

where ϕ_s is the saturated vapor pressure, given by Noggle (1985) as

$$\phi_s = 237.7 \exp \left[-\frac{M_w L}{R_u} \left(\frac{1}{T} - \frac{1}{T_s} \right) \right] \quad [3.23]$$

Differentiating Eq. [3.21] with respect to h yields

$$\frac{\partial \rho_v}{\partial h} = \left(\phi_s g_s \frac{M_w}{R_u T} \right) \left(g_s \rho_L \frac{M_w}{R_u T} \right) \exp \left[g_s h \frac{M_w}{R_u T} \right] \quad [3.24]$$

and with respect to T gives

$$\frac{\partial \rho_v}{\partial T} = D1 * D2 - \left(\phi g_a \rho_L \frac{M_w}{R_u T^2} \right) \quad [3.25]$$

where

$$D1 = \left(g_a \rho_L \frac{M_w}{R_u T} \right), \quad D2 = \left[\frac{\partial \phi_g}{\partial T} D3 + \phi_g g_a h \frac{M_w}{R_u T^2} D3 \right]; \quad D3 = \exp \left(g_a h \frac{M_w}{R_u T} \right)$$

Variation in saturated vapor pressure with temperature is given by

$$\frac{\partial \phi_g}{\partial T} = \left(- \frac{237.7 M_w L}{R_u T^2} \right) \exp \left[- \frac{M_w L}{R_u} \left(\frac{1}{T} - \frac{1}{T_r} \right) \right] \quad [3.26]$$

The vapor diffusion coefficients are determined as (Milly and Eagleson, 1980)

$$D_{hv} = \left(\frac{D_a \tau_a \theta_a}{\rho_L} \right) \frac{\partial \rho_v}{\partial h}, \quad D_{zv} = \left(\frac{D_a f \xi}{\rho_L} \right) \frac{\partial \rho_v}{\partial T} \quad [3.27]$$

with

$$\tau_a = \theta_a^{2/3}, \quad f = \theta_T \text{ for } \theta_L < \theta_k, \quad f = \theta_a + \left(\frac{\theta_a}{\theta_T - \theta_k} \right) \theta_T \text{ for } \theta_L > \theta_k \quad [3.28]$$

where D_a is a molecular diffusion coefficient of water vapor in air, τ_a is an air-phase tortuosity factor, f is vapor path correction for liquid islands, θ_T is total porosity, θ_k is the water content at which liquid continuity breaks during desaturation, and ξ ($= 1.7$) is a temperature-gradient enhancement factor for vapor.

Specific heat is estimated from the methods of deVries (1963) as

$$C = X_s c_s + X_{st} c_{st} + X_c c_c + X_{om} c_{om} + C_L \theta_L + C_v \theta_v \quad [3.29]$$

where X_s , X_{st} , X_c , and X_{om} are the volume fractions of sand, silt, clay, and organic matter, respectively, and c_s , c_{st} , c_c , c_{om} , C_v are the volumetric heat capacities of sand, silt, clay, organic matter, and water vapor, respectively. The specific heat of water vapor is given by Noggle (1985) as

$$C_v = \frac{30.54 + 0.01029 T}{0.0180015} \quad [3.30]$$

The apparent thermal conductivity can be estimated as a harmonic mean of the soil constituents (de Vries, 1963)

$$\lambda = 1.25 \left(\frac{\sum_{i=s, st, c, o, \theta} k_i^* X_i \lambda_i}{\sum_{i=s, st, c, o, \theta} k_i^* X_i} \right); \quad k_i^* = \frac{1}{3} \sum_{j=1, \dots, 4} \left[1 + \left(\frac{\lambda_i}{\lambda_a} - 1 \right) g_j \right]^{-1} \quad [3.31]$$

where λ_i represents the respective thermal conductivities of the soil constituents, g_j are shape factors for the soil constituents, and λ_a is the thermal conductivity of air.

The incoming global radiation for the soil/atmospheric boundary condition must be partitioned into a flux-density distribution for daylight hours. Chung and Horton (1987) suggested a sine wave distribution

$$R_g = \frac{\pi}{2} \frac{R_{dg}}{DL} \sin \left[\left(t - SN + \frac{DL}{2} \right) \frac{\pi}{DL} \right] \quad [3.32]$$

where R_{dg} is daily global radiation, DL is day length, SN is solar noon, and t is the time of day. The air and dew-point temperature distributions can also be expressed as sine functions

$$T_a = \bar{T}_a + A_a \sin \left(\frac{2\pi t_m}{86400} + \pi \right), \quad T_d = \bar{T}_d + A_d \sin \left(\frac{2\pi t_m}{86400} + \pi \right) \quad [3.33]$$

where the bar indicates average temperature; T_a and T_d are air and dew point temperatures, respectively; A_a and A_d are air and dew point temperature amplitudes, respectively; t_m is the time from midnight; and the maximum temperature is assumed to occur at solar noon.

The soil surface emissivity, ϵ_s , and albedo, ρ_s , are described by the method of van Bavel and Hillel (1975, 1976) as

$$\begin{aligned} \epsilon_s &= 0.9 + 0.18\theta_L, \quad \rho_s = 0.25 \text{ for } \theta_L \leq 0.10, \\ \rho_s &= 0.35 - \theta_L \text{ for } 0.10 < \theta_L < 0.25, \quad \rho_s = 0.10 \text{ for } \theta_L \geq 0.25 \end{aligned} \quad [3.34]$$

CHAPTER 4 MODEL VERIFICATION AND VALIDATION

Numerical solutions to differential equations require testing to ensure that numerical instabilities have not been introduced into the solution due to round-off or truncation errors and that the solution converges on a reasonable estimate of the exact solution. A numerical scheme is stable if, with increasing time, the difference between the numerical solution and the exact solution tends uniformly to zero at all nodes (Benjamin, 1989). Convergence is satisfied if the numerical solution approaches the exact solution as spatial- and temporal-step sizes approach zero. Proper testing also ensures the correctness of mathematical representation for the physical system being modeled and the validity of any assumptions made in the model.

Testing of a model may be achieved in multiple ways. One such way is by comparing the model results with analytical (exact) solutions for greatly simplified conditions, and another is by comparing the model results with observed data from carefully designed experiments. Unfortunately, no analytical solution to the governing equations for coupled heat and water transport is known to exist. Hence, portions of the model were tested with observed data and analytical solutions for simplified conditions, where available.

Isothermal Water Flow

Model results were compared with data for transient one-dimensional, isothermal water flow through sand as reported by Haverkamp et al. (1977), with vapor flow ignored. Haverkamp et al. (1977) reported K_{sat} , θ_r , θ_s , and soil bulk density to be $34.0 \text{ (cm h}^{-1}\text{)}$, 0.287 , 0.075 , and 1.66 g cm^{-3} , respectively. An analytical model by van Genuchten (1980) was fitted to the soil water content versus matric potential data in order to provide optimum values for the hydraulic parameters α and η . A uniform initial water content of 0.10 was specified and water content at the 0.70 m depth was kept constant at this value. A constant water influx of 13.69 cm h^{-1} was specified at the top boundary. Results of the numerical simulation, and experimental data for different times, are shown in Fig. 4-1. The numerical solution was stable and converged upon a close approximation of the experimental values. The model accurately described the movement of the water front in the column of sand.

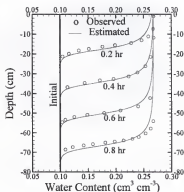


Figure 4-1. Observed and computed distributions of water content in a sand column during constant flux infiltration.

Uncoupled Heat Flow

Next, the numerical solution for heat flow was verified with field-measured temperature data (Horton and Chung, 1991) for a Nicollet clay loam soil profile with a bare surface located near Ames, IA. The effect of water flow was ignored. Representative values of heat capacity and thermal conductivity for loam soil were used. Initial conditions as specified by Horton and Chung (1991) were used in the model and temperature at the 60-cm depth was held constant at 20 °C. Temperatures observed for the soil surface were used in the model to provide the surface boundary condition. One-dimensional numerical results (Fig. 4-2) for the 5- and 15-cm soil depths provided satisfactory representation of temporal temperature profiles for each depth.

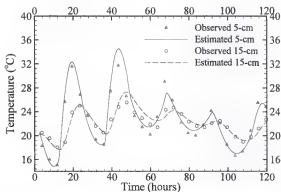


Figure 4-2. Observed and computed temperatures for two depths in a field soil.

Coupled Water and Heat Flow

In order to test the capacity of the numerical solution to predict coupled heat and water transfer, simulation using the experimental data of Nassar and Horton (1989a) was performed. Nassar and Horton (1989a) conducted laboratory experiments of heat and mass transfer with controlled temperature gradients in sealed columns (14 cm in length) of silt loam soil with initially uniform water content (0.117). The column ends were subjected to different temperatures (19.03 °C and 9.36 °C) in order to create a temperature gradient. The experiment was run for a period of 31 days. The observed mean value of saturated hydraulic conductivity for the soil was 0.964 cm hr^{-1} , with a corresponding soil water retention curve having been determined by Nassar and Horton (1989b).

The van Genuchten (1980) model was fitted to the soil water retention curve in order to obtain optimum hydraulic parameters for the soil ($\alpha = 0.03137 \text{ cm}^{-1}$, $n = 1.33308$, $\theta_s = 0.65$, $\theta_r = 0.05$) for silt loam soil. A numerical simulation was carried out for 31 days using zero flux boundaries at both ends for water flow and Dirichlet boundaries for heat flow. Observed and predicted water contents are given in Fig. 4-3. Good agreement was noted everywhere except in the vicinity of the cold end of the soil column with elevated water content. The predicted total water content in the column was slightly higher than the observed value. Since the computed mass balance error was less than 1.0 % in the numerical simulation, the possibility exists for a small systematic error in the measurement of either initial or final water contents during the actual experiment.

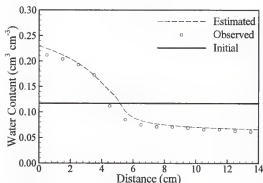


Figure 4-3. Observed and computed water content after 31 days under the influence of both matric head and thermal gradients.

Isothermal 1-D Solute Transport during Steady Water Flow

The model component for solute transport was tested against data reported by van Genuchten (1981) for the movement of a pulse of boron (H_3BO_3) during steady water flow through a column of Glendale clay loam. The solute-transport parameters (Šimůnek and van Genuchten, 1994) used were: $D^* = 2.042 \text{ cm}^2 \text{ hr}^{-1}$, $\theta_s = 0.445$, $\rho = 1.222 \text{ g cm}^{-3}$, $k_d = 1.14 \text{ cm}^3 \text{ g}^{-1}$, $\beta = 1.0$, $\eta = 0.0$, $f_r = 0.47$, and $\omega = 1.33 \times 10^{-2}$. The initial concentration was zero and a pulse of aqueous solution containing a boron concentration of 20.0 mmol L^{-1} was applied at a constant flux of 713.0 cm hr^{-1} for a duration of 121.44 hr. Assuming two-site chemical non-equilibrium sorption, a simulation was run for 20 pore volumes of effluent. A comparison of numerical and experimental results (Fig. 4-4) verified that the model described the transport process with satisfactory accuracy.

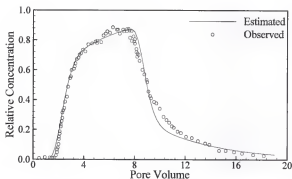


Figure 4-4. Observed and computed break through curves for boron.

Isothermal 2-D Solute Transport during Steady Water Flow

The mathematical accuracy of 2-D numerical simulations for isothermal steady water flow, was verified employing a simple analytical solution. Solute (non-volatile) transport in a homogenous, isotropic porous medium during steady-state unidirectional groundwater flow can be written as

$$R \frac{\partial c}{\partial t} = D_T \frac{\partial^2 c}{\partial x^2} + D_L \frac{\partial^2 c}{\partial z^2} - v_z \frac{\partial c}{\partial z} - \mu_L R c \quad [4.1]$$

where D_T and D_L are transverse and longitudinal dispersion coefficients, respectively, and v_z is average pore-water velocity in the downward vertical direction. The initially solute-free medium is subjected to a solute source, C_o , of unit concentration. The source covers a length $2a$ along the inlet boundary at $z = 0$, and is located symmetrically about the coordinate $x = 0$. The transport region of interest is the half-plane ($z < 0; -\infty < x < \infty$). The boundary conditions can be written as

$$c(x, 0, t) = C_0 \quad -a \leq x \leq a; \quad c(x, 0, t) = 0 \quad \text{other values of } x$$

$$\lim_{z \rightarrow \infty} \frac{\partial c}{\partial z} = 0; \quad \lim_{x \rightarrow \pm a} \frac{\partial c}{\partial x} = 0 \quad [4.2]$$

An analytical solution to the above transport problem is given by Leij and Bradford (1994) as

$$c(x, z, t) = \frac{C_0 z}{4(\pi D_L)^{1/2}} \exp\left(\frac{v_z z}{2D_L}\right) \int_0^R \exp\left[-\left(\mu_L R + \frac{v_z^2}{4D_L}\right) \tau_w - \frac{z^2}{4D_L \tau_w}\right] \tau_w^{-3/2} \left[\operatorname{erf}\left(\frac{a-x}{2(D_T \tau_w)^{1/2}}\right) + \operatorname{erf}\left(\frac{a+x}{2(D_T \tau_w)^{1/2}}\right) \right] d\tau_w \quad [4.3]$$

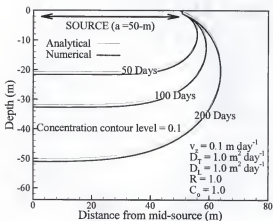


Figure 4-5. Location of solute concentration fronts for three times as estimated numerically and with the analytical solution.

The numerical simulation assumed a source-width of $2a = 100 \text{ m}$. Because of symmetry, computations were carried out only for the half plane where $x \geq 0$.

Figure 4-5 shows the estimated solute concentration fronts (0.1) at selected times

and various values of the parameters as used in the computations. Results predicted by the numerical model were similar to those given by the analytical solution.

Isothermal 1-D Solute Transport with Nitrification Chain during Steady Water Flow

To verify the numerical solution capacity in simulating multiple linked species in a chain, comparison was done with results generated from an analytical solution published by van Genuchten (1985) for 1-D transport of solutes involved in sequential first-order decay reactions. The analytical solution holds for a homogenous, isotropic porous medium with steady-state uni-directional groundwater flow. The solute-transport Eqs. [3.4] and [3.5] for this case reduces to

$$R_1 \frac{\partial c_1}{\partial t} = D^z \frac{\partial^2 c_1}{\partial x^2} - v_x \frac{\partial c_1}{\partial x} - \mu_{L,1} R_1 c_1 \quad [4.4]$$

and

$$R_i \frac{\partial c_i}{\partial t} = D^z \frac{\partial^2 c_i}{\partial x^2} - v_x \frac{\partial c_i}{\partial x} + \mu_{L,i-1} R_{i-1} c_{i-1} - \mu_{L,i} R_i c_i ; \quad i = 2, 3 \quad [4.5]$$

A simulation was performed here that involves a three-species nitrification chain



and follows van Genuchten (1985) and Cho (1971).

A NH_4^+ solution was applied to an initially solute-free medium. The input transport parameters used for the simulation were

$v_x =$	1.00 m h ⁻¹	$R_1 =$	2.0 [-]
$D_L =$	0.18 m ² h ⁻¹	$R_2 =$	1.0 [-]
$\mu_1 =$	0.01 h ⁻¹	$R_3 =$	1.0 [-]
$\mu_2 =$	0.10 h ⁻¹	$c_i =$	0.0 [-]
$\mu_3 =$	0.0 h ⁻¹	$c_{0,i} =$	1.0 [-]

The simulation was conducted for 200 hours. Figure 4-6 shows the concentration profiles for all three solutes at time 200 hr, calculated both numerically and with the analytical solution from the CHAIN code of van Genuchten (1985). The numerical solution duplicated the analytical results almost exactly.

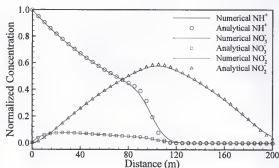


Figure 4-6. Analytically determined and numerically computed concentration profiles at 200 hours.

Isothermal 1-D Solute Transport involving Gas Flow

The capacity of the numerical solution in simulating gas transport was tested against an analytical solution given by Crank (1975). Considering uniform constant water content in a homogenous 1-D soil column, for a chemical species existing in the gaseous phase undergoing hydrolysis (represented as first-order loss, μ_g), the transport equation (Eq. [3.4]) reduces to

$$\frac{\partial g}{\partial t} = D^g \frac{\partial^2 g}{\partial x^2} - \mu_g g \quad (4.7)$$

For an application of finite source (g_0) at one end with zero flux BC and zero gradient BC at the other end, an analytical solution is (Crank, 1975)

$$g(x, t) = e^{-\mu_y t} \cdot \frac{1}{2} g_0 \sum_{n=-\infty}^{\infty} \left[\operatorname{erf} \frac{a+2nL-x}{2\sqrt{D^g t}} + \operatorname{erf} \frac{a-2nL+x}{2\sqrt{D^g t}} \right] \quad (4.8)$$

where a is the initial source length. Prior to deriving the analytical solution the transformation $g = g^* \exp(-\mu_y t)$ was used to simplify Eq. [4.7] to

$$\frac{\partial g^*}{\partial t} = D^g \frac{\partial^2 g^*}{\partial x^2} \quad (4.9)$$

A numerical simulation was conducted for 5 hours with $g_0 = 50$ moles, $a = 1$ cm, $D^g = 47.52 \text{ cm}^2 \text{ hr}^{-1}$, and $\mu_y = 0.055 \text{ hr}^{-1}$. The numerical solution duplicated the results of analytical solution at 1, 3, and 5 hours (Fig. 4-7).

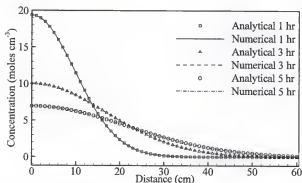


Figure 4-7. Analytically determined and numerically computed concentration profiles at 1, 3, and 5 hours.

Summary

All major components of the numerical model were tested for mathematical accuracy, the adapted numerical scheme, and its ability to represent the physical systems. Both analytical solutions for simplified cases and published data were used to check against simulation results from the numerical model. Excellent agreement was observed in nearly all the cases undertaken for testing of heat-flow, water-flow, and solute-transport model components. The coupled water-heat flow component was also successfully tested. The model could not be tested in its entirety as a single unit, because no analytical solution exists at present for coupled water-heat and solute transport. Also, no published data set was found to test all the features of the model together as a single unit. However, successful testing of individual model components provides confidence in the application of the model simulations conducted in this work.

CHAPTER 5 MODEL APPLICATION

Fate and Transport of Methyl Bromide Fumigation in Soils

Methyl bromide (MBr) is an odorless, colorless toxic gas used in agriculture throughout the world. The United States uses it on more than 100 crops as a soil fumigant, a post-harvest treatment, and as a plant quarantine treatment to control a variety of pests. MBr is also used to fumigate structures such as grain storage warehouses, flour mills, and ships carrying agricultural commodities. California and Florida are the primary users of MBr, followed by Hawaii.

MBr, a broad-spectrum pesticide, is utilized heavily as a very effective agricultural fumigant during vegetable and fruit production in Florida, California, and Hawaii. MBr is very effective for eradicating insects, nematodes, fungi, bacteria, and weeds. In the United States, strawberries (16 % of U.S. total) and tomatoes (24 % of U.S. total) are the crops which use the most MBr, consuming about 6,500 tons annually. Other crops which use this pesticide as a soil fumigant include tobacco, peppers, grapes, and nut crops (USEPA, 1997).

In the United States, the U.S. Clean Air Act requires that the production and importation of any substance defined as an ozone depleter by the Montreal Protocol of 1991 be phased out (USDA ARS, 1997). Therefore, despite its economic value, the

U.S. Environmental Protection Agency (USEPA) plans to phase out the use of MBr by January 1, 2001. Since the Clean Air Act allows no exceptions, all uses of MBr, including plant quarantine, will be banned. In addition to being a toxic gas, MBr is a significant ozone-depleting substance, with recent scientific evidence estimating that bromine from this material is at least 50 times more effective at destroying ozone than chlorine from carbonylfluorocarbons on a per-molecule basis (USEPA, 1997). MBr has an average residence time of 1.5-2.0 years in the atmosphere (Hacherl, 1994). However, there are also other natural sources, primarily forest fires and marine organisms besides anthropogenic sources, which contribute significant quantities of MBr to the atmosphere.

Table 5-1. Earlier estimates for source-contributions of MBr to the atmosphere (Grojesan, 1991; Khalil et al., 1993; Lobert et al., 1990; Manó and Andreae, 1994; Yagi et al., 1993; and Zurer, 1993).

MBr Source	Quantity in atmosphere (in ton y ⁻¹)
Oceanic	30,000 (30 %)
Bio-mass burning	30,000 (30 %)
Industrial	15,000 (15 %)
Agricultural	25,000 (25 %)
Total	100,000

Quantification of MBr release to the atmosphere is extremely difficult, since limited data exist for the total balance of MBr in the earth's atmosphere. Based upon information from several sources, atmospheric release can be broadly attributed to 4 major sources (Table 5-1), with agricultural use of MBr being attributed to 25 % of

the atmospheric MBr. Recently, Yagi et al. (1993) estimated that agricultural use contributes 80 % of anthropogenic MBr in the atmosphere. MBr is used industrially as a methylating agent and a degreaser.

More recent investigations emphasize new facets (Table 5-2) of the uncertainty of various source contributions and sinks for atmospheric MBr. New modeling studies based upon recent monitoring data suggest that the ocean absorbs more MBr from the atmosphere than previously thought. Rapid removal by the ocean shortens the average estimated life-time of atmospheric MBr to just 0.7 year, much less than an earlier estimate of 2 years (Friebele, 1997).

Table 5-2. A recently revised budget for atmospheric MBr (Yvon-Lewis and Butler, 1997).

MBr Sources	Emissions (Gg y ⁻¹)	MBr Sinks	Uptake (Gg y ⁻¹)
Oceans	56	Oceans	77
Fumigation (soils, durables, perishables and structures)	46	Hydrolysis and uv	86
Gasoline, leaded	15	Soils	43
Biomass Burning	20	Plants	?
Total	137	Total	206

These new results with regard to the role of oceans in the level of atmospheric MBr (Friebele, 1997) raise a question about the contribution that anthropogenic MBr plays in destroying the ozone layer. A newly revised MBr budget (Table 5-2) presented by Yvon-Lewis and Butler (1997) estimates that sinks (206 Gg y⁻¹) greatly exceed sources (137 Gg y⁻¹). These estimates imply that MBr

should not accumulate in the atmosphere. Obviously, high uncertainty prevails regarding sources and sinks for the accumulation of atmospheric MBr. The buffering role of oceans implies that reducing agricultural sources will not affect atmospheric MBr to any great extent, and yet could cause unnecessary economic stress on the agricultural community. Thus, the economic value and efficacy of MBr fumigation to control pathogens in agricultural soils warrant renewed research efforts. Modeling MBr fate and transport during agricultural use (soil fumigation) is particularly needed to provide improved insight of system dynamics with regard to atmospheric emissions resulting from MBr fumigation and to provide guidelines for future research needs.

Table 5-3. Selected chemical and physical properties of MBr (CH_3Br) (Adapted from Hacherl, 1994).

Selected Property	Magnitude
Molecular weight (g mole^{-1})	94.94
Boiling point ($^{\circ}\text{C}$)	4.6
Solubility in water (g kg^{-1}) at 20°C	13.4
Gas density (g L^{-1} at 20°C)	3.974
Diffusion coefficient ($\text{cm}^2 \text{s}^{-1}$ in free air at 20°C)	0.0903
Henry's Law constant at 20°C	0.251
Vapor pressure (mm Hg at 20°C)	1420

MBr is an odorless hydrocarbon (CH_3Br) except at extremely high concentrations, where it has a sweet odor. It has a low boiling point (4.6°C) and thus remains in gaseous form at temperatures normally encountered under field conditions. The important chemical properties of MBr are listed in Table 5-3. Lethal

toxicity of MBr to humans has been noted at 1600 ppm in air for 10-20 hours, or at 7900 ppm for 1.5 hours (USEPA, 1986). The lowest inhalation level found to cause toxicity in humans is 35 ppm in air (EXTONET, 1997).

Transport Mechanisms for MBr Fumigant in Soil

Although MBr is extremely volatile, it is commonly injected as a liquid from a pressurized cylinder. The formulation injected is typically a mixture of 98 % MBr with 2 % chloropicrin (Hacherl, 1994). Chloropicrin is added to act as a lachrymatory warning agent. Transport of gaseous MBr in the soil environment is mainly via diffusion through interconnected air-filled soil pores. Mass flow of gases in the soil environment has been proposed by several mechanisms, primarily controlled by changes in temperature and barometric pressure, effects of wind, and forced movement due to infiltrating water (Bever et al., 1972).

The diffusion coefficient for MBr in free air has been reported to be $325 \text{ cm}^2 \text{ hr}^{-1}$ at $20 \text{ }^\circ\text{C}$ (Siebering and Leistra, 1979). The temperature-dependence of the diffusion coefficient in free air can be defined by use of Eq. [2.15]. Estimation of the diffusion coefficient of gases in a porous soil system is done by taking into account the air porosity and tortuosity of the soil system. The tortuosity can be determined by use of Eq. [3.28].

Maharajh and Walkley (1973) measured MBr diffusion in water for temperatures ranging from 9.9 to $34.9 \text{ }^\circ\text{C}$ (Fig. 5-1). An almost linear increase in the diffusion coefficient was observed with temperature over the range of investigation.

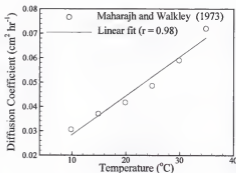


Figure 5-1. Temperature dependence of MBr diffusion in water (Data from Maharajh and Walkley, 1973).

Fate of MBr Fumigant in Soil

The fate of MBr is not only dependent upon transport by diffusion in the gaseous phase, but also upon partitioning between the gaseous and liquid water phases as well as between the liquid water and solid phases. Reactions in the water and solid phases greatly influence MBr fate and transport. In general, two ways exist by which the fate of MBr in soil is affected. The first includes factors that affect MBr movement in soil in a reversible manner, such as sorption to solids and dissolution in water. The second includes factors which contribute to the irreversible chemical degradation or destruction of MBr molecules, such as hydrolysis.

Gaseous MBr reversibly partitions into both the solid matrix and the liquid phase. This partitioning may be described by instantaneous linear sorption under equilibrium conditions such as (Brown and Rolston, 1980)

$$s = k_s c \quad ; \quad k_s = \left[\frac{\theta_s (R - 1)}{\theta_L \rho_L + \rho} \right] \quad [5.1]$$

where k_p is a partitioning coefficient between the gaseous phase and the combination of soil + water phase. Goring (1962) reported the Henry's Law constant as 0.244 [-] at 20 °C for the partitioning of gaseous MBr into liquid water. Mutziger et al. (1996) reported lab-measured Henry's Law constant values over a temperature range for the partitioning of MBr into water (Fig. 5-2).

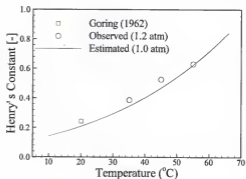


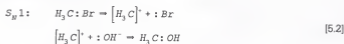
Figure 5-2. Laboratory-measured and estimated Henry's Law constants at different temperatures for the partitioning of MBr into water (Adapted from Mutziger et al., 1996).

Reversible partitioning reactions are characterized by the fact that, as gaseous phase MBr concentrations decrease, MBr molecules will desorb from soil solids or volatilize from water and thus be returned to the gaseous phase.

Irreversible chemical or biological degradation reactions, on the other hand, are ones in which MBr is converted into another compound in such a way that it cannot return to the gas phase and thus is permanently lost from the system.

In an irreversible hydrolysis reaction, MBr is known to react with hydroxide ions (OH^-) in aqueous solutions through both unimolecular and bimolecular nucleophilic substitutions to form methanol and the bromide (Br^-) ion as shown in

the following reactions (Moje, 1960)



The rate of these hydrolysis reactions is greatly enhanced in the presence of ultraviolet light, although light from the visible spectrum has no effect (Castro and Belser, 1981; and Gentile et al., 1989, 1992). Increased pH and increased temperatures also show an enhancing effect upon the hydrolysis of MBr (Hacherl, 1994).

Moje (1960) indicated that unimolecular nucleophilic substitution should be the major mechanism for the hydrolysis of MBr in water. Thus, the hydrolysis reaction becomes first-order. Reactions of MBr in soil water with soil organic matter involve the transfer of methyl groups to the organic matter (Maw and Kempton, 1973). These reactions are expected to be first-order due to the large excess of organic matter reaction sites (Brown and Rolston, 1980). Brown and Rolston (1980) measured the appearance of Br^- in the soil solution resulting from the decomposition of MBr as a function of time for three different soils. The production of Br^- for a given introduction of MBr was greatest for organic soil, intermediate for loam soil, and lowest for sand. The results thus suggest that mechanisms of decomposition involving clay particles and soil organic matter are significant to the decomposition of MBr in soils during fumigation. A first-order hydrolysis rate coefficient of 0.014-hr^{-1} was reported for Yolo loam soil by Rolston and Glauz (1982). Hornsby et al.

(1996) reported the soil organic carbon sorption coefficient (k_{oc}) for MBr to be 22.0 ml g⁻¹ of organic carbon. In a recent study by Jin and Jury (1995), on a Pachappa fine sandy loam soil with 0.49 % organic carbon, the degradation rate of MBr was observed to be first-order and was insensitive to changes in soil water content (Table 5-4). However the MBr degradation rate showed a slight increase at water saturation. These results confirmed earlier work showing that organic matter is the major factor influencing degradation of MBr in soils.

Table 5-4. Measured degradation rate coefficient and half life of MBr as a function of soil water content (Adapted from Jin and Jury, 1995).

Degree of Water Saturation in % (Water Content, θ_r)	Half-life (days)	Rate coefficient (hr ⁻¹)
45 ($\theta_L = 11.5$)	12.5	0.0023
76 ($\theta_L = 19.4$)	12.5	0.0023
100 ($\theta_L = 25.6$)	10.7	0.0027

Although hydrolysis deactivates toxic MBr molecules, toxic levels of bromide may accumulate in the soil water of treated soils (Macartney and Price, 1988; and Maw and Kempton, 1982). High levels of bromide accumulation have also been found in crops such as tomato, carrot, lima bean, lettuce, radish, tobacco, wheat, orange, and lemon grown on initially fumigated soils (Hoffman and Malkomes, 1979; and Maw and Kempton, 1973).

Permeation/Transmission of MBr through Polyethylene Mulch

Open-field fumigation without a plastic soil cover (mulch) may provide a large input of MBr into the atmosphere. In plastic-mulch culture, atmospheric

emission occurs by diffusive transport (or permeation) through the plastic mulch (within the bed) as well as by diffusion through uncovered soil surfaces in furrows between parallel soil beds. Several environmental factors contribute to diffusive flux through the soil in furrows and through the plastic mulch in beds. Environmental factors with the greatest impact upon diffusive flux include the temperature gradient across the plastic mulch, the moisture or condensed water layer on the underside of the plastic mulch, and the sweeping effect of wind over the surface (overland wind velocity).

The physical dynamics of water and heat transport beneath plastic-mulched soil surfaces are quite complex (as discussed in Chapter-2.). Temperature increases at the plastic mulch during the daytime by as much as 15 to 20 °C due to solar radiation are not uncommon (Ham and Kluitenberg, 1994). Such temperature increases during daylight hours enhance the water evaporation rate, thereby increasing relative humidity of the air gap and of soil beneath the plastic mulch. Since the plastic cools faster than the soil, the condensation of water from the humid soil air tends to occur on the underside of the plastic mulch during nighttime hours. As a result, permeability of the plastic mulch to MBr would be reduced due to a blocking effect by the layer of condensed water. As the mulch temperature increases during daytime hours, evaporation then removes the condensed water layer. In cases where permeating MBr is soluble in or sorbs to the plastic material, the rate of movement by diffusion would further be reduced, thus delaying the equilibrium. As such, only operational value for the diffusion coefficient can be envisioned.

Table 5-5. Rate[†] of escape of MBr through several films at various temperatures (Adapted from Kolbezen and Abu-El-Haj, 1977).

Temp. (°C)	LDPE [‡] (1-mil)	HDPE-1 ^{††} (1-mil)	HDPE-2 ^{††} (1-mil)	Polybutene (1-mil)	Saran (0.5-mil)	Black LDPE (6-mil ^{‡‡})
23	8.2	2.7	1.4	2.9	Nil	1.6
30	11.1	3.5	1.7	4.0	Nil	2.2
40	15.1	5.0	2.9	6.3	Nil	3.4
50	20.1	6.8	3.9	9.1	0.18	5.9
60	30.6	8.8	5.2	11.8	0.41	9.2

[†] Units are $\text{ml hr}^{-1} \text{m}^{-2} \text{ml}^{-1} \text{L}^{-1}$.

[‡] low density polyethylene,

^{††} high density polyethylene sample 1,

^{††} high density polyethylene sample 2, and

^{‡‡} 1 mil = 2.544×10^{-3} cm.

Few investigations have been conducted to measure the diffusion coefficient of MBr through polyethylene sheets used for mulching. Kolbezen and Abu-El-Haj (1977) measured rates of escape of gaseous MBr through six selected films at different temperatures. The escape rates increased with temperature for all films. MBr escape rates ranged from 0.41 to 30.6 $\text{ml hr}^{-1} \text{m}^{-2} \text{ml}^{-1} \text{L}^{-1}$ for the six materials. The authors found one of the high-density polyethylenes (Table 5-5) to be an effective barrier to MBr transport, with minimum escape rate over the temperature range investigated.

During a field experiment for unbedded mulched soil in California Yagi et al. (1993) observed that the cumulative emission of MBr decreased as the thickness of LDPE plastic increased (1.03, 1.29, 1.37, and 1.6 mil thickness were used). Unpublished results from field investigations for mulched soil bed system at the

University of Florida Green Acres Experimental Station, near Gainesville, FL, with black LDPE (1.2 mil) and clear laminated plastic (relatively thicker than black LDPE) showed emission fluxes differed between the two plastic materials.

Emissions were reported for both the plastic-covered beds and uncovered furrows in between the parallel beds.

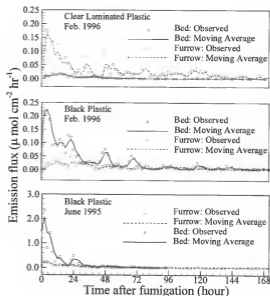


Figure 5-3. MBr emission fluxes in plastic mulched beds during fumigation at the University of Florida Green Acres Experimental Station located near Gainesville, FL.

MBr was applied at the rate of 450 kg ha^{-1} with a 3-nozzle applicator at a depth of 20 and 33 cm during the summer of 1995 and winter of 1996, respectively, in soil beds of Arredondo Fine Sand soil used for vegetable production. As expected, higher magnitudes of the emission fluxes were observed in the summer shallow

injection over winter deeper injection during fumigation (Fig. 5-3). A diurnal cyclical pattern was evident in the emission fluxes to the atmosphere due to non-isothermal conditions. The relatively thicker clear laminated plastic was able to retain slightly more MBr in the soil bed over black LDPE (Fig. 5-3). However, material balance estimations from emission fluxes and soil Br⁻ residue measurements for MBr applied during fumigation revealed that 39, 46, and 70 % of applied MBr were unaccountable in bed systems with black LDPE (June, 1995), black LDPE (Feb., 1996), and clear laminated plastic (Feb., 1996) mulches, respectively. Hence, definite conclusions were not feasible from these field investigations of MBr fumigation in plastic mulched vegetable beds (personal communication with investigators¹).

Hacherl (1994) conducted laboratory investigations measuring the diffusion through black LDPE (1.25 mil) film commonly used in agriculture. Figure 5-4 shows the results of diffusion investigations by Hacherl (1994) and Kolbezen and Abu-El-Haj (1977) for black LDPE with 1.25-mil and 1.00-mil thicknesses, respectively. The results revealed a near-linear increase of diffusion coefficient with temperature, with lower values in the case of Hacherl (1994) corresponding to thicker LDPE. In another study (Jin and Jury, 1995), from the data presented, the diffusion coefficient was estimated to be $0.005969 \text{ cm}^2 \text{ hr}^{-1}$ for black LDPE (1.0 mil).

¹ A. G. Hornsby, L.T. Ou, D. Dickson, S.J. Locascio, and P.S.C. Rao

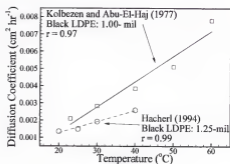


Figure 5-4. MBr diffusion through black LDPE of different thicknesses (Data from Hacherl, 1994; and Kolbezen and Abu-El-Haj, 1977).

Modeling of MBr Transport during Fumigation

Only a few prior modeling efforts have been attempted to describe MBr transport in soil during fumigation. Hemwall (1969) described a two-dimensional model for gaseous diffusion of MBr in soil with relatively low water content. The model assumed a small constant water content and isothermal soil conditions. Typical simulations were presented to demonstrate time-dependent patterns of fumigant concentration and biological control within an uncovered soil profile after fumigation.

Siebering and Leistra (1979) presented a one-dimensional model for gaseous diffusion of MBr under isothermal conditions. Water content was held constant and small, such that water flow could be ignored. Comparison of model simulations with experimental results for MBr concentrations during soil fumigation applied to soil under cover in a greenhouse matched only in the upper part of the soil profile (to 40 cm) but deviated substantially elsewhere.

Roiston and Glauz (1982) proposed a model describing radial diffusive transport of gaseous MBr away from injection chisels during fumigation of a field profile. The model was based on similar work done by Hemwall (1959, 1960) and Siebering and Leistra (1979). The model included the dissolution-distillation of MBr gas on soil solids and in soil water, using both kinetic and equilibrium relationships and hydrolysis to yield Br^- ions according to first-order kinetics. The model considered the case where the soil surface was covered with a barrier totally impermeable to the diffusion of gas along with the case of a bare soil surface. Reported simulation results provided a better match with the experimental data of Abdalla et al. (1974), which involved a mulch barrier, when no barrier was considered at the soil surface during simulations. Sensitivity analysis of input parameters showed reaction kinetics to be unimportant, so they could be safely ignored. Water flow and non-isothermal temperature effects were ignored in all simulations. Also, in that model, the boundary conditions (BC) at the soil surface were unrealistically handled by making the plastic mulch impermeable and applying a zero-concentration fixed BC at the soil surface.

Mignard and Benet (1989) considered a kinetic relationship for MBr partitioning between the gaseous and solution phases. Synthetic simulations were conducted and compared with equilibrium models, and profiles were developed to forecast the treatment zones and behavior of MBr. The authors inferred from their analysis that a kinetic partitioning relationship is important only for rapidly changing boundary conditions. This model also ignored water and temperature variations in the soil.

Recently Wang et al. (1997) adopted a two-dimensional (2-D) finite-element model, CHAIN_2D (Šimůnek and van Genuchten, 1994) to simulate the fate and transport of MBr fumigant in soil. CHAIN_2D numerically solves the partial differential equations for 2-D nonlinear, nonequilibrium simultaneous transport of water and heat, (but not coupled heat-water) and solute in a vanably saturated porous medium. The temperature dependence of various coefficients (such as D^g , K_p , etc.) were described in similar fashion to the present work. However, the model lacked a realistic description of the soil-surface plastic-mulch/atmospheric boundary. Placement of a plastic mulch significantly changes the energy balance at the soil/atmospheric interface (as discussed in Chapter-3) and requires proper redefinition of the energy exchange and balance at the interface to simulate non-isothermal soil conditions. The transfer of MBr to the atmosphere was described (Wang et al., 1997) by introducing a transfer coefficient (h_{TK}) as

$$Flux = -\frac{D^g}{d_b}(g - g_{atm}) = h_{TK}(g - g_{atm}) \quad [5.4]$$

where d_b (cm) was considered a composite boundary thickness inclusive of an air gap below the mulch, the mulch thickness, and an overlying atmospheric boundary layer; and where h_{TK} was described as a transfer coefficient (cm s^{-1}). The d_b parameter was shown to be temperature-dependent through use of an equation similar to Eq. [2.14], but the scientific basis for doing so was not explained. Although a cyclic nature in emission flux in accordance with non-isothermal conditions was demonstrated, model simulations failed to accurately describe (Fig. 5-5) the cyclic field-measured emission flux reported by Yates et al. (1996).

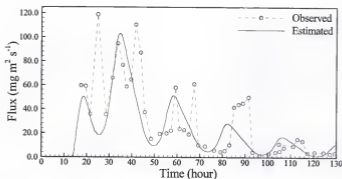


Figure 5-5. Simulated and measured flux density through plastic-mulched surface. Adapted from Wang et al. (1997).

It is thus evident that, in modeling MBr fate and transport, various investigators have made simplifying assumptions (such as small and constant soil water content and isothermal conditions) that reflect unrealistic field conditions. Also, BCs at the soil surface which are more realistically described by a Neumann-type in the case of MBr fumigation have been improperly designated (such as a zero concentration fixed BC at nodes exposed to the atmosphere for uncovered soil). The dissolution (Henry's Law constant) and diffusion (both in air and water) of MBr are temperature-dependent, and variably saturated soil-water flow is a common occurrence under field conditions. This is particularly true for humid climates.

Analysis of Fate and Transport of MBr Fumigant

The model presented in this dissertation represents many improvements over earlier efforts (Hemwall, 1959; Mignard and Benet, 1989; Rolston and Glauz, 1982; and Siebering and Leistra, 1979), for it includes coupled transient flows of both heat and water based upon PDT theory. Realistic plastic-mulch boundary conditions are described thoroughly by inclusion of optical properties of the plastic mulch in the energy balance at the soil/atmospheric interface. This model provides opportunity to consider the effect of improved temperature upon estimates of solute transport (both in the liquid and gaseous phases).

Modeling investigations (synthetic simulations) of the fate and transport of MBr fumigant were conducted to obtain improved insight into the system dynamics for MBr fumigation of soils. Modeling simulations of MBr fumigation prior to this research have utilized overly simplified assumptions, such as gaseous diffusive transport in air-filled soil pores under isothermal conditions with the effects of transient liquid-water flow neglected. Simulations reported here utilized an assumption that was more realistic of actual field conditions; i.e., non-isothermal soil conditions that fluctuate diurnally due to net solar radiation, thus altering vapor and liquid water flow as well as MBr diffusion. Objectives were as follows:

- 1) To investigate important major processes influencing MBr fate and transport including volatilization and degradation in fumigated soil beds used for vegetable and fruit production in Florida,

- 2) To investigate the effect of non-isothermal and variably saturated soil conditions on material balance of MBr during simulated fumigations,
- 3) To evaluate the effectiveness of the current management technique-i.e., plastic-mulching of soil beds-in minimizing MBr emission from fumigated soil beds to the atmosphere, and
- 4) To examine alternative management methods for decreasing MBr emission during commercial use of soil fumigation.

Approach

Simulation analysis was designed considering major factors known to affect the fate and transport of MBr. The following factors were considered in the design of simulations:

- I. Effect of variable water saturation in the soil bed: Two levels of heterogeneous water saturation were selected to represent a relatively dry soil and a reasonably wet profile. The effects of hydrolysis (degradation) on MBr material balance were considered for different levels of soil water saturation.
- II. Effect of variable temperature regime in the soil bed:
 - A. Non-isothermal conditions: Effects of transient thermal conditions were considered upon the following input parameters for the model
 1. MBr diffusion coefficient in the air phase (D^a),
 2. MBr diffusion coefficient in the water phase (D^w),
 3. MBr partition coefficient between gaseous and aqueous phases (Henry's Law constant, K_g),

4. Diffusion coefficient of MBr through polyethylene film ($D_{plastic}^{\theta}$).
- B. Isothermal conditions: Uniform thermal conditions were provided for comparison (average daily temperature was assumed to exist uniformly over the simulation domain).
- III. MBr diffusion through plastic mulch: Due to uncertainty in published data and based on reported field investigations of MBr emissions from plastic-mulched soil, different magnitudes for the MBr diffusion coefficient through plastic film were used to examine the material balance of MBr.
 - IV. Depth of fumigant injection: Two depths of fumigant injection zones were investigated:
 - A. Typical shallow injection zone: 33 cm depth total
 - B. Deep injection zone: 66 cm depth total (arbitrarily chosen for comparison)
 - V. Effect of irrigation (dousing of water on the bed): Effect of irrigation was examined to evaluate the surface-sealing effect (due to wetness) on reduction of gaseous emissions for MBr.
 - VI. Fumigation Efficiency: Soil sterilization during fumigation was investigated based on the nematotoxic level of MBr (20 ppm or greater) and exposure time (minimum 24 hr) for 2nd-stage juveniles of root knot nematode (Mckenry and Hesse, 1978).
 - VII. Hydrolysis of MBr: As no data for the hydrolysis rate of MBr in Florida soils was available, sensitivity analysis was carried out for 3 rates; 1) 0.014 hr⁻¹ (for California, Yolo loam soil, Rolston and Glauz (1980)), 2) 0.007 hr⁻¹, and 3) 0.0035 hr⁻¹.

VIII. Diurnal water and heat dynamics in soil bed: The influence of atmospheric interactions with the soil surface (both bare furrow and mulched bed) were examined by analyzing the water and heat dynamics in the soil bed system over a diurnal period of 24 hrs.

Methodology

Arredondo Fine Sand (Grossarenic Paleudults, loamy, siliceous, hyperthermic), a coarse-textured soil at the IFAS Green Acres farm near Gainesville and commonly found in north central Florida, was selected for the modeling investigation. Representative soil properties were taken from 'Soil Science Research Report # 88-1, 1988¹'. The soil consisted of five horizons namely, Ap (0-23 cm), E1 (23-66 cm), E2 (66-99 cm), Bt1 (99-165 cm), and Bt2 (165-203 cm). The weather data for simulation purposes were taken from a weather station at the Green Acres Farm of IFAS located west of Gainesville. The month of February was selected for all simulations, since MBr fumigations are normally performed for the Gainesville area at that time of the year.

A spatial profile discretization of the cross-sectional soil bed resulted in 2782 elements with 1474 nodes (Fig. 5-6). Bed symmetry was assumed, so only a half-section (AB-BC-CD-DE-FE-AF) of the soil bed needed be considered for simulations.

¹Compiled by Univ. of Florida, IFAS, Soil Science Dep. Soil Characterization Lab. in cooperation with the USDA-SCS.

No flow BCs on the left- and right-hand sides (AF and DE) were defined for heat, water, and solutes. The DE boundary represents a vertical symmetry line through the middle of a furrow between two parallel soil beds. The AF boundary represents a vertical symmetry line through the middle of a soil bed. The lower boundary (FE) was designated as a zero thermal gradient with gravitational water flow ($= K(h, T)$).

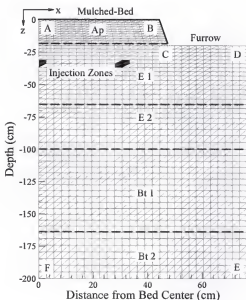


Figure 5-6. Schematic of the discretized simulation domain of the soil bed.

For solute transport, both convective (in the liquid phase) and diffusive (both in the aqueous liquid and gaseous phases) transport were allowed at the bottom (FE), with the assumption that solute leaving the lower boundary is lost from the

flow domain (i.e., there is no return flow). The emission loss of MBr to the atmosphere (AB-BC) was described through diffusive flux, assuming a 1-cm boundary layer and zero concentration on the atmospheric side of the boundary layer. These emission fluxes may be defined explicitly as

a) For Bed

$$J_{gas}^{Bed} = - \left[D_{plastic}^g \left(\frac{g_s - g_{s+1}(air)}{z_s - z_{s+1}(air)} \right) \right]$$

b) For Furrow

$$J_{gas}^{Furrow} = - \frac{1}{2} \left[D_{free\ air}^g \left(\frac{g_s - g_{s+1}(air)}{z_s - z_{s+1}(air)} \right) + \theta_{air} D_{soil}^g \left(\frac{g_{s-1} - g_s}{z_{s-1} - z_s} \right) \right]$$

where the subscripts s , $s+1$, and $s-1$ represent nodes at the soil surface, above the surface, and below the surface, respectively.

Table 5-6. Physical properties for 5 distinct horizons of a profile of Arredondo fine sand soil .

Soil Layer	Sand (%)	Silt (%)	Clay (%)	OC [†] (%)	BD [‡] (g cm ⁻³)	K _{sat} ¹ (cm hr ⁻¹)
Ap	91.9	3.3	4.8	0.83	1.52	6.2
E1	92.0	3.3	4.7	0.28	1.54	16.7
E2	91.4	3.0	5.6	0.14	1.52	15.1
Bt1	86.0	3.7	10.3	0.11	1.56	6.4
Bt2	75.2	3.0	21.8	0.20	1.57	2.4

[†] OC- Organic Carbon,

[‡] BD- Bulk Density

The data for physical properties of the soil profile used are presented in

Table 5-6, with other related parameter values in Table 5-7. The soil water

characteristic data used for estimating (van Genuchten, 1980) hydraulic-function parameters were taken from the report mentioned earlier. Average weather parameters¹ used in simulations for the month of February were: 1) average daily temperature - 11.6 °C, 2) temperature amplitude - 7.7 °C, 3) wind velocity - 11×10^4 cm hr⁻¹, 4) day-length - 11.0 hrs, and 5) global daily radiation - $1400 \text{ J cm}^{-2} \text{ day}^{-1}$.

Table 5-7. Parameter values for 5 distinct horizons of a profile of Arredondo fine sand soil.

Soil Layer	μ_{L1} [†] (hr ⁻¹)	K_{d1} [‡] (cm ³ g ⁻¹)	K_{d2} ^{††} (cm ³ g ⁻¹)	van Genuchten Parameters			
				α (cm ⁻¹)	η	θ_s	θ_r
Ap	0.014	0.1826	0	0.0225	2.124	0.43	0.03
E1	0.014	0.0616	0	0.0216	2.762	0.42	0.04
E2	0.014	0.0308	0	0.0271	2.626	0.43	0.04
Bt1	0.014	0.0242	0	0.0211	2.091	0.41	0.06
Bt2	0.014	0.0440	0	0.0307	1.557	0.41	0.13

[†] - hydrolysis rate coefficient for MBr,

[‡] - soil sorption coefficient for MBr, and

^{††} - soil sorption coefficient for bromide ion.

Temperature-dependence of the diffusion coefficients for MBr in gaseous and aqueous phases of the soil were defined by use of Eq. [2.15] and data reported in Fig. 5-1 from Maharajh and Walkley (1973), respectively. As information is unavailable for the temperature dependence of the hydrolysis rate coefficient (μ_{L1}), a fixed value of 0.014 hr^{-1} was used (Rolston and Glauz, 1982). The diffusion coefficient

¹Climatological Data, Agronomy Department and NOAA Cooperating, 1996.

for the plastic mulch was defined using the data of Hacherl (1994). The MBr fumigant was assumed to be applied at a rate of 450 kg ha^{-1} with a three-shank applicator, so that 1½ shank ($3591 \mu\text{moles}$) injections occur within the flow domain shown in Fig. 5-6. Unless otherwise noted, the depth of the injection and time of day for injection for all the simulations were set at 33 cm and 9:00 AM, respectively. Black LDPE of thickness 1.25 mil was assumed as the plastic mulch in all the simulations. Mass and energy balance errors were less than 1.0 % for all simulations reported in this work.

Results and Discussion

Plastic-Mulching of Soil Beds to Control MBr Loss to the Atmosphere

Preliminary simulations conducted using the laboratory-measured data (Fig. 5-7, Level-1) of Hacherl (1994) for diffusion through plastic (black LDPE, 1.25-mil thick) provided estimates for the atmospheric losses of MBr during fumigation of the soil bed that were very low (23 % during the 1st day) compared to reported values of 40 to 60 % for recent investigations (Yagi et al., 1993; Yates et al. 1996). Hence, parallel elevated temperature-dependent levels were designed (Fig. 5-7) for investigation. The use of an experimentally measured diffusion coefficient for a 1.25-mil thick black LDPE by Hacherl (1994) in simulations showed that very little MBr escaped (0.02 % of that applied) through the plastic mulch into the atmosphere (i.e. from the bed excluding the furrow) during the 1st day. The

diffusive flux (Fig. 5-8: Level-1, and Fig. 5-9: a, Level-1) based upon the measured diffusion coefficient of plastic mulch from the soil bed was very low and it was also

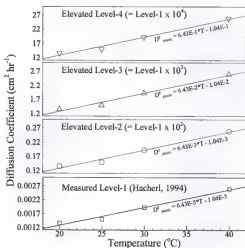


Figure 5-7. Measured and elevated levels of diffusion coefficients through 1.25-mil black LDPE plastic mulch used in the model simulations.

demonstrated by the material balance after 1 and 3 days (Table 5-8) that only 23.4 and 45.8 % of the applied MBr, respectively, was lost from the system (mulched soil-bed plus bare furrow) to the atmosphere. This result is much lower than the 40 to 60 % atmospheric losses earlier reported from field investigations (Yagi et al., 1993; Yates et al., 1996), which were carried out under unbedded conditions with complete mulch cover of the soil. Initial average fluxes both from the bed and the furrow were substantially higher than for later periods (after 24 hours) when the

concentrations in soil had decreased due to spreading, hydrolysis, and loss of MBr to the atmosphere. Also note that emission fluxes from the furrow were nearly 5 times larger than for the bed, except for elevated plastic-mulch diffusion Level-4, due to the absence of a mulch barrier over the furrow.

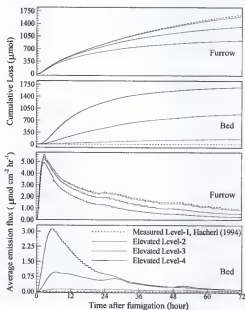


Figure 5-8. Losses of MBr to the atmosphere through soil bed and furrow surfaces using measured and elevated diffusion coefficients for MBr through plastic mulch¹.

¹Small steps in some of the figures resulted from the need for plotting more points within certain time periods.

Use of elevated levels of diffusion coefficients for plastic mulch showed more losses of MBr into the atmosphere from the system (Level-2 = 25.1 %; Level-3 = 34.7 %; and Level-4 = 51.7 %) one day after fumigant injection. In all cases, emission fluxes from the bare soil furrow were highest near the bed due to close proximity to the injection zone. Figure 5-9: a shows MBr fluxes in the bed 6 hours after fumigant injection, when peak emission fluxes occurred from the bed (Fig. 5-8).

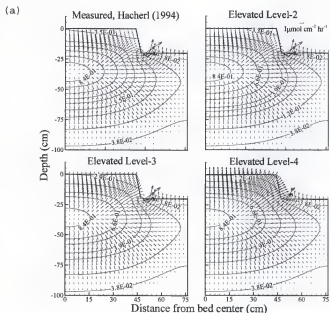


Figure 5-9. MBr total concentration ($\mu\text{mol cm}^{-3}$) contours and gaseous MBr flux vectors ($\mu\text{mol cm}^{-2} \text{hr}^{-1}$) in the bed 6 hrs after injection of MBr fumigant.

- a) 4 levels of diffusion coefficients through the plastic mulch,
 b) non-mulched bed.

Emission fluxes (Fig. 5-9: a) increased from the mulched bed with elevated levels of diffusion coefficients for the plastic mulch. Also to be noted here is the fact that the trend of diffusive flux was reversed in the furrow compared to that for the bed, and lower diffusion coefficients for plastic mulch showed higher diffusive flux and more cumulative loss from the furrow (Fig. 5-8, Fig. 5-9: a, and Table 5-8). Figure 5-9: b shows the emission of MBr in furrow and bed without a plastic mulch, for comparison purposes. The emission fluxes were higher from soil-surface regions close to the fumigant injection zone (Fig. 5-9: b).

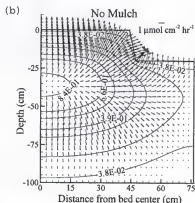


Figure 5-9--continued

Overall, total material losses of MBr from the simulated soil-system to the atmosphere (Table 5-8) increased when elevated levels of diffusion coefficients for plastic mulch were used in the simulations. Three-day simulations were appropriate, as the results showed that most of the MBr losses occur within the initial 24 to 30 hrs after fumigation (Fig. 5-8 and Table 5-8). Atmospheric losses were

observed to continue in small amounts even after 3 days, as long as undegraded MBr is present in the soil.

Obviously much uncertainty prevails regarding the diffusion coefficient of MBr in plastic mulches. The use of a lab-measured diffusion coefficient for simulating field conditions greatly under-estimated published results from the field investigations done in the past. However, the use of elevated diffusion coefficients (Level-2, Level-3, and Level-4) improved simulation results. It was, therefore, decided to use the Level-3 diffusion coefficient for all other simulations, as results obtained from this level were close to those from the published field investigations.

Table 5-8. Material balance (unit: %) of MBr under measured and enhanced levels of diffusion coefficient for plastic mulch.

Day-1	Total MBr in Profile	Atmospheric Emission Losses			Hydrolyzed	Deep Down-flow
		Bed	Furrow	Total		
Level-1	69.55	0.02	23.39	23.41	7.04	0
Level-2	67.91	1.81	23.29	25.10	6.98	0
Level-3	58.54	13.15	21.57	34.72	6.73	0
Level-4	42.24	34.24	17.41	51.65	6.11	0
No-Mulch	37.29	-	-	56.92	5.79	0
Day-3						
Level-1	36.38	0.20	45.63	45.83	17.79	0
Level-2	33.94	4.24	44.42	48.66	17.39	0
Level-3	23.46	24.55	36.52	61.07	15.46	0
Level-4	15.05	46.32	25.84	72.16	12.79	0
No-Mulch	13.40	-	-	74.68	11.91	0

Non-Isothermal versus Isothermal Soil-Conditions

An isothermal simulation was performed in order to compare with non-isothermal simulations existing under a black LDPE. Thermal effects on solute transport (involving D^f , D^v , k_g , $D^f_{plastic}$ parameters) were ignored in isothermal (with respect to solute transport only) simulations. However, the coupled heat and water flow model was used in its original form, with solute transport being made independent of temperature fluctuations. The parameters for solute transport were estimated and kept constant for a daily average temperature of 11.6 °C, typically existing during the month of February in the vicinity of Gainesville (diffusion coefficient in air = 308 cm² hr⁻¹, Henry's Law constant = 0.15 (-)).

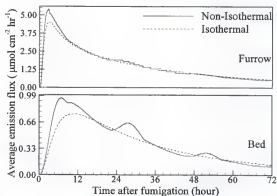


Figure 5-10. Emission fluxes of MBr through bed and furrow under isothermal and non-isothermal transport of fumigant.

The isothermal and non-isothermal simulations conducted for a 3-day period showed (Fig. 5-10) that MBr emission fluxes from both bed and furrow were affected by non-isothermal conditions. Figure 5-10 shows the diurnal fluctuations in MBr emissions from bed and furrow in the case of non-isothermal simulations for black-LDPE, whereas a similar cyclical nature of MBr emission was missing in isothermal simulations. This emission pattern has been reported earlier (Fig. 5-5) for field investigations (Yagi et al., 1993; and Yates et al., 1996). Higher diffusive flux rates for MBr were observed initially from the furrow, which subsequently flattened out due to lower concentration gradients as increasing amounts of MBr were lost to the atmosphere. The delay in reaching the initial peak emission flux (Fig. 5-10) from the bed occurred due to a build-up time for MBr concentrations beneath the mulch and an increase in temperature of the plastic mulch as the day progressed (application time - 9:00 AM), whereas the bare furrow surface offered a quick passageway to the atmosphere.

Table 5-9. Material balance (unit: %) of MBr for fumigation under isothermal and non-isothermal conditions.

Day-1	Total MBr in Profile	Atmospheric Emission Losses			Hydrolyzed	Deep Down-flow
		Bed	Furrow	Total		
Isothermal	61.28	11.42	20.33	31.75	6.97	0
Non-Isothermal	58.55	13.44	21.59	34.73	6.72	0
Day-3						
Isothermal	25.96	22.37	35.45	57.82	16.21	0
Non-Isothermal	23.46	24.56	36.51	61.07	15.46	0

The results suggest that inclusion of non-isothermal conditions is essential to correctly estimate the fate and transport of volatile chemicals. Non-inclusion of temperature effects on solute transport may underestimate (Table 5-9) material losses to the atmosphere in the case of volatile chemicals such as MBr. The isothermal simulation estimated 260.2 kg ha^{-1} (57.8 % of application) emission loss to atmosphere compared to 274.8 kg ha^{-1} (61.1 % of application) as a non-isothermal estimate over a 3-day period.

Variable Water Saturation of Soil

Volumetric water contents present in the soil bed at the time of fumigation not only affect the hydrolysis of MBr but also its transport in the soil. Two different wetting regimes were selected for the simulations. An initially saturated soil profile was allowed to drain and evaporate water for 40 days. Two wetting levels were then selected to provide the soil water regime:

- 1) Level-1 (WL-1): 3292 cm^3 total water content in the flow domain, and
- 2) Level-2 (WL-2): 1864 cm^3 total water content in the flow domain.

The simulations revealed (Fig. 5-11) that larger amounts of MBr were lost to the atmosphere when there was less water ($WL-2 < WL-1$) in the soil profile. This result was expected, due to less hydrolysis and enhanced diffusion. Higher temperatures and lower water contents existed (Fig. 5-12) near the surface in the case of the drier soil system (WL-2). Greater diffusion pathways (larger diffusion volume due to lower water contents) at higher diffusion rates also existed in the drier profile. This resulted in a higher MBr emission flux from both the bed and

furrow in the case of the drier (WL-2) profile (Fig. 5-12). The emission fluxes from the bed were also higher (Fig. 5-11) during the later periods (after approximately 34 hrs) in WL-1. This was due to the higher water contents in WL-1 causing larger amounts of MBr to partition into the aqueous phase, which were then released to the gaseous phase as atmospheric losses occurred in order to maintain equilibrium between the aqueous and gaseous phases (controlled by the Henry's Law constant).

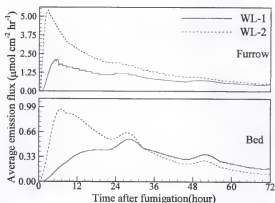


Figure 5-11. Emission fluxes of MBr through bed and furrow during fumigation performed under different profile water-saturation scenarios.

Figure 5-12 shows the plots of water content, temperature, MBr concentration, and MBr fluxes in the bed under different water saturations (WL-1 and WL-2) for 0.5, 3, 6, 12, 18, and 24 hours after fumigant injection. Temperatures under the bed and at the bare soil surface were higher in WL-2 as compared to WL-1, whereas water contents were lower in WL-2 as compared to WL-1 at the

same locations. The wetter profile (WL-1) maintained a higher water content at the mulched soil surface, due to vapor movement. This also contributed to lesser emission of MBr through both bed and furrow surfaces due to partial blockage of soil pores. Though not obvious, a cyclical diurnal pattern in the temperature profile can be identified (Fig. 5-12). This demonstrates that MBr fate and transport would be affected by the non-isothermal conditions within the bed. Figure 5-12: a shows the conditions existing ½ hour after the MBr fumigant injection. To be noted in this plot is the difference in spread of fumigant from the injection point. More rapid movement of MBr is clearly noticeable in the case of the drier bed (WL-2), whereas restricted spread of MBr is noticed in the case of the wetter bed (WL-1), due to partitioning with water and restricted passageways due to higher moisture contents. The discontinuity in the water content distributions (Fig. 5-12) was due to horizons of different porosity and texture in the soil profile.

As time progressed after injection (Fig. 5-12: c-f), the injection masses at the injection points coalesced showing the center of fumigant mass in the center of the bed. Figure 5-12: d-f in isolation would give an uninformed observer an impression that there was only one fumigant injection point. The coalescence occurs as a result of MBr transport and loss to the atmosphere; thus, higher concentrations remained in the center of the bed.

Material balances after fumigant injection indicated that more MBr was hydrolyzed in the wetter profile (WL-1), as would be expected. During the 1st day, nearly 20 % higher emission loss to the atmosphere (Table 5-10) was observed in the drier soil system (WL-2) as compared to the wet profile (WL-1). By the end of the

3rd day, the amount of MBr retained in the wet profile (WL-1) was 10 % more than for the drier one (WL-2). However, nearly 12 % more MBr was hydrolyzed in the wet profile (WL-1) than the drier one (WL-2) over a 3-day period. This indicates that the wet profile was able to retain more MBr compared to the dry one, but resulted in more bromide formation as a decomposition product. The higher retention of MBr in WL-1 was partly due to smaller quantities of available diffusion volume in the gaseous phase, partly due to more MBr partitioning into the aqueous phase at the higher water contents. Diffusion in the aqueous phase was very slow (by a factor of 10^3) compared to the gaseous phase.

Table 5-10. Material balance of MBr (unit: %) under different water saturations for one and 3 days after fumigant injection.

Day-1	Total MBr in Profile	Atmospheric Emission Losses			Hydrolyzed	Deep Down-flow
		Bed	Furrow	Total		
WL-1 (Wet)	72.53	5.54	9.44	14.98	12.48	0
WL-2 (Dry)	58.55	13.44	21.59	34.73	6.72	0
Day-3						
WL-1 (Wet)	34.45	18.16	19.78	37.94	27.61	0
WL-2 (Dry)	23.46	24.56	36.51	61.07	15.46	0

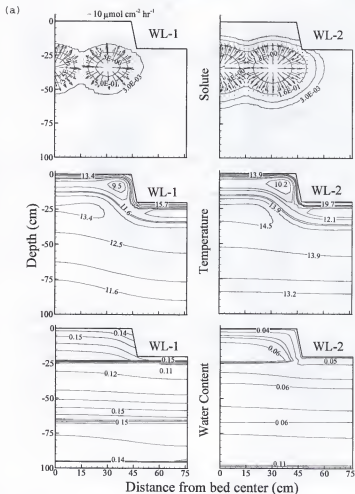


Figure 5-12. Contours of water content ($\text{cm}^3 \text{cm}^{-3}$), temperature ($^{\circ}\text{C}$), and MBr concentration (μmol) with gaseous fluxes ($\mu\text{mol cm}^{-2} \text{hr}^{-1}$) of MBr under 2 different soil-water saturation scenarios after fumigation.

a) $\frac{1}{2}$ hour; b) 3 hours; c) 6 hours; d) 12 hours; e) 18 hours; f) 24 hours.

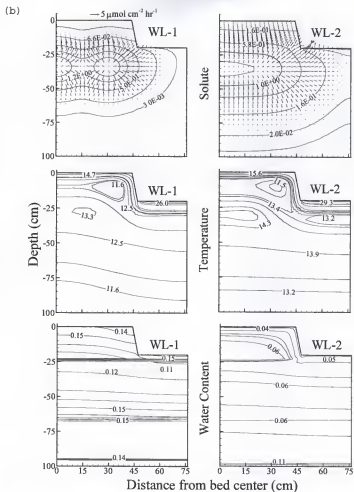


Figure 5-12-continued

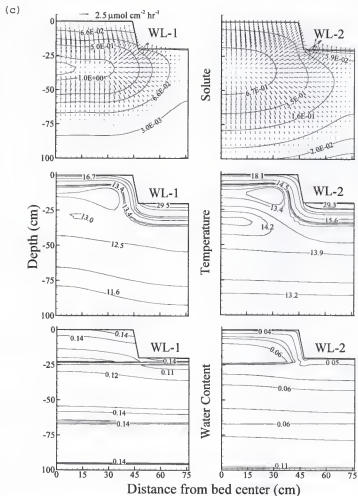


Figure 5-12-continued

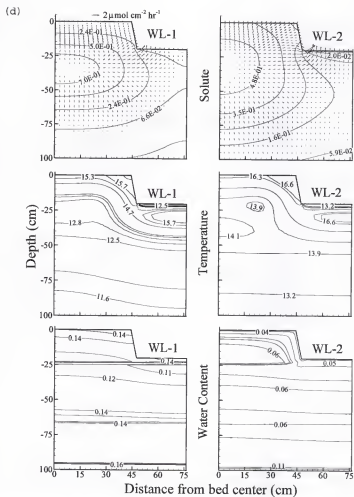


Figure 5-12-continued

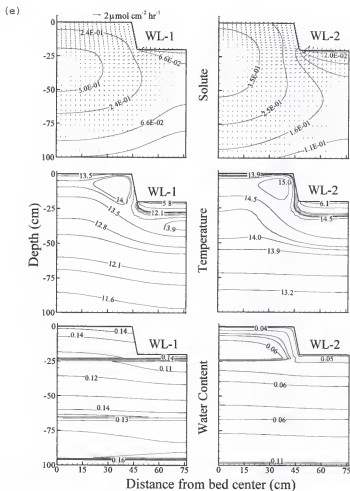


Figure 5-12—continued

(f)

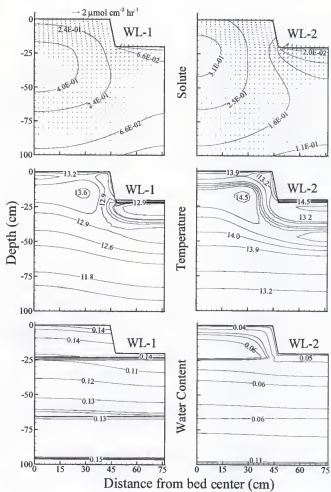


Figure 5-12-continued

Depth of Fumigant Injection

Influence of the depth of the fumigant injection zone upon MBr distribution and loss was investigated using two injection depths, 33-cm (shallow) and 66-cm (deep). Results for the shallow (33-cm) injection depth with variable water saturation are presented in Fig. 5-11 and Table 5-10.

In case of deeper injection of MBr at 66 cm (Fig. 5-13), the emission fluxes were smaller than those for the 33-cm injection zone. This was partly due to higher water contents in the 66-cm injection zone due to the presence of a differential soil horizon (Fig. 5-12), resulting in more MBr in the aqueous phase and partly due to greater distance to the emission surface from the center of MBr mass.

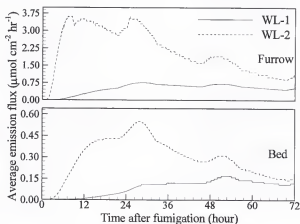


Figure 5-13. Emission fluxes of MBr under different water saturations for a 66-cm injection zone during the first 3 days after fumigant injection.

Table 5-11. Material balance of MBr (unit: %) during fumigation under different water saturations for 65-cm injection zone.

Day-1	Total MBr in Profile	Atmospheric Emission Losses			Hydrolyzed	Deep Down-flow
		Bed	Furrow	Total		
WL-1 (Wet)	81.30	0.30	1.85	2.15	16.54	0
WL-2 (Dry)	67.57	4.74	17.96	22.70	9.72	0
Day-3						
WL-1 (Wet)	46.05	4.77	10.41	15.18	38.76	0
WL-2 (Dry)	27.21	13.82	38.44	52.26	20.53	0
Day-7						
WL-1 (Wet)	13.56	10.05	18.36	28.41	58.03	0
WL-2 (Dry)	6.76	17.21	46.91	64.12	29.12	0

Negligible amounts of MBr were lost to the atmosphere during the 1st day in the wet profile (WL-1), and only 28.4 % was lost after 7 days following injection. Also, in the case of drier soil system (WL-2), deeper injection resulted in 8.8 % less emission to the atmosphere compared to the shallower injection depth (33 cm) over the first 3 days after injection. Thus, deeper injection is potentially conducive to controlling atmospheric emissions of MBr irrespective of profile wetness.

Effect of Irrigation (Water Dousing of the Bed Surface)

The large initial losses of MBr to the atmosphere were assumed to possibly be minimized by dousing water on the bed just before unrolling and placement of plastic mulch on the bed surface. A numerical experiment was run by simulating

such a situation. This was achieved by modifying the initial conditions for matric suction ($h = -5$ cm) on the top nodal layer of the bed surface. An initial water content of $0.42 \text{ cm}^3 \text{ cm}^{-3}$ (97 % water saturation) on the bed surface was achieved in this way, representing dousing of water compared to the undoused situation ($0.03 \text{ cm}^3 \text{ cm}^{-3}$, 6 % degree of water saturation). Only the top surface of the bed was doused with water (the sides of the bed, and the furrow, were excluded).

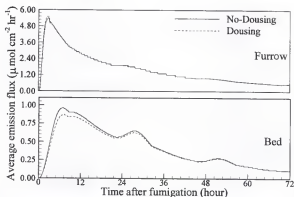


Figure 5-14. Effect of water dousing on the MBr emission fluxes from the soil bed during fumigation.

The results for emission flux for both situations revealed that dousing slightly reduced the emission flux from the bed, but only initially (Fig. 5-14). Dousing saturated the pores of the soil under the plastic mulch with water, thus temporarily blocking MBr gas passage to the atmosphere through the plastic mulch (Fig. 5-15). However, this effect lasted only for a short time in the coarse-textured soil, due to rapid redistribution of water. If the soil were fine-textured, one would expect the

reduction in emission flux to last longer. The material balance (Table 5-12) also showed that, during the 1st day, = 5.4 kg ha⁻¹ of MBr emission losses were prevented

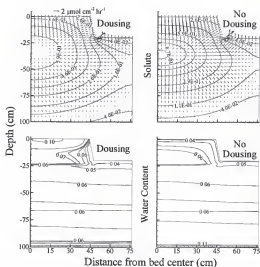


Figure 5-15. Contours of water content, temperature, and MBr concentration with gaseous fluxes of MBr at 9 hours after fumigation under water dousing and no-dousing on the bed-surface.

Table 5-12. Material balance (unit: %) of MBr under water dousing and no-dousing.

Day-1	Total MBr in Profile	Atmospheric Emission Losses			Hydrolyzed	Deep Down-flow
		Bed	Furrow	Total		
No-Dousing	58.55	13.44	21.59	34.73	6.72	0
Dousing	59.14	12.25	21.67	33.92	6.94	0
Day-3						
No-Dousing	23.46	24.56	36.51	61.07	15.46	0
Dousing	23.92	23.48	36.67	60.15	15.93	0

from the bed when the bed surface was doused with water immediately after fumigation.

Fumigation Efficiency Analysis

Effective soil fumigation is achieved when the target pathogen and/or pest is successfully eradicated from the desired soil zones. The primary goal of soil fumigation is to provide a pest-free growing environment to the crop plant in order to obtain economically viable yields. To achieve this goal, an optimum fumigant dosage must be determined. This is crucial when a fumigant such as MBr is not only environmentally hazardous due to its high toxicity to humans but also is detrimental to the atmosphere's ozone layer. The determination of optimum fumigant dosage is expected to depend upon

- 1) Fumigant exposure time and concentration required for eradication of a specific target pathogen and/or pest,
- 2) Level of pathogen and/or pest infestation,
- 3) Soil texture and structure,
- 4) Fumigant fate and transport in soil,
- 5) Desired eradication zones (soil volumes), and
- 6) Extent of sterilized buffer zones (pathogens are mobile and can reenter a sterilized zone again from surrounding uneradicated zones after fumigation).

Mckenry and Hesse (1978) reported that 20 ppm or greater concentration of MBr fumigant for a 24-hr period is required to completely eradicate the 2nd stage of

root knot nematode (RKN) juveniles. A literature search and personal communication with University of Florida nematologists did not reveal additional information on nematotoxic levels and exposure periods for MBr. It was, therefore, decided to use the data from Mckenry and Hesse (1978) as a basis for investigating soil sterilization efficiency for different scenarios. Simulations were conducted for 3-day periods to record 24-hour residence times for concentrations ≥ 10 ppm, ≥ 20 ppm (Mckenry and Hesse, 1978), and ≥ 30 ppm. The 10- and 20-ppm levels were chosen to provide improved insight of eradication patterns if there exists uncertainty in the data reported by Mckenry and Hesse (1978).

To identify the eradication zones for RKN, flood contour plots in the soil bed were used to demarcate those zones which satisfied the conditions of exposure time (24 hrs) for the related level of exposure concentration (≥ 10 ppm, ≥ 20 ppm, and ≥ 30 ppm). Full-bed plots were generated for clarity, using the mirror image of the simulated domain. Figure 5-16a shows the demarcated zones using criterion based on Mckenry and Hesse (1978). No-mulch (A) was observed to be very ineffective and full-mulch (bed plus furrow) (B) the most effective. The current practice of mulching the bed (C) provides adequate sterilization if a single crop row were grown in the center of the bed. The same may become inadequately sterilized if the crops were grown in two rows on the same bed, however. It was very clear, from this analysis, that deep injection in either dry or wet soil does not provide adequate soil sterilization in the root zone where it is desired (Fig. 5-16: a).

The analysis provided different results (Fig. 5-16: b) when the required MBr exposure concentration for RKN eradication was changed to concentrations ≥ 10

ppm. The eradication zone under no-mulch increased substantially, though it still remained inadequate. In all other cases, eradication increased substantially to provide excellent sterilization except for case (E), which remained inadequate. A single-row crop seemed feasible in case (D), which received adequate sterilization with exposure concentrations of ≥ 10 ppm (Fig. 5-16: b).

Lastly, the analysis for exposure concentrations ≥ 30 ppm showed (Fig. 5-16: c) that adequate sterilization was not achieved in any of the cases, implying that the soil bed was under-fumigated (at the rate of 450 kg ha^{-1}). This exercise reveals that reliable information on toxic concentration levels along with exposure-time levels is very necessary to correctly estimate fumigant dosages. Information on pathogen mobility is also required, to determine the size of buffer zones so that a correct estimation of soil zones and/or volumes (in the case of spot treatments for orchard plantings) requiring sterilization can be made.

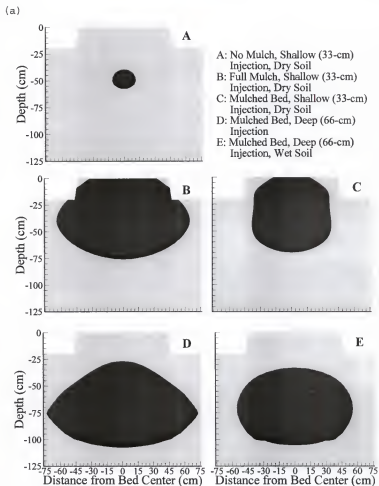


Figure 5-16 Soil sterilization zones for different scenarios 3 days after MBr fumigation using different criteria.
 a) MBr concentration ≥ 20 ppm for 24 hrs (Mckenry and Hesse, 1978);
 b) MBr concentration ≥ 10 ppm for 24 hrs;
 c) MBr concentration ≥ 10 ppm for 24 hrs.

(b)

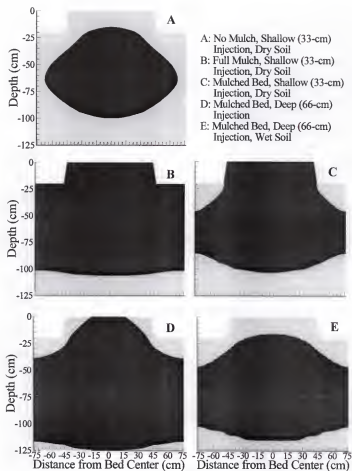


Figure 5-16—continued

(c)

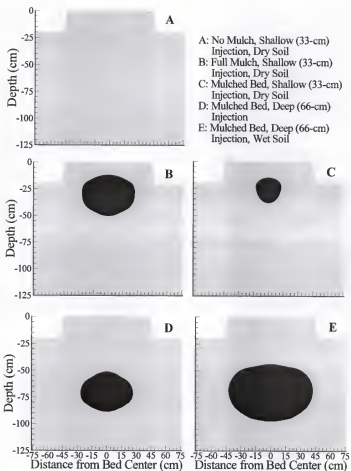


Figure 5-16—continued

Hydrolysis of MBr (Sensitivity Analysis)

Information on the rate of MBr hydrolysis in Florida soils is lacking. It is expected that sandy soils will have lower hydrolysis rates compared to fine textured soils and soils with higher organic matter. Three-day simulations were conducted for three rates of hydrolysis which were; 1) 0.014 hr^{-1} (HR-1), 2) 0.007 hr^{-1} (HR-2), and 3) 0.0035 hr^{-1} (HR-3). HR-1 represents a value for Yolo loam soil from California (Rolston and Glauz, 1982). The effect of different rates of hydrolysis on material balance of MBr reflected that model simulations are very sensitive to this input parameter (Fig. 5-17). Material balance showed that over a period of 3 days an amount of 69.6 kg ha^{-1} , 37.5 kg ha^{-1} , and 19.5 kg ha^{-1} of MBr was hydrolyzed, respectively, for HR-1, HR-2, and HR-3. The amount of material hydrolyzed showed a linear relation with the hydrolysis rate coefficient (Fig. 5-17). Thus the results indicate that both the water saturation of the soil and the hydrolysis rate coefficient play significant roles in determining the fate and transport of MBr fumigant.

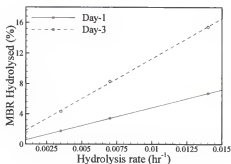


Figure 5-17. Loss of MBR (unit: %) under different rates of hydrolysis of MBr.

Diurnal Water and Heat Dynamics in a Plastic Covered Soil Bed

Interactions of the soil surface with overlying atmosphere due to solar radiation, evaporation, and wind cause disturbances in the system by altering the thermal regime and water content. For a soil system at static equilibrium with respect to water content and heat, a change in boundary conditions controlling the thermal or hydraulic state of the medium causes the system to adjust in a transient unsteady state manner both in water and heat if the flows of water and heat are assumed to be coupled.

The effects of overlying atmosphere on the bed system were analyzed for a period of 24 hrs starting at 12:00 noon on the second day after fumigant injection and mulch application in cases of both initially 'wet' and 'dry' soils. Figure 5-18: a-c and Fig. 5-19: a-c present the cases of a wet soil and a dry soil, respectively. Simulated data exhibiting the contours of water content and temperature along with flux vectors of water, vapor, and heat are presented in these figures for time intervals of 3 hr depicting the status and system dynamics in the bed. Flux vectors for the heat, water, and vapor on the upper boundary nodes are suppressed as these were controlled by imposed boundary conditions.

Patterns of thermal energy distributions were similar in both wet and dry soils (Fig. 5-18: a, Fig. 5-19: a) over the diurnal period. Diurnal temperature amplitudes were greater for unmulched furrow surfaces than for the mulched bed surfaces both under wet and dry soils. The bedded soil surface under mulch showed smaller temperature amplitude because of a 0.5 cm air gap assumed to exist

between the soil surface and mulch. This resulted in contact resistance which impeded the flow of thermal energy and thus caused insulation of soil under the bed (Ham and Kluitenberg, 1994). The assumption of a 0.5 cm air gap was realistic for field conditions since perfect contact (0 cm air gap) between the mulch and soil surface is never obtained due to surface roughness of the soil. However, the actual temperature of the plastic mulch was higher than the underlying soil surface during the day (data not shown). Black plastic has a high absorbance (0.96) and a very low transmittance (0.01) and reflectance (0.03) (Table 2.2). In conditions where the air gap is practically zero, the soil surface and mulch would have similar temperatures (Ham and Kluitenberg, 1994). Whereas, the behavior of the system (i.e., interactions of soil surface with plastic mulch) is entirely opposite for a clear plastic mulch. The high transmittance (0.84) for clear plastic permits direct heating of the soil surface resulting in high temperatures. With an air gap between the surface and mulch, flow of thermal energy back to the atmosphere is impeded. Thus the soil surface beneath a clear plastic mulch (with some air gap in between) would show higher temperatures during daytime hours. However, with no air gap, the soil surface mulched with black plastic would show higher temperatures because of higher absorbance than the clear plastic.

Thermal energy fluxes were in general inward to the soil system during the day time (due to input of solar radiation energy) and outward to the atmosphere during the night time at the surface. To be noted in Fig. 5-18: a and Fig. 5-19: a are the presence of 'hot spots' (closed contours regions, Fig. 5-18: a and Fig. 5-19: a; 12:00 PM to 9:00 AM) that develop in the upper corners of the beds. This was due to

larger exposure area towards the edges which had higher energy levels flowing in and out. Location of the hot spots differed slightly between the wet and dry soils. As thermal conductivity is greatly affected by water content, lower conductivity in a dry soil would result in lesser dissipation of thermal energy being exhibited by higher temperature. For this reason hot spots in the dry soil showed slightly higher temperatures than the ones in wet soil.

Liquid water movement in the wet soil under the bed was mostly downward due to gravitational drainage. However, under the furrow surface it was both downward and upward for the depths depending upon time of the day (Fig. 5-18: b). Upward liquid water movement in the furrow occurred as a result of atmospheric evaporative demand. Loss of water due to evaporation generated high matric suction at the surface allowing liquid water to move in response to potential gradients overcoming thermal gradients. The fluxes were higher near the surface in response to higher evaporative demand during peak solar radiation hours (12:00 AM and 3:00 PM) which subsequently reduced during cooler atmospheric periods.

A similar behavior was observed for liquid water movement in dry soil in the furrow (Fig. 5-19: b). However, the spatial pattern for flow of liquid water differed both beneath the bed and furrow in that it was mostly upward in the dry soil. This was due to lower matric potentials in the upper profile in the dry soil. The magnitude of the liquid water flux was ten fold (see the reference vectors in Fig. 5-18: b and Fig 5-19: b) smaller in the dry soil.

The system behavior is also influenced by the vapor movement in response to thermal energy (as vapor movement, water movement and heat flow are highly

coupled). Vapor water losses to the atmosphere occurred only from the unmulched furrow surface. Both downward and upward movement of vapor was observed in wet and dry soils (Fig. 5-18: c and Fig. 5-19: c). The pattern was generally similar except for the magnitude of fluxes. During the day time the vapor fluxes (excluding the evaporative fluxes from the top layer which were imposed as boundary conditions in the solution of flow equations and hence not shown in the figures) were primarily downward due to heating of the uppermost soil layer. The magnitude of these fluxes were highest during the peak solar radiation hours (corresponding to the times 12:00 AM-3:00 PM as shown in Fig. 5-18: c and Fig. 5-19: c). Direction reversal of flux vectors occurred during the night time when the upper soil profile cooled and the deeper soil profile remained warm. During these periods, the vapor fluxes were upward. Also to be noted in conjunction with Figs. 5-18: a and 5-19: a (showing thermal status) is that vapor fluxes coincided with hot spots near the bed edges. A transitional phase occurred around 9:00 AM (Fig. 5-18: c and Fig. 5-19: c) when the upper soil surface began warming due to the onset of solar radiation. During this period the fluxes from the upper soil region were downward and fluxes from still warm lower region were upward. The coalescence of this fluxes occurred at a depth of 25-30 cm in the simulation results (Fig. 5-18: c and Fig. 5-19: c).

This analysis reveals the complex nature of system behavior and dynamics under a plastic mulched soil bed during diurnal periods. However, the actual behavior would depend upon the specific soil system under consideration (such as soil type and layering within the soil, water saturation, winter versus summer

weather conditions, plastic material, etc). In a closed soil column system in the laboratory the non-isothermal and coupled flow is easy to demonstrate (for e.g. Fig. 4-3) where different constant temperatures can be imposed at opposite ends of the column for long periods. In an open field system such as plastic mulched bed where the boundary conditions change diurnally, the effects are imperceptible and masked due to system driving towards a state of equilibrium with the open surroundings. A field system is also more complex due to inherent heterogeneity of the soil system (such as layering present in the soil used in model simulations). This results in variable hydraulic and thermal characteristics of the soil medium exhibiting differences in porosity (affecting vapor movement), differences in water contents for the similar potential (affecting water movement), and differences in soil texture, structure and mineralogy (affecting heat capacity and thermal conductivity). Given the complexities of such a system, inference can be drawn that the fate and transport of volatile chemicals would definitely be influenced by interactions of water, vapor, and heat in such a system.

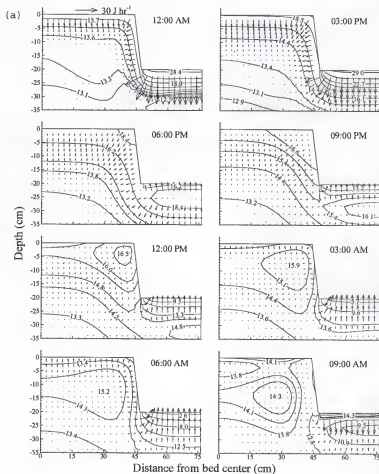


Figure 5-18 Diurnal water and heat dynamics in a mulched bed for a wet soil.
 a) Contours of temperature ($^{\circ}C$) and heat flux vectors ($J hr^{-1}$);
 b) Contours of liquid water content ($cm^3 cm^{-3}$) and water flux vectors ($cm hr^{-1}$);
 c) Contours of liquid water content ($cm^3 cm^{-3}$) and vapor flux vectors ($mg cm^{-2} hr^{-1}$).

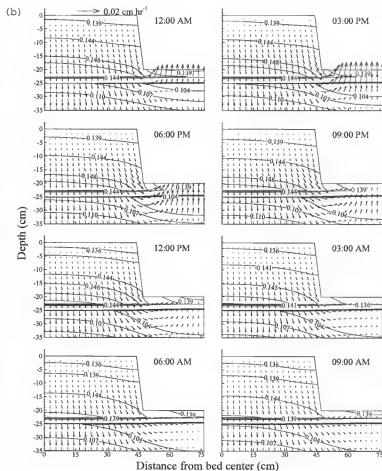


Figure 5-18—continued

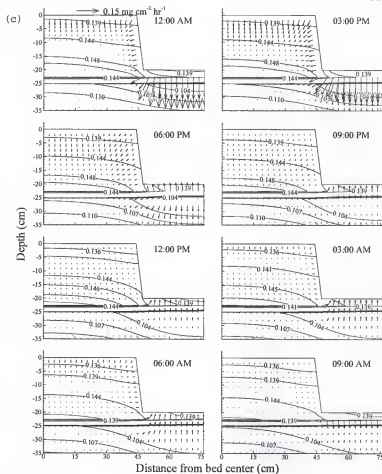


Figure 5-18—continued

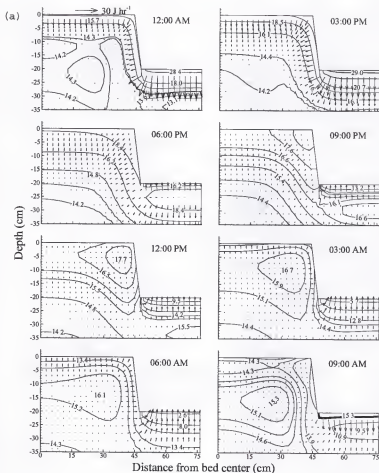


Figure 5-19 Diurnal water and heat dynamics in a mulched bed for a dry soil.
 a) Contours of temperature ($^{\circ}\text{C}$) and heat flux vectors (J hr^{-1});
 b) Contours of liquid water content ($\text{cm}^3 \text{cm}^{-3}$) and water flux vectors (cm hr^{-1});
 c) Contours of liquid water content ($\text{cm}^3 \text{cm}^{-3}$) and vapor flux vectors ($\text{mg cm}^{-2} \text{hr}^{-1}$).

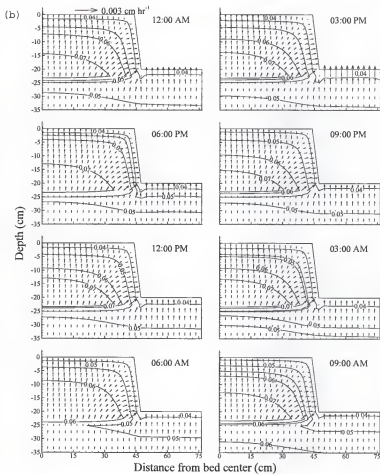


Figure 5-19—continued

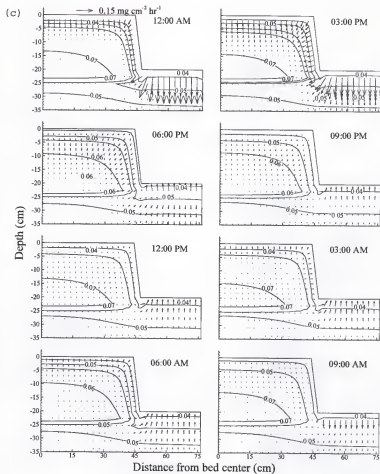


Figure 5-19—continued

Summary and Conclusions

A numerical investigation including sensitivity analysis was conducted using a coupled heat-water and solute transport model developed in the present work, to analyze the fate and transport of MBr during fumigation of soil beneath plastic-mulched beds. The investigation provided improved insight into the dynamics of MBr fumigation in relation to critical management and environmental impacts. Specific observations made during this investigation include:

1. A need exists for improved determination of diffusion coefficients for MBr diffusion through plastic mulch under field conditions. Use of lab-measured data for field simulations under predicted MBr emission losses implies that polyethylene-plastic mulch is relatively effective in controlling atmospheric losses of MBr. However, this result is in direct contradiction to reported field studies from the scientific literature.
2. Non-isothermal soil conditions were shown to be especially important to solute transport in plastic-mulched soil beds, particularly in cases where highly volatile chemicals like MBr are used for soil fumigation.
3. A wetter soil profile was shown to retain more (approximately 10-20 % depending on injection depth over 3 day period) MBr than a drier one, due to partitioning into water, but also to result in more bromide production due to increased hydrolysis. Higher wetness of the soil restricted the MBr passageway from spreading quickly. Substantial reductions (approximately

23-36 % depending on injection depth over 3 day period) in MBr emission losses to the atmosphere were observed due to higher water-saturation of the soil.

4. Deeper injection (66 cm) of MBr fumigant provided less (approximately 10 and 23 % in dry and wet soil, respectively) emission losses to the atmosphere, irrespective of soil wetness, than a shallow injection zone (33 cm).
5. Fumigant efficiency analysis based upon Mckenry and Hesse (1978) data for nematotoxic concentration and exposure time for root knot nematode showed that current practice of MBr fumigation and dosage used (450 kg ha^{-1}) provides adequate soil sterilization in the crop root zone of the bed. However, it was also revealed that deeper injection (66 cm) is not conducive for sterilization of the crop root zone even though it is environmentally less hazardous. Such analysis is site-specific, and does not apply to general recommendations.
6. For a sandy soil, dousing of water on the soil bed immediately after injection and before placing the plastic mulch was shown to slightly decrease MBr emission losses to the atmosphere, by sealing off the soil pores to gaseous diffusion during the initial hours after mulch placement. Dousing of finer-textured soil would be expected to provide more effective control of MBr emissions.
7. Utilizing a slightly wet profile, a slightly deeper injection zone, and dousing water on the surface of the bed offers potential fumigant management opportunities to decrease MBr atmospheric losses.

8. Information on hydrolysis of MBr in Florida soils is lacking. Sensitivity analysis showed that a linear relation of hydrolysis rate occurred with the amount of MBr hydrolyzed. This information is critical for improved estimation of MBr fate and transport in wet soils.
9. Information on pathogen toxic concentration and exposure time is quite limited. This information is very important to optimize fumigant dosage in order to achieve effective soil sterilization and avoid environmental hazards through over-fumigation.
10. Decreased atmospheric emission of MBr due to improved fumigant management in agricultural soils may result in greater MBr retention by soils and ultimate decomposition to bromide ions during hydrolysis. However, this may undesirably increase bromide concentration in crops and groundwater over long periods of time.
11. Carefully-controlled field experiments are needed to validate conclusions based upon the model simulations.
12. Results from model simulations provide improved insight of system dynamics, as needed in the design of future field experiments.

APPENDIX A
SOIL MOISTURE FLOW

The total mass of water in the system may be defined as

$$\rho_L M^w = \rho_L \theta_L + \rho_v \theta_a ; \quad M^w = \theta_L + \frac{\rho_v}{\rho_L} \theta_a \quad [A-1]$$

where M^w represents the total water (liquid + vapor) storage. The liquid is assumed here to be incompressible.

The liquid water flux for an isotropic unsaturated media is defined by Darcy's equation as

$$\frac{q_L}{\rho_L} = -K \nabla h - K k \quad [A-2]$$

Equation [A-2] applies to media with properties either constant/or continuously varying in space.

An intuitive extension of Fick's law applied to porous media for vapor water flow (Philip and de Vries, 1957) can be expressed as

$$q_v = -D_a \nu \tau_a \theta_a \nabla \rho_v \quad [A-3]$$

where ν is a mass flow factor and τ_a is tortuosity of the air-filled pore space. Water vapor distribution in the air phase is found to be (Edlefsen and Anderson, 1943)

$$\rho_v = \rho_o R_h = \rho_o (T) \exp\left(\frac{h g_a}{R_u T}\right) \quad [A-4]$$

where ρ_o is saturation water vapor density over a free water surface, R_h is relative

humidity, and g_s is the acceleration of gravity. Equation [A-4] is based on the assumption of thermodynamic equilibrium between the liquid and vapor phases and is valid for the natural system.

Expanding $\rho_v(h, T)$ in Eq. [A-3] and with v being generally reported as unity, it follows that

$$q_v = -D_s \tau_s \theta_s \left[\frac{\partial \rho_v}{\partial h} \Big|_T \nabla h + \frac{\partial \rho_v}{\partial T} \Big|_h \nabla T \right] \quad [\text{A-5}]$$

Introducing a correction factor for 'liquid islands' and the temperature gradient differences between the whole media and the air-filled pores as described by Philip and de Vries (1957) leads to

$$q_v = -D_s \tau_s \theta_s \frac{\partial \rho_v}{\partial h} \Big|_T \nabla h - D_s (\theta_s + \theta_L) \frac{\partial \rho_v}{\partial T} \Big|_h \xi \nabla T; \quad \xi = \frac{(\nabla T)_s}{\nabla T} \quad [\text{A-6}]$$

where $(\nabla T)_s$ is the average temperature gradient in the air phase.

For generalizing over a range of θ_L values, where the liquid phase is continuous, the quantity $(\theta_s + \theta_L)$ in Eq. [A-6] is replaced by $(\theta_s + f \theta_L)$, where f goes to zero as θ_s goes to zero. The form of f is linear with θ_s in this regime. This leads to

$$\begin{aligned} q_v &= -D_s \tau_s \theta_s \frac{\partial \rho_v}{\partial h} \Big|_T \nabla h - D_s f \xi \frac{\partial \rho_v}{\partial T} \Big|_h \nabla T \\ \Rightarrow q_v &= -\rho_L D_{hv} \nabla h - \rho_L D_{Tv} \nabla T \end{aligned} \quad [\text{A-7}]$$

where

$$D_{hv} = \frac{D_s}{\rho_L} \tau_s \theta_s \frac{\partial \rho_v}{\partial h} \Big|_T, \quad D_{Tv} = \frac{D_s}{\rho_L} f \xi \frac{\partial \rho_v}{\partial T} \Big|_h$$

$$\theta (= \theta_s + \theta_L) \text{ for } \theta_s \leq \theta_k, \quad f = \theta_s + \frac{\theta_s}{\theta_L - \theta_k} \theta_L \text{ for } \theta_s > \theta_k$$

The total mass flux can be defined as

$$\begin{aligned} \frac{q_w}{\rho_L} &= \frac{q_L}{\rho_L} + \frac{q_v}{\rho_L} \\ \rightarrow \frac{q_w}{\rho_L} &= -K \nabla h - Kk - D_{hv} \nabla h - D_{Tv} \nabla T \rightarrow \frac{q_w}{\rho_L} = -(K + D_{hv}) \nabla h - D_{Tv} \nabla T - Kk \end{aligned} \quad [A-8]$$

The continuity equation of water mass now can be stated as

$$\frac{\partial}{\partial t} \left(\theta_L + \frac{\rho_v}{\rho_L} \theta_s \right) = \nabla \cdot \left[(K + D_{hv}) \nabla h + D_{Tv} \nabla T + Kk \right] \quad [A-9]$$

with,

$$\frac{\partial}{\partial t} (\theta_L + \theta_s) = 0 \rightarrow \frac{\partial \theta_s}{\partial t} = -\frac{\partial \theta_L}{\partial t}, \quad \frac{\partial}{\partial t} \left(\frac{\rho_v}{\rho_L} \theta_s \right) = \frac{\rho_v}{\rho_L} \frac{\partial \theta_s}{\partial t} + \frac{\theta_s}{\rho_L} \frac{\partial \rho_v}{\partial t} \quad [A-10]$$

it follows that,

$$\left(1 - \frac{\rho_v}{\rho_L} \right) \frac{\partial \theta_L}{\partial t} + \frac{\theta_s}{\rho_L} \frac{\partial \rho_v}{\partial t} = \nabla \cdot \left[(K + D_{hv}) \nabla h + D_{Tv} \nabla T + Kk \right] \quad [A-11]$$

Considering that $\theta_L = \theta_L(h, T)$ and $\rho_v = \rho_v(h, T)$, it is seen that

$$\frac{\partial \theta_L}{\partial t} = \frac{\partial \theta_L}{\partial h} \frac{\partial h}{\partial t} + \frac{\partial \theta_L}{\partial T} \frac{\partial T}{\partial t}, \quad \frac{\partial \rho_v}{\partial t} = \frac{\partial \rho_v}{\partial h} \frac{\partial h}{\partial t} + \frac{\partial \rho_v}{\partial T} \frac{\partial T}{\partial t} \quad [A-12]$$

Substituting Eq. [A-12] into Eq. [A-11] and considering the effect of heat of wetting

(Kay and Groenevelt, 1974) on the pressure-head field and resulting flow leads to

$$\begin{aligned} & \left[\left(1 - \frac{\rho_v}{\rho_L} \right) \frac{\partial \theta_L}{\partial h} \Big|_T + \frac{\theta_s}{\rho_L} \frac{\partial \rho_v}{\partial h} \Big|_T \right] \frac{\partial h}{\partial t} + \left[\left(1 - \frac{\rho_v}{\rho_L} \right) \frac{\partial \theta_L}{\partial T} \Big|_h + \frac{\theta_s}{\rho_L} \frac{\partial \rho_v}{\partial T} \Big|_h \right] \frac{\partial T}{\partial t} \\ & = \nabla \cdot \left[(K + D_{hv}) \nabla h + (D_{Tv} + D_{Ts}) \nabla T + Kk \right] \end{aligned} \quad [A-13]$$

where D_{Ts} is a transport coefficient for adsorbed liquid (film) flow due to thermal gradients. However, in sandy soils with the specific surface area being comparatively very low, heat of wetting can be safely neglected as shown by Milly and Eagleson (1980) to obtain the form of Eq. [3.1] which was given in Chapter-3.

APPENDIX B
SOIL HEAT FLOW

The total flux of sensible and latent heat in a porous medium, considering convection of air and radiative heat transfer negligible, is given by de Vries (1958) as

$$q_h = -\lambda \nabla T + L_0 q_v + C_v (T - T_0) q_v + C_L (T - T_0) q_L \quad [B-1]$$

in which λ accounts for the Fourier heat diffusion.

From basic thermodynamic relationships it is observed that

$$L_0 + C_v (T - T_0) = L + C_L (T - T_0) \Rightarrow L_0 = L + C_L (T - T_0) - C_v (T - T_0)$$

which gives

$$q_v L_0 = q_v L + C_L (T - T_0) q_v - C_v (T - T_0) q_v \quad [B-2]$$

Substituting Eq. [B-2] into Eq. [B-1] leads to

$$q_h = -\lambda + L q_v + C_L (T - T_0) q_w \quad ; \quad q_w = q_L + q_v \quad [B-3]$$

Including advection of the heat of wetting due to pressure-head gradients (Groenevelt and Kay, 1974), and substituting Eq. [A-7] for q_w , it follows that

$$\begin{aligned} q_h &= -\lambda - L \rho_L (D_{hv} \nabla h + D_{Tv} \nabla T) + \rho_L g_s T D_{Ts} \nabla h + C_L (T - T_0) q_w \\ &\Rightarrow q_h = -(\lambda + L \rho_L D_{Tv}) \nabla T - \rho_L (L D_{hv} + g_s T D_{Ts}) \nabla h + C_L (T - T_0) q_w \\ &\Rightarrow q_h = -\lambda^* \nabla T - \rho_L (L D_{hv} + g_s T D_{Ts}) \nabla h + C_L (T - T_0) q_w \end{aligned} \quad [B-4]$$

where λ^* accounts for the combined effect of simple Fourier heat diffusion and latent heat transport by temperature-induced vapor diffusion.

The bulk volumetric heat content of the porous medium, H , is given by

$$H = C_d(T - T_0) + L_0 \rho_v \theta_s + C_v \rho_v \theta_s (T - T_0) + C_L \rho_L \theta_L (T - T_0) - \rho_L \int_{t_0}^t W \frac{d\theta_L}{dt} dt \quad [B-5]$$

$$-H = (C_d + C_L \rho_L \theta_L + C_v \rho_v \theta_s)(T - T_0) + L_0 \rho_v \theta_s - \rho_L \int_{t_0}^t W \frac{d\theta_L}{dt} dt$$

This equation assumes local thermal equilibrium among soil particles, the water, and the air.

Equating the change in stored energy, Eq. [B-5], to the sum of the convergence of the heat flux, Eq. [B-4], yields

$$\left(C + H_1 \frac{\partial \rho_v}{\partial T} \Big|_h + H_2 \frac{\partial \theta_L}{\partial T} \Big|_h \right) \frac{\partial T}{\partial t} + \left(H_1 \frac{\partial \rho_v}{\partial h} \Big|_T + H_2 \frac{\partial \theta_L}{\partial h} \Big|_T \right) \frac{\partial h}{\partial t} = \nabla \left[\lambda \nabla T + \rho_L (L D_{hv} + g_s T D_{Ts}) \nabla h - C_L (T - T_0) q_w \right] \quad [B-6]$$

where $C = C_d + C_L \rho_L \theta_L + C_v \rho_v \theta_s$, $H_1 = [L_0 + C_v (T - T_0)] \theta_s$,
 $H_2 = (C_L \rho_L - C_v \rho_v) (T - T_0) - \rho_L W - \rho_v L_0$

W , the differential heat of wetting (de Vries, 1958; Edlefsen and Anderson, 1943) is defined as

$$W = -j^{-1} g_s \left(h - T \frac{\partial h}{\partial T} \Big|_0 \right) \quad [B-7]$$

in which j is a conversion factor relating mechanical work to thermal energy. The quantity W is the amount of heat released per unit mass of added water when an infinitesimal quantity of free liquid water is added to the medium. In sandy soils, surface area being small, the heat of wetting can be neglected to give the form of Eq. [3.2] presented in Chapter-3.

APPENDIX C
CHEMICAL TRANSPORT

Šimůnek et al. (1992) and Šimůnek and van Genuchten (1994) presented equations for solute fate and transport assuming that solutes can exist in all three phases (liquid, solid, and gaseous) and that the decay and production processes are different in each case. Non-equilibrium solute transport was considered to be caused by the kinetic sorption on some (or all) of the soil sorption sites. Solutes were considered to be transported by three different mechanisms: by convection and dispersion in the liquid phase, and by diffusion in the gas phase. Following their approach, which is relatively general, the governing Eqs. [3.4], [3.5] were formulated. Non-equilibrium interaction between the solution (c) and adsorbed (s) concentrations of solutes, and equilibrium interaction between the solution (c) and gas (g) concentrations, can be assumed for solutes in the soil system. Following Šimůnek and van Genuchten (1994), the adsorption isotherm relating s_i and c_i (where i designates the specie number) can be described via a general nonlinear empirical equation

$$s_i = \frac{k_{d,i} c_i^{\beta_i}}{1 + \eta_i c_i^{\beta_i}} ; \quad i = 1, \dots, n_s$$

$$-\frac{\partial s_i}{\partial t} = \frac{k_{d,i} \beta_i c_i^{\beta_i - 1}}{(1 + \eta_i c_i^{\beta_i})^2} \frac{\partial c_i}{\partial t} + \frac{c_i^{\beta_i}}{1 + \eta_i c_i^{\beta_i}} \frac{\partial k_{d,i}}{\partial t} - \frac{k_{d,i} c_i^{2\beta_i}}{(1 + \eta_i c_i^{\beta_i})^2} \frac{\partial \eta_i}{\partial t} \quad [C-1]$$

$$+ \frac{k_{d,i} c_i^{\beta_i} \ln c_i}{(1 + \eta_i c_i^{\beta_i})^2} \frac{\partial \beta_i}{\partial t} ; \quad i = 1, \dots, n_s$$

where $k_{d,i}$, β_i , and η_i are empirical constants. The Freundlich, Langmuir, and linear adsorption equations are special cases of Eq. [C-1]. When $\beta_i = 1$, Eq. [C-1] becomes the Freundlich equation, and when both $\beta_i = 1$ and $\eta_i = 0$, Eq. [C-1] there results a linear adsorption isotherm. Solute transport without adsorption is described when $k_{d,i} = 0$.

The concept of two reaction sites on soil surfaces (van Genuchten and Wagnert, 1969) assumes that sorption sites can be divided into two fractions as

$$s_i = s_i^e + s_i^k ; \quad i = 1, \dots, n_s \quad [C-2]$$

Sorption on the first fraction, s_i^e , is assumed to be instantaneous, while sorption on the second (remaining) fraction, s_i^k , is considered to be time-dependent. At equilibrium, for Type-1 (equilibrium) and Type-2 (kinetic) sites, it follows that

$$s_i^e = f_r s_i, \quad s_i^k = (1 - f_r) s_i ; \quad i = 1, \dots, n_s \quad [C-3]$$

where f_r is the fraction of sorption sites assumed to be at equilibrium with the solution. The time dependence of Type-1 sites represents the sorption on these sites as

$$\frac{\partial s_i^e}{\partial t} = f_r \frac{\partial s_i}{\partial t} ; \quad i = 1, \dots, n_s \quad [C-4]$$

The transfer of mass from the solution to Type-2 sorption sites can be described by a first-order kinetic sorption law. The mass balance for Type-2 sites then becomes

$$\frac{\partial s_i^k}{\partial t} = \omega_i \left[(1 - f_r) \frac{K_{d,i} C_i^{\beta_i}}{1 + \eta_i C_i^{\beta_i}} - s_i^k \right] - \mu_{s,i} s_i^k + (1 - f_r) V_{s,i} ; \quad i = 1, \dots, n \quad [C-5]$$

where ω_i is the first-order rate adsorption constant for the i^{th} solute.

The concentrations g_i (gaseous) and c_i (solution) can be related by a linear relation as

$$g_i = k_{g,i} c_i; \quad i = 1, \dots, n_s \quad [C-6]$$

where $k_{g,i}$ is an empirical constant equal to $(K_H R_u T)^{-1}$ (Stumm and Morgan, 1981), where K_H is obtained from Henry's Law.

Substituting Eqs. [C-1] through [C-6] and the continuity equation describing flow of liquid water in a variably saturated medium

$$\frac{\partial \theta_L}{\partial t} = -\nabla q_L \quad [C-7]$$

into Eqs. [3.4] and [3.5] yields

$$\theta_L R_i \frac{\partial c_i}{\partial t} + q_L \nabla c_i - \nabla (\theta_L D_i \nabla c_i) - T_i^f c_i - G_i = 0; \quad i = 1, \dots, n_s \quad [C-8]$$

The effective dispersion coefficient tensor D_i can be described as

$$\theta D_i = \theta_L D_i^L + \theta_a D_i^g k_{g,i}; \quad i = 1, \dots, n_s \quad [C-9]$$

The coefficients T_i^f and G_i in Eq. [C-8] are defined as

$$T_i^f c_i = -(\mu_{L,i} + \mu_{L,i}^*) \theta_L - (\mu_{s,i} + \mu_{s,i}^*) \rho f_r \frac{k_{a,i} c_i^{\beta_i - 1}}{1 + \eta_i c_i^{\beta_i}} - (\mu_{s,g} + \mu_{s,g}^*) \theta_a k_{g,i} + k_{g,i} \frac{\partial \theta_L}{\partial t} - \theta_a \frac{\partial k_{g,i}}{\partial t}; \quad i = 1, \dots, n_s \quad [C-10]$$

$$G_i(c_i) = \gamma_{L,i} \theta_L + \gamma_{g,i} f_r \rho + \gamma_{a,i} \theta_a - \omega_i \rho \left[\frac{(1-f_r) k_{s,i} c_i^{\beta_i}}{1 + \eta_i c_i^{\beta_i}} - s_i^k \right] - g_i(c_i) \quad [C-11]$$

$$G_i(c_i) = \left(\mu_{L,i-1}^* \theta_L + \mu_{S,i-1}^* f_r \rho_b \frac{k_{d,i-1} c_i^{\beta_{i-1}-1}}{1 + \eta_{i-1} c_i^{\beta_{i-1}}} + \mu_{G,i-1} \theta_a k_{g,i-1} \right) c_{i-1} - g_i(c_i) +$$

$$Y_{L,i} \theta_L + Y_{S,i} f_r \rho_b + Y_{G,i} \theta_a - \omega_i \rho_b \left[\frac{(1-f_r) k_{d,i} c_i^{\beta_i}}{1 + \eta_i c_i^{\beta_i}} - s_i^k \right]; \quad i = 2, \dots, n_s \quad [C-12]$$

where g_i is defined as

$$g_i(c_i) = \rho_b f_r \left[\frac{c_i^{\beta_i}}{1 + \eta_i c_i^{\beta_i}} \frac{\partial k_{d,i}}{\partial t} - \frac{k_{d,i} c_i^{2\beta_i}}{(1 + \eta_i c_i^{\beta_i})^2} \frac{\partial \eta_i}{\partial t} + \frac{k_{d,i} \ln c_i c_i^{\beta_i}}{(1 + \eta_i c_i^{\beta_i})^2} \frac{\partial \beta_i}{\partial t} \right];$$

$$i = 1, \dots, n_s \quad [C-13]$$

The retardation factor R_i is defined as

$$R_i(c_i) = 1 + \frac{\rho_b}{\theta_L} \frac{f_r k_{d,i} \beta_i c_i^{\beta_i-1}}{(1 + \eta_i c_i^{\beta_i})^2} + \frac{\theta_a k_{g,i}}{\theta_L}; \quad i = 1, \dots, n_s \quad [C-14]$$

In order to solve Eq. [C-10], it is necessary to know the liquid water content and the volumetric flux. Both variables are obtained the solutions of the modified Philip and de Vries equation. If it is assumed that μ_L^* , μ_S^* , μ_G^* , η_i , and k_{g_i} are equal to zero, and that f_r and β_i are equal to one, the entire system of Eqs. [3.4], [3.5], and [C-1] through [C-14] simplifies into a system of mutually-independent solutions as described by Šimůnek et al. (1992). The components of the dispersion tensor in the liquid phase, D^L , were given by Bear (1972) as

$$\theta_L D^L = D_T |q_L| \delta_{ij} + (D_L - D_T) \frac{q_{Lj} q_{Li}}{|q_L|} + \theta_L D_w \tau_w \delta_{ij} \quad [C-15]$$

where D_w is the molecular diffusion coefficient in free water, τ_w is a tortuosity factor in the liquid phase, $|q|$ is the absolute value of the fluid flux density, δ_{ij} is the Kronecker delta function ($\delta_{ij} = 1$ if $i = j$, and $\delta_{ij} = 0$ if $i \neq j$), and D_L and D_T are the

longitudinal and transverse dispersivities, respectively. After adding the diffusion contribution from the gas phase, the individual components of the effective dispersion tensor in the soil matrix for two-dimensional transport are as follows

$$\begin{aligned} \theta D_{xx} &= D_L \frac{q_{Lx}^2}{|q_L|} + D_T \frac{q_{Lz}^2}{|q_L|} + \theta_L D_w \tau_w + \theta_s D_g k_g \tau_s \\ \theta D_{zz} &= D_L \frac{q_{Lz}^2}{|q_L|} + D_T \frac{q_{Lx}^2}{|q_L|} + \theta_L D_w \tau_w + \theta_s D_g k_g \tau_s \\ \theta_L D_{xz} &= (D_L - D_T) \frac{q_{Lx} q_{Lz}}{|q_L|} \end{aligned} \quad [C-16]$$

where D_g is the molecular diffusion coefficient in the gas phase and τ_s is the tortuosity factor in the gas phase

$$\tau_w = \frac{\theta_L^{7/3}}{\theta_s^2} \quad \text{and} \quad \tau_s = \frac{\theta_s^{7/3}}{\theta_L^2} \quad [C-17]$$

APPENDIX D NUMERICAL APPROACH

The Finite Element Method presented here follows the methodology given by Istok (1989) and Segerlind (1984). A short description of the method as related to the present work is presented here. A more detailed and complete description of the method can be found in Pinder and Gray (1977), Segerlind (1984), and Istok (1989).

The first step in the solution of a water/heat flow or solute-transport problem by the finite-element method is to discretize the problem domain (the soil profile). Discretization is done by replacing the problem domain with a collection of nodes and elements referred to as the finite-element mesh. Different element types are available for one-, two-, and three-dimensional problems, and also for problems with axisymmetry. Elements may be of any size, the size and shape of each element in the mesh can be different, and several different types of elements can be used in a single mesh. Values of the material properties are usually assumed to be constant within each element, but are allowed to vary from one element to the next.

When preparing the finite-element mesh it is important to remember that the precision of the solution obtained and the level of computational effort required to obtain a solution are determined to a great extent by the number of nodes in the mesh. A coarse mesh has a smaller number of nodes and will give a lower precision than a fine mesh. However, the larger the number of nodes in the mesh, the greater will be the required computational effort and cost.

Each node in the mesh is assigned a unique node number with no skips in-between. The nodes are then assigned a set of nodal coordinates. These could be (x) , (x,y) , (x,y,z) , or (r,z) coordinates of the nodes. The nodes have to be numbered in a fashion so as to minimize the semi-bandwidth (SBW) of the matrix for the resulting system of linear equations. When the SBW is large and the system of equations is operated on in matrix form, the storage capacity of current desktop computers can be easily exceeded. The SBW for any mesh can be computed from: $SBW = R^{node} + 1$, where R^{node} is the maximum difference between any two node numbers within a single element in the mesh.

The Method of Weighted Residuals

The second step in solving the governing flow or transport equation involves deriving an integral formulation. This integral formulation leads to a system of algebraic equations that can be solved for the values of the field variables (h , T or c for this work).

In the method of weighted residuals, an approximate solution to the boundary- or initial-value problem is defined. When this approximate solution is substituted into the governing differential equation, an error or residual occurs at each point in the problem domain. The weighted average of the residuals for each node is then forced to zero.

Let us consider a differential equation of the form

$$L(\Phi, z) - F(x, y, z) = 0 \quad [D-1]$$

where L is the differential operator, Φ is the field variable, and F is a known

function. We can define an approximate solution $\hat{\Phi}$ of the form

$$\hat{\Phi}(x, y, z) = \sum_{i=1}^m N_i(x, y, z) \Phi_i \quad [D-2]$$

where N_i are interpolation functions, Φ_i represents (unknown) values of the field variable at the nodes, and m is the number of nodes in the mesh. When the approximate solution is substituted into Eq. [D-1], the differential equation is no longer satisfied exactly

$$L(\hat{\Phi}(x, y, z)) - F(x, y, z) = R_{es}(x, y, z) \neq 0 \quad [D-3]$$

where R_{es} is the residual or error due to the approximate solution. R_{es} varies from node to node within the solution domain.

In the method of weighted residuals, the weighted average of the residuals at the nodes is forced to be equal to zero

$$\int_{\Omega} W(x, y, z) R_{es}(x, y, z) d\Omega = 0 \quad [D-4]$$

where $W(x, y, z)$ is a weighting function and Ω represents the problem domain. Ω becomes a length for a 1-D problem, an area for a 2-D problem, and a volume for a 3-D problem. Substituting Eq. [D-3] into Eq. [D-4] results in

$$\int_{\Omega} W(x, y, z) [L(\hat{\Phi}(x, y, z)) - F(x, y, z)] d\Omega \quad [D-5]$$

To evaluate Eq. [D-5], the mathematical form of the approximate solution $\hat{\Phi}$ and the weighting function W must be specified. $\hat{\Phi}$ is defined in a piece-wise fashion over the problem domain. The value of $\hat{\Phi}$, within any element e , $\hat{\Phi}^{(e)}$, is given by

$$\hat{\Phi}^{(e)}(x, y, z) = \sum_{i=1}^n N_i^{(e)} \Phi_i \quad [D-6]$$

where $N_i^{(n)}$ are interpolation functions and n is the number of nodes within the element. It is to be noted that, in Galerkin's Method, the weighting function for a node is identical to the interpolation function used to define the approximate solution, $\hat{\phi}$. Galerkin's method is a subset of the method of weighted residuals that is most commonly used to solve water-flow and solute-transport problems for a porous medium.

After specifying the form of $\hat{\phi}$ and W , the integral in Eq. [D-5] is evaluated in order to obtain a system of linear equations of the form

$$[C]\{\phi\} = \{F\} \quad [D-7]$$

that can be solved for the values of Φ at each node in the mesh.

Evaluation of the integral containing the time derivative of Φ requires that the time derivative of $\hat{\phi}$ be defined over the volume of the element. This can be done using interpolation functions and the values of the time derivatives at the nodes, in the same manner that $\hat{\phi}$ is defined over the volume of the element using the interpolation functions and the values of $\hat{\phi}$ at the nodes. Depending on the type of interpolation function used, the procedure is called either a 'consistent' or a 'lumped' element formulation. Both formulations are used in practice. However, the lumped formulation is less susceptible to problems of 'numerical oscillation' than is the consistent formulation (Segerlind, 1984). The lumped formulation assumes that the variation of $\partial\Phi/\partial t$ with respect to x , y , and z is constant between the midpoints of adjacent elements and that the weighting functions are the same as used for the spatial derivatives.

Element Type and Interpolation Function

A commonly used 2-D element, a linear triangle (Fig. D-1), was used in the present work. Linear interpolation functions for this type of element are derived in Segerlind (1984). The interpolation functions are also commonly referred to as shape functions or as basis

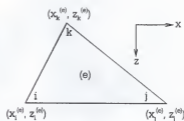


Figure D-1. Linear triangular element

functions. For the 2-D triangular element used in this work, the functions were

$$\begin{aligned}
 N_i^{(e)}(x, z) &= \frac{1}{2A^{(e)}}(a_i + b_i x + c_i z) \\
 N_j^{(e)}(x, z) &= \frac{1}{2A^{(e)}}(a_j + b_j x + c_j z) \\
 N_k^{(e)}(x, z) &= \frac{1}{2A^{(e)}}(a_k + b_k x + c_k z)
 \end{aligned}
 \tag{D-8}$$

where

$$\begin{aligned}
 a_i &= x_j^{(e)} z_k^{(e)} - x_k^{(e)} z_j^{(e)} & b_i &= z_j^{(e)} - z_k^{(e)} & c_i &= x_k^{(e)} - x_j^{(e)} \\
 a_j &= x_k^{(e)} z_i^{(e)} - x_i^{(e)} z_k^{(e)} & b_j &= z_k^{(e)} - z_i^{(e)} & c_j &= x_i^{(e)} - x_k^{(e)} \\
 a_k &= x_i^{(e)} z_j^{(e)} - x_j^{(e)} z_i^{(e)} & b_k &= z_i^{(e)} - z_j^{(e)} & c_k &= x_j^{(e)} - x_i^{(e)}
 \end{aligned}
 \tag{D-9}$$

and

$$A^{(e)} = \begin{vmatrix} 1 & x_i^{(e)} & z_i^{(e)} \\ 1 & x_j^{(e)} & z_j^{(e)} \\ 1 & x_k^{(e)} & z_k^{(e)} \end{vmatrix}
 \tag{D-10}$$

Derivatives of the interpolation functions are

$$\begin{aligned} \frac{\partial N_i^{(e)}}{\partial x} &= \frac{b_i}{2A^{(e)}} & \frac{\partial N_j^{(e)}}{\partial x} &= \frac{b_j}{2A^{(e)}} & \frac{\partial N_k^{(e)}}{\partial x} &= \frac{b_k}{2A^{(e)}} \\ \frac{\partial N_i^{(e)}}{\partial z} &= \frac{c_i}{2A^{(e)}} & \frac{\partial N_j^{(e)}}{\partial z} &= \frac{c_j}{2A^{(e)}} & \frac{\partial N_k^{(e)}}{\partial z} &= \frac{c_k}{2A^{(e)}} \end{aligned} \quad [D-11]$$

The element matrices for the linear triangle element can be estimated as (Segerlind, 1984)

$$\int_{A^{(e)}} \left(N_i^{(e)}\right)^a \left(N_j^{(e)}\right)^b \left(N_k^{(e)}\right)^c dA = \frac{a! b! c!}{(a+b+c)!} 2A^{(e)} \quad [D-12]$$

where a , b , and c are exponents of the interpolation functions $N_i^{(e)}$, $N_j^{(e)}$, and $N_k^{(e)}$.

Matrix Equations

Application of the finite-element method, as described, results in the linearized matrix form of the water flow governing equation

$$[A_w] \left(\frac{\partial h}{\partial t} \right) + [B_w] \left(\frac{\partial T}{\partial t} \right) + [C_w] \{h\} + [D_w] \{T\} = \{E_w\} - \{Q_w\} \quad [D-13]$$

where elements in the $n \times n$ coefficient matrices and $n \times 1$ vectors are

$$\begin{aligned} A_{w1j} &= \sum_e \left[\left(\frac{A_e}{9} \right) (A_{w1} + A_{w2} + A_{w3}) \delta_{1j} \right], & B_{w1j} &= \sum_e \left[\left(\frac{A_e}{9} \right) (B_{w1} + B_{w2} + B_{w3}) \delta_{1j} \right] \\ C_{w1j} &= \sum_e \left[C_w \frac{(b_1 b_j + c_1 c_j)}{4A_e} \right], & D_{w1j} &= \sum_e \left[D_w \frac{(b_1 b_j + c_1 c_j)}{4A_e} \right] \\ E_{w1} &= \sum_e (E_w c_1), & Q_{w1} &= \sum_e \left[\frac{(L_j V_w)_1}{2} \right] \quad (m = 1, 2) \end{aligned} \quad [D-14]$$

The values of the coefficients C_w , D_w , and E_w for each element are estimated as the

average of the nodal values. The subscripts i , j , and k on the A_w and B_w coefficients indicate the value of the coefficient at the respective local node of a particular element. The Q_w vector is used to satisfy a Neumann boundary condition where V_w is a prescribed or known flux density across the side of the element, L_s is the length of the boundary side, and m represents the local nodes of the element side on the boundary.

For an isotropic heterogenous medium the coefficients in Eq. [D-13] are described as (Milly and Eagleson, 1980)

$$A_w = \left(1 - \frac{\rho_v}{\rho_L} \right) \frac{\partial \theta_L}{\partial h} \Big|_T + \frac{\theta_s}{\rho_L} \frac{\partial \rho_v}{\partial h} \Big|_T \quad \text{[D-13a]}$$

$$B_w = \left(1 - \frac{\rho_v}{\rho_L} \right) \frac{\partial \theta_L}{\partial T} \Big|_h + \frac{\theta_s}{\rho_L} \frac{\partial \rho_v}{\partial T} \Big|_h \quad \text{[D-13b]}$$

$$C_w = K + D_{hv} \quad \text{[D-13c]}$$

$$D_w = D_{Tv} \quad \text{[D-13d]}$$

$$E_w = Kk \quad \text{[D-13e]}$$

A fully implicit finite-difference scheme was used to integrate the time derivatives. The time domain was divided into a sequence of finite intervals, Δt , and the time derivatives were replaced by finite differences. After rearrangement to combine known terms on the right hand side of the equation, the resultant matrix equation was obtained as

$$\left[\frac{A_w^p}{\Delta t} + C_w^p \right] \{h^p\} = - \left[\frac{B_w^p}{\Delta t} + D_w^p \right] \{T^p\} + \left[\frac{A_w^p}{\Delta t} \right] \{h^{p-1}\} + \left[\frac{B_w^p}{\Delta t} \right] \{T^{p-1}\} - \{E_w^p - Q_w^p\} \quad \text{[D-15]}$$

where p denotes the current time step for which a solution is sought and $p-1$ denotes the previous time step. Storage and transport properties of the elements in A_w , B_w , C_w , D_w , and E_w are evaluated at the current time step.

An exactly similar procedure was applied to develop the matrix equation for heat flow. The two equations for water flow and heat flow, being highly nonlinear in nature, are solved iteratively and sequentially until a desired level of convergence is reached.

The standard Galerkin's method was also applied to solute transport, resulting in

$$[R] \left\{ \frac{dc}{dt} \right\} + [Q^s] \{c\} + [D] \{c\} + [T^s] \{c\} + \{G\} = \{O\} \quad [D-16]$$

where $[R]$ is the retardation matrix, $[Q^s]$ is the convection matrix, $[D]$ is the diffusion matrix, $[T^s]$ is the transformation matrix, $\{G\}$ is the temperature effects vector, and $\{O\}$ is the force vector. Elements in the $n \times n$ coefficient matrices and $n \times 1$ vectors are

$$\begin{aligned} R_{ij} &= -\sum_e \left(\frac{A_e}{3} R_{ij}^{td} \delta_{ij} \right), \quad Q_{ij}^s = -\sum_e \left(\frac{b_i q_{Lx} + c_i q_{Lz}}{6} \right) \\ D_{ij} &= -\sum_e \left[\frac{b_i b_j D_{xx} + (b_i b_j + c_i c_j) D_{xx} + c_i c_j D_{zz}}{4A_e} \right] \\ T_{ij}^s &= \sum_e \left[\frac{A_e}{24} (F_i + F_j) (1 + \delta_{ij}) \right], \quad G_i = \sum_e \left(\frac{A_e}{3} G_i \right) \end{aligned} \quad [D-17]$$

A fully implicit finite-difference method was used to integrate the time derivative to obtain

$$\left[\frac{R^p}{\Delta t} + Q_s^p + D^p + T^p \right] \{C^p\} = - \left[\frac{R^p}{\Delta t} \right] \{C^{p-1}\} - \{G^p\} + \{Q^p\} \quad [D-18]$$

where the superscript p represents a future time level.

The matrix equations were programmed in FORTRAN-90 language using Microsoft[®] Fortran PowerStation™ Version 4.0 (Microsoft Corporation, 1995)¹. Matrix solvers provided with the package (Microsoft IMSL™ mathematical and statistical libraries²) were used for solving the assembled matrices. The simulation results from the model were visualized using TECPLOT[®] (Amtec Eng., Inc., 1996)³.

Mulch Energy Balance

Given known meteorological conditions, system optical and thermal properties, and temperatures T_s and T_1 , Eq. [3.7] and [3.8] are unique functions of T_s and T_m . An algorithm was developed for solving nonlinear equations using the

¹Microsoft is a registered trademark, and PowerStation is-trademark, of Microsoft Corporation in the United States and/or other countries.

²IMSL is a registered trademark of Visual Numerics, Inc.

³TECPLOT is a registered trademark of Amtec Engineering, Inc.

Newton-Raphson technique (Press et al., 1986). Partial derivatives required for the

Newton-Raphson solution are as follows

$$\begin{aligned} \frac{\partial f_1}{\partial T_a} &= 4e_a \sigma T_a^3 (e_a(1 - e_s) \rho_{ir}^* - 2) - \frac{1}{r_c} - \frac{C_a}{r_{a,b}}, \quad \frac{\partial f_1}{\partial T_s} = 4e_s e_a \sigma T_s^3 \rho_{ir}^* + \frac{1}{r_c} \\ \frac{f_2}{T_a} &= 4e_s e_a \sigma T_a^3 \rho_{ir}^* + \frac{1}{r_c}, \quad \frac{\partial f_2}{\partial T_s} = 4e_s \sigma T_s^3 (e_s \rho_{e,ir} \rho_{ir}^* - 1) - \frac{1}{r_c} - \frac{\lambda^*}{\Delta z} - \frac{C_s \Delta z}{2\Delta t} \end{aligned} \quad [D-19]$$

where functions f_1 and f_2 represent energy balance Eqs. [3.7] and [3.8], respectively.

LIST OF REFERENCES

- Abdalla, N., D.J. Raski, B. Lear, and R.V. Schmitt. 1974. Distribution of methyl bromide in soils treated for nematode control in replant vineyards. *Pestic. Sci.* 5: 259-269.
- Amtec Eng., Inc. 1996. TEC PLOT Version 7: Productive Power for Data Visualization. Bellevue, WA.
- Anderson, D.M. and A. Linville. 1960. Temperature fluctuations accompanying water movement through porous media. *Science* 101: 1370-1371.
- Anderson, M.P. and W.W. Woessner. 1992. Applied Groundwater Modeling: Simulation of Flow and Advective Transport. Academic Press, Inc., San Diego, CA.
- Bach, L.B. 1992. Soil water movement in response to temperature gradients: experimental measurements and model evaluation. *Soil Sci. Soc. Am. J.* 56: 37-46.
- Barnes, C.J. and G.B. Allison. 1984. The distribution of deuterium and ^{18}O in dry soils. 3. Theory for non-isothermal water movement. *J. Hydrol.* 74: 119-135.
- Barnes, C.J., G.B. Allison, and M.W. Hughes. 1989. Temperature gradient effects on stable isotope and chloride profiles in dry soils. *J. Hydrol.* 112: 69-87.
- Baver, L.D., W.H. Gardner, and W.R. Gardner. 1972. Soil Physics. John Wiley and Sons, Inc., New York.
- Bear, J. 1972. Dynamics of Fluid in Porous Media. Elsevier, New York.
- Bear, J. and A. Verruijt. 1987. Modeling Groundwater Flow and Pollution. D. Reidel Publishing Company, Dordrecht, Holland.
- Benjamin, J.G. 1989. Coupled water and heat transport in nonuniform soils. *Ph.D. Thesis*. Iowa State University, Ames, Iowa.
- Bird, R.B., W.E. Stewart, and E.N. Lightfoot. 1960. Transport Phenomenon. John Wiley and Sons, Inc., New York.

- Brown, B.D. and D.E. Rolston. 1980. Transport and Transformation of methyl bromide in soils. *Soil Sci.* 130: 68-75.
- Cary, J.W. 1966. Soil moisture transport due to thermal gradients: practical aspects. *Soil Sci. Soc. Am. Proc.* 30: 428-433
- Cary, J.W. and S.A. Taylor. 1962a. The interaction of the simultaneous diffusion of heat and water vapor. *Soil Sci. Soc. Am. Proc.* 26: 413-416.
- Cary, J.W. and S.A. Taylor. 1962b. Thermally driven liquid and vapor phase transfer of water and energy in soil. *Soil Sci. Soc. Am. Proc.* 26: 417-420.
- Cassel, D.K., D.R. Nielsen, and J.W. Biggar. 1969. Soil water movement in response to imposed temperature gradients. *Soil Sci. Soc. Am. Proc.* 33: 493-500.
- Castro, C.E. and N.O. Belser. 1981. Photohydrolysis of methyl bromide and chloropicrin. *J. Agric. Food. Chem.* 29: 1005-1008.
- Cho, C.M. 1971. Convective transport of ammonium with nitrification in soil. *Can. J. Soil Sci.* 51: 339-350.
- Chung, S.O. and R. Horton. 1987. Soil heat and water flow with a partial surface mulch. *Water Resour. Res.* 23: 2175-2186.
- Clark, M.M. 1996. Transport Modeling for Environmental Engineers and Scientists. John Wiley & Sons, Inc., New York.
- Cohen, Y. and P.A. Ryan. 1989. Chemical transport in the top soil zone - the role of moisture and temperature gradients. *J. Haz. Materials* 22: 283-304.
- Cohen, Y., H. Taghavi, and P.A. Ryan. 1988. Chemical volatilization in nearly dry soils under non-isothermal conditions. *J. Environ. Qual.* 17: 198-204.
- Constantz, J. 1982. Temperature dependence of unsaturated hydraulic conductivity of two soils. *Soil Sci. Soc. Am. J.* 46: 466-470.
- Crank, J. 1975. The Mathematics of Diffusion. Oxford University Press, London, Great Britain.
- Daniels, F. and R.A. Alberty. 1961. Physical Chemistry. John Wiley & Sons, Inc., New York.
- de Silans, P.A., L. Bruckler, J.L. Thony, and M. Vauclin. 1989. Numerical modeling of coupled heat and water flows during drying in a stratified bare soil - comparisons with field observations. *J. Hydrol.* 105: 109-138.

- de Vries, D.A. 1968. Simultaneous transfer of heat and moisture in porous media. *Trans. Am. Geophys. Union* 39: 909-916.
- de Vries, D.A. 1963. Thermal properties of soils. In: Physics of Plant Environment (Ed. W.R. van Wijk). North Holland Publishing Co., Amsterdam, pp 210-235.
- Edlefsen, N.E. and A.B.C. Anderson. 1943. Thermodynamics of soil moisture. *Hilgardia* 15: 31-298.
- Ekern, P.C. 1967. Soil moisture and soil temperature changes with the use of black vapor-barrier mulch and their influence on pineapple growth in Hawaii. *Soil Sci. Soc. Am. Proc.* 31: 270-275.
- Enfield, C.G. 1970. An irreversible thermodynamic approach to simultaneous movement of water, heat, and salt through unsaturated soils. Report UC-51, Geology and Mineralogy, Battelle Memorial Institute, Pacific Northwest Laboratories, Richland, WA.
- Evans, D.D. and T.J. Nicholson. 1987. Flow and transport through unsaturated fractured rock: An overview. In: Flow and Transport Through Unsaturated Fractured Rock (Eds. D.D. Evans and T.J. Nicholson). Geophysical Monograph 42, pp 1-10.
- EXTONET. 1997. The EXtension TOXicology NETwork. A pesticide information project of cooperative extension offices at Cornell Univ., Michigan State Univ., Oregon State Univ., and Univ. of California at Davis. <http://ace.ace.orst.edu/info/extoxnet/>.
- Fnebele, E. 1997. Partial picture of methyl bromide demands more pieces. *EOS, Trans. Am. Geophys. Union* 78: 245-246.
- Friedman, R., C. Ansell, S. Diamond, and Y.Y. Haimes. 1984. The use of models for water resources management, planning and policy. *Water Resour. Res.* 20: 793-802.
- Geiger, R. 1957. The Climate Near the Ground. Harvard University Press, Cambridge, MA.
- Gentile, I.A., L. Ferraris, S. Crespi, and A. Belligno. 1989. The degradation of methyl bromide in some natural fresh water influence of temperature, pH, and light. *Pestic. Sci.* 25: 261-272.
- Gentile, I.A., L. Ferraris, M. Sanguinetti, M. Tipngan and G. Fisichella. 1992. Methyl bromide in natural fresh waters hydrolysis and volatilisation. *Pestic. Sci.* 34: 297-301.

- Ghildyal, B.P. and R.P. Tripathi. 1987. Soil Physics. Wiley Eastern Limited, New Delhi, India.
- Goring, C.A.I. 1962. Theory and principles of soil fumigation. *Adv. Pest Control Res.* 5: 47-84.
- Groenevelt, P.H. and B.D. Kay. 1974. On the interaction of water and heat transport in frozen and unfrozen soils, 2. The liquid phase. *Soil Sci. Soc. Am. Proc.* 38: 400-404.
- Grojesan, D. 1991. Atmospheric chemistry of toxic contaminants. 4. Saturated halogenated aliphatics: methyl bromide, epichlorhydrin, phosgene. *J. Air Waste Manage. Assoc.* 41: 56-61.
- Gurr, C.G., T.J. Marshall, and J.T. Hutton. 1952. Movement of water in soil in response to temperature gradients. *Soil Sci.* 74: 335-345.
- Hacherl, E.L. 1994. Diffusion of methyl bromide through polyethylene films and soil: Effects of temperature and moisture content. *M.S. Thesis*. University of Florida, Gainesville, FL.
- Ham, J.M. and G.J. Kluitenberg. 1994. Modeling the effect of mulch optical properties and mulch-soil contact resistance on soil heating under plastic mulch culture. *Agric. For. Meteorol.* 71: 403-424.
- Ham, J.M., G.J. Kluitenberg, and W.J. Lamont. 1993. Optical properties of plastic mulches affect the field temperature regime. *J. Am. Soc. Hort. Sci.* 118: 188-193.
- Hares, M.A. and M.D. Novak. 1992. Simulation of surface energy balance and soil temperature under strip tillage: I. Model description. *Soil Sci. Soc. Am. J.* 56: 22-29.
- Havercamp, R., M. Vauclin, J. Tovina, P.J. Wierenga, and G. Vachaud. 1977. A comparison of numerical simulation models for one-dimensional infiltration. *Soil Sci. Soc. Am. Proc.* 41: 285-294.
- Hemwall, J.B. 1959. A mathematical theory of soil fumigation. *Soil Sci.* 88: 184-190.
- Hemwall, J.B. 1960. Theoretical considerations of several factors influencing the effectivity of soil fumigants under field conditions. *Soil Sci.* 90: 157-168.
- Hillel, D. 1980. Fundamentals of Soil Physics. Academic Press, Inc., New York.

- Hoffman, G.M. and H.P. Malkomes. 1979. The fate of fumigants. In: Soil Disinfestation (Ed. D. Mulder). Elsevier Scientific Publishing Co., Amsterdam, The Netherlands. pp. 291-335.
- Hornsby, A.G., R.D. Wauchope, and A.E. Herner. 1996. Pesticide Properties in the Environment. Springer-Verlag New York, Inc., New York.
- Horton, R. and S. Chung. 1991. Soil Heat Flow. In: Modeling Plant and Soil Systems. (Eds. J. Hanks and J. Ritchie). Monograph 31, Am. Soc. of Agronomy, Madison, WI. pp. 397-348.
- Istok, J. 1989. Groundwater Modeling by the Finite Element Method. Water Resources Monograph 13, American Geophysical Union, Washington, DC.
- Jackson, R.D. 1967. Osmotic effects on water flow through a ceramic filter. *Soil Sci. Soc. Am. Proc.* 31: 713-715.
- Jin, Y. and W.A. Jury. 1995. Methyl bromide diffusion and emission through soil columns under various management techniques. *J. Environ. Qual.* 24: 1002-1009.
- Jones, H.E. and H. Kohnke. 1952. The influence of soil moisture tension on vapor movement of soil water. *Soil Sci. Soc. Am. Proc.* 16: 245-248.
- Jury, W.A. 1973. Simultaneous transport of heat and moisture through a medium sand. *PhD Thesis*, University of Wisconsin, Madison, WI.
- Kay, B.D. and P.H. Groenevelt. 1974. On the interaction of water and heat in frozen and unfrozen soils, 1. Basic theory; the vapor phase. *Soil Sci. Soc. Am. Proc.* 38: 395-400.
- Kemper, W.D. and D.E.L. Maasland. 1964. Reduction in salt content of solution on passing through thin films adjacent to charged surfaces. *Soil Sci. Soc. Am. Proc.* 28: 318-823.
- Kemper, W.D. and J.B. Rollins. 1966. Osmotic efficiency coefficients across compacted clays. *Soil Sci. Soc. Am. Proc.* 30: 529-534.
- Khalil, M.A.K., R.A. Rasmussen, and R. Gunawardena. 1993. Atmospheric methyl bromide trends and global mass balance. *J. Geophys. Res.* 98: 2887-2896.
- Kolbezan, M.J. and Fawzi J. Abu-El-Haj. 1977. Permeability of plastic films to fumigants. *Proc. International Agricultural Plastics Congress*, San Diego, CA, April 11-16.

- Leij, F.J. and S.A. Bradford. 1994. 3DADE: A computer program for evaluating three-dimensional equilibrium solute transport in porous media. Research Report No. 134, U.S. Salinity Lab., USDA, ARS, Riverside, CA.
- Letey, J. and W.D. Kemper. 1969. Movement of water and salt through a clay-water system experimental verification of Onsager reciprocal relation. *Soil Sci. Soc. Am. Proc.* 33: 25-29.
- Lobert, J.M., D.H. Scharffe, W.M. Hao, and P.J. Crutzen. 1990. Importance of biomass burning in the atmospheric budgets of nitrogen-containing gases. *Nature* 346: 552-554.
- Low, P.F. 1955. Effect of osmotic pressure on diffusion rate of water. *Soil Sci.* 80: 95-100.
- Macartney, L. and T.V. Price. 1988. Bromide residues in glasshouse soils in Victoria following bromomethane fumigation. *Soil Bio. Biochem.* 20: 393-397.
- Maharajh, D.M. and J. Walkley. 1973. The temperature dependence of Ar, CO₂, CH₄, CH₃CL, CH₃BR, and CHCL₂F in water. *Can. J. Chem.* 51: 944-952.
- Mahrer, Y., O. Naot, E. Rawitz, and J. Katan. 1984. Temperature and moisture regimes in soils mulched with transparent polyethylene. *Soil Sci. Soc. Am. J.* 48: 362-367.
- Manó, S. and M.O. Andreae. 1994. Emission of methyl bromide from biomass burning. *Science* 263: 1255-1257.
- Marshall, T.J. and J.W. Holmes. 1979. *Soil Physics*. Cambridge University Press, Cambridge.
- Maw, G.A. and R.J. Kempton. 1973. Methyl bromide as a soil fumigant. *Soils Fert.* 36: 41-47.
- Maw, G.A. and R.J. Kempton. 1982. Bromine in soils and peats. *Plant and Soil.* 65: 103-109.
- Mckenry, M.V. and C.O. Hesse. 1978. Preplant fumigations of planting sites. *California Agriculture* 32: 14-15.

- Microsoft Corporation. 1995. Microsoft® Fortran PowerStation™ Version 4.0¹: Development System for Windows 95™ and Windows NT™ Workstation. Redmond, WA.
- Mignard, E. and J.C. Benet. 1969. Diffusion of methyl bromide in soil. *J. Soil Sci.* 40: 151-165.
- Milly, P.C.D. 1984. A simulation analysis of thermal effect on evaporation from soil. *Water Resour. Res.* 20: 1087-1098.
- Milly, P.C.D. and P.S. Eagleson. 1980. The coupled transport of water and heat in a vertical soil column under atmospheric excitation. Tech. Rep. no. 258. R.M. Parsons Lab., Dep. Civil Eng., Mass. Inst. Technol., Cambridge.
- Moje, W. 1960. The chemistry and nematocidal activity of organic halides. *Adv. Pest Control Res.* 3: 181-217.
- Mutziger, A.J., S.R. Yates, D. Wang, W.F. Spencer, F.F. Ernst, and J. Gan. 1996. Modeling methyl bromide diffusion in a field soil. *Soil Sci. Soc. Am. Annual Meeting*, Indianapolis, Indiana, Nov. 3-8, 1996.
- Nassar, I.N. and R. Horton. 1989a. Water transport in unsaturated non-isothermal salty soil: I. Experimental results. *Soil Sci. Soc. Am. J.* 53: 1330-1337.
- Nassar, I.N. and R. Horton. 1989b. Water transport in unsaturated non-isothermal salty soil: II. Theoretical development. *Soil Sci. Soc. Am. J.* 53: 1330-1337.
- Nassar, I.N. and R. Horton. 1992. Simultaneous transfer of heat, water, and solute in porous media: I. Theoretical development. *Soil Sci. Soc. Am. J.* 56: 1350-1356.
- Noborio, K. 1995. A two-dimensional finite-element model for solution, heat, and solute transport in furrow-irrigated soil. *Ph.D. Thesis*. Texas A & M University, College Station, TX.
- Noggle, J.H. 1985. Physical Chemistry. Little, Brown and Co., Boston.

¹Microsoft and Windows 95 are registered trademarks, and Windows NT and PowerStation are trademarks, of Microsoft Corporation in the United States and/or other countries.

- Philip, J.R. and D.A. de Vries. 1957. Moisture movement in porous materials under temperature gradients. *Trans. Am. Geophys. Union* 38: 222-232.
- Pinder, G.F. and W.G. Gray. 1977. Finite Element Simulation in Surface and Subsurface Hydrology. Academic Press, New York.
- Press, W.H., B.P. Flannery, S.A. Teukolsky, and W.T. Vetterling. 1986. Numerical Recipes: The Art of Scientific Computing. Cambridge University Press, New York.
- Qayyum, M.A. and W.D. Kemper. 1962. Salt concentration gradients in soils and their effects on moisture movement and evaporation. *Soil Sci.* 93: 333-342.
- Richards, L.A. 1931. Capillary conduction of liquids in porous mediums. *Physics*. 1: 318-333.
- Rollins, R.L., M.G. Spangler, and D. Kirkham. 1954. Movement of soil moisture under a thermal gradient. *Highway Res. Board Proc.* 33: 492-508.
- Rolston, D.E. and R.D. Glauz. 1982. Comparison of simulated with measured transport and transformation of methyl bromide gas in soils. *Pestic. Sci.* 13: 653-664.
- Rosenberg, N.J., B.L. Blaid, and S.B. Verma. 1983. Microclimate: The Biological Environment. John Wiley & Sons, Inc., New York.
- Scanlon, B.R. 1992. Evaluation of liquid and vapor water flow in desert soils based on chlorine 36 and tritium tracers and non-isothermal flow simulations. *Water Resour. Res.* 28: 285-297.
- Schwarzenbach, R. P., P. M. Gschwend, and D.M. Imboden. 1993. Environmental Organic Chemistry. John Wiley & Sons, Inc., New York.
- Segerlind, L.J. 1984. Applied Finite Element Analysis. John Wiley & Sons, Inc., New York.
- Siebering, H. and M. Leistra. 1979. Computer simulation of fumigant behaviour in soil. In: Soil Disinfestation (Ed. D. Mulder). Elsevier Scientific Publishing Co., Amsterdam, The Netherlands. pp 135-161.
- Šimůnek, J. and D.L. Suarez. 1993. Modeling of carbon dioxide transport and production in soil: 1. Model development. *Water Resour. Res.* 29: 487-497.
- Šimůnek, J. and M.Th. van Genuchten. 1994. The CHAIN_2D code for simulating two-dimensional variably saturated water flow, heat transport and transport

of solutes involved in sequential first-order decay reactions. Research Report No. 136. U.S. Salinity Lab., ARS, USDA, Riverside, CA.

- Šimůnek, J., T. Vogel, and M.Th. van Genuchten. 1992. The SWMS_2D Code for simulating water flow and solute transport in 2-D variably saturated media, Ver. 1.1, Research Report No. 126. U.S. Salinity Lab., USDA, ARS, Riverside, CA.
- Smith, W.O. 1943. Thermal transfer of moisture in soils. *Trans. Am. Geophys. Union* 24: 511-523.
- Sophocleous, M. 1979. Analysis of water and heat flow in unsaturated-saturated porous media. *Water Resour. Res.* 15: 1195-1206.
- Staple, W.J. and Lehane, J.J. 1954. Movement of moisture in unsaturated soils. *Can. J. Agric. Sci.* 34: 329-342.
- Stumm, W. and J.J. Morgan. 1981. Aquatic Chemistry: An introduction emphasizing chemical equilibria in natural waters. John Wiley & Sons, Inc., New York.
- Taylor, S.A. and J.W. Cary. 1960. Analysis of the simultaneous flow of water and heat or electricity with the thermodynamics of irreversible processes. *Trans. Intern. Congr. Soil Sci.*, 7th Cong. Madison 1: 80-90.
- Taylor, S.A. and L. Cavazza. 1964. The movement of soil moisture in response to temperature gradients. *Soil Sci. Soc. Am. Proc.* 18: 351-358.
- USDA ARS. 1997. ARS Methyl Bromide Research newsletter. <http://www.ars.usda.gov/is/mb/mebrweb.html>.
- USEPA. 1986. Chemical Fact Sheet for Methyl Bromide. *Fact Sheet No. 98*. 22 August 1986.
- USEPA. 1997. Stratospheric Ozone. Methyl Bromide Information. <http://www.epa.gov/docs/ozone/MBR/MBRqa.html>.
- Van Bavel, C.H.M. and D.I. Hillel. 1975. A simulation study of soil heat and moisture dynamics as affected by a dry mulch. *Proc. Summer Computer Simulation Conf.*, 1975. pp 815-821.
- Van Bavel, C.H.M. and D.I. Hillel. 1976. Calculating potential and actual evapotranspiration from a bare soil surface by simulation of concurrent flow of water and heat. *Agricultural Meteorology* 17: 453-476.

- Van de Hulst, H.C. 1980. Multiple Light Scattering: Tables, Formulas, and Applications. Academic Press, New York. 299 pp.
- van Genuchten, M. Th. 1980. A closed-form equation for predicting the hydraulic conductivity of unsaturated soils. *Soil Sci. Soc. Am. J.* 44: 892-898.
- van Genuchten, M. Th. 1981. Non-equilibrium transport parameters from miscible displacement experiments. Research Report No. 119, U.S. Salinity Laboratory, Riverside, CA.
- van Genuchten, M. Th. 1985. Convective-dispersive transport of solutes involved in sequential first-order decay reactions. *Computers & Geosciences* 11: 129-147.
- van Genuchten, M. Th., and R.J. Wagenet. 1989. Two-site/two-region models for pesticide transport and degradation theoretical development and analytical solutions, *Soil Sci. Soc. Am. J.* 53: 1303-1310.
- Waggoner, P.E., P.M. Miller, and H.C. DeRoo. 1960. Plastic mulching - principles and benefits. Bull. No. 634, Conn. Agric. Exp. Stn., New Haven.
- Wang, D., S.R. Yates, and J. Gan. 1997. Temperature effect on methyl bromide volatilization in soil fumigation. *J. Environ. Qual.* 26: 1072-1079.
- Wescott, D.W. and P.J. Wierenga. 1972. Transfer of heat by conduction and vapor movement in a closed soil system. J. Article No. 456, Agri. Exp. St., New Mexico State Univ, Las Cruces.
- Wiegand, C.L. and S.A. Taylor. 1962. Temperature depression and temperature distribution in drying soil columns. *Soil Sci.* 94: 75-79.
- Woodside, W. and J.B. Cliffe. 1959. Heat and moisture transfer in closed systems of two granular materials. *Soil Sci.* 87: 75-82.
- Yagi, K., J. Williams, N.Y. Wang, and R.J. Cicerone. 1993. Agricultural soil fumigation as a source of atmospheric methyl bromide. *Proc. Natl. Acad. Sci. USA.* 90: 8420-8423.
- Yakrevich, A., P. Berliner, and S. Sorek. 1997. A model for numerical simulation of evaporation from bare saline soil. *Water Resour. Res.* 33: 1021-1033.
- Yates, S.R., J. Gan, F.F. Ernst, F. Gao, and D. Wang. 1996. Methyl bromide emissions from a covered field: III. Correcting chamber flux for temperature. *J. Environ. Qual.* 25: 892-898.

- Yvon-Lewis, S.A. and J.H. Butler. 1997. The potential effect of oceanic biological degradation on the lifetime of atmospheric CH_3Br . *Geophysical Research Letters*, 24: 1227-1230.
- Zurer, P.S. 1993. Proposed ban on methyl bromide opposed by producers, users. *Chem. & Eng. News*. February 1: 23-24.

BIOGRAPHICAL SKETCH

Dilip Shinde was born on August 29, 1962, in the city of Gwalior, Madhya Pradesh (MP) State, India. He graduated from St. Paul's Higher Secondary School, Indore, MP, at the age of 16. After studying one year of higher mathematics and science at MVM Science College, Bhopal University in the State Capital, Bhopal, he entered the College of Agriculture at Indore city, an affiliate of Jawaharlal Nehru Agricultural University at Jabalpur, MP. He graduated with honors in 1983 and continued for a master's program in agronomy at the same institution. He obtained his master's degree, also with Honors, in 1985.

In January 1986, he received an Australian Government Scholarship to pursue a master's program in soil and water engineering at the Asian Institute of Technology (AIT), Bangkok, Thailand. After graduating from AIT in August, 1987, he returned to India and accepted a position as scientist with the Jawaharlal Nehru Agricultural University. His work as a scientist was focused on watershed management in dryland-rainfed agriculture until he came to the University of Florida in January 1992.

He started a Ph.D. program in the Soil and Water Science Department on an international 'Freedom From Hunger' scholarship awarded by 'The Rotary Foundation of The Rotary International'. The doctoral program occurred within the interdepartmental hydrologic sciences program, with a strong emphasis on soil physics.

I certify that I have read this study and that in my opinion it conforms to acceptable standards of scholarly presentation and is fully adequate, in scope and quality, as a dissertation for the degree of Doctor of Philosophy.


Robert S. Mansell, Chair
Professor of Soil and Water Science


I certify that I have read this study and that in my opinion it conforms to acceptable standards of scholarly presentation and is fully adequate, in scope and quality, as a dissertation for the degree of Doctor of Philosophy.


Arthur G. Hornsby, Cochair
Professor of Soil and Water Science


I certify that I have read this study and that in my opinion it conforms to acceptable standards of scholarly presentation and is fully adequate, in scope and quality, as a dissertation for the degree of Doctor of Philosophy.


Palakurthis S. C. Rao
Graduate Research Professor of Soil
and Water Science

I certify that I have read this study and that in my opinion it conforms to acceptable standards of scholarly presentation and is fully adequate, in scope and quality, as a dissertation for the degree of Doctor of Philosophy.


Brian L. McNeal
Professor of Soil and Water Science

I certify that I have read this study and that in my opinion it conforms to acceptable standards of scholarly presentation and is fully adequate, in scope and quality, as a dissertation for the degree of Doctor of Philosophy.


Pedro S. Zazueta
Professor of Agricultural and
Biological Engineering

This dissertation was submitted to the Graduate Faculty of the College of Agriculture and to the Graduate School and was accepted as partial fulfillment of the requirements for the degree of Doctor of Philosophy.

December, 1997


Dean, College of Agriculture

Dean, Graduate School

LD
1780
1997
.S556

